ANALYTICAL AND EXPERIMENTAL MODELLING OF ICEBERG SCOURS

KAVURI SIVA RAMA PRASAD

ANALYTICAL AND EXPERIMENTAL MODELLING OF ICEBERG SCOURS

By

Kavuri Siva Rama Prasad, B.Tech., M.Tech.

A thesis submitted to the School of Graduate Studies in partial fulfillment of the requirements for the degree of Master of Engineering

Faculty of Engineering and Applied Science
Memorial University of Newfoundland

August 1985

St. John's Newfoundland Canada

ABSTRACT

The discovery of oil and gas in the iceberg infested waters off the coast of Newfoundland and Labrador has generated increased interest in icebergs. There is a need to find solutions to potential iceberg hazards in order to optimize the production schemes. This thesis is a continuation of the ongoing research on geotechnical aspects of iceberg scours.

The earlier analytical model has been extended to incorporate the nonlinear velocity of the iceberg during scouring. This study examines the scouring potential of icebergs which roll due to instability, increase their draft, and penetrate the seabed before scouring. For a given iceberg, if such initial penetration depth is more than a certain upper bound, only a pockmark will be left on the seafloor. For initial penetration depths smaller than a certain lower bound, the resulting maximum scour depth would be as if there were no initial penetration of the seafloor.

The influence of keel shape on the maximum depth gouged by an iceberg was studied experimentally. Six models of different keel shape were instrumented and pushed horizontally into a sloping sand bed. The measured front face resistance for each model was correlated with the computed values using available theoretical methods. The experimental results were extrapolated to the scour model.

It is shown that the influence of keel shape on the estimated scour depth is within an acceptable range of variation and thus scour depths predicted using an idealized shape are realistic.

ACKNOWLEDGEMENTS

This thesis was completed at Memorial University of Newfoundland as part of a project partially funded by the Natural Sciences and Engineering Research Council of Canada. The receipt of a University Fellowship and graduate supplement by the author during the period of this study is gratefully acknowledged.

The author is greatly indebted to Dr. T. R. Chari, Professor and Associate Dean of Engineering, for his excellent guidance, understanding, cooperation and careful review of the manuscript. Thanks are due to Dr. G. R. Peters, Dean of Engineering, for his encouragement and the facilities provided. Dr. F. A. Aldrich, Dean of Graduate Studies has been the source of inspiration and his help is highly appreciated.

Thanks are due to the Technical Staff who made their services readily available at every stage of this project. The author is grateful to Dr. D. W. Bass for several useful discussions. Special thanks are due to Mr. Bhimavarapu Subba Reddy, Mr. Jae Shik Joo, and Mr. V. Neelakantan who provided physical and moral support on many occasions. The help of Miss Moya Grouchy who typed this manuscript and Mr. Barry Bowers who drafted several figures is appreciated.

Finally, the author would like to record his appreciation towards his wife, Annapurna, without whose patience, understanding and cooperation this work would not have taken shape.

TABLE OF CONTENTS

LIST OF TABLES

LIST OF FIGURES

NOTATIONS

The notation adopted in this thesis is in confirmation to that recommended by Barsvary et al (1980). The symbols are defined at their first appearance. However, a list of symbols used in this thesis are given below.

A	projected area of the submerged iceberg normal to the propelling currents
B	width of the idealized iceberg, also width of scour
c	shear strength of cohesive soil, also cohesion of cohesive frictional soil
C_d	drag coefficient
C_u	uniformity coefficient
d	depth of scour at any instant of time during scouring
D	maximum depth of scour
D_s	depth of scour profile
E_{drg}	cumulative energy due to hydrodynamic drag
E_{net}	residual kinetic energy of the iceberg
E_s	cumulative energy expended in overcoming soil resistance
F	shear resistance on the bottom of trial wedge
F'	shear resistance on each side of trial wedge
F_d	drag force on a decelerating iceberg
g	acceleration due to gravity
H	final height of surcharged soil in front of the berg
h	height of surcharged soil at any instant during scouring (obtained from the geometry of scour trench)
I_s	inside sloping length of scour track
K_0	at rest earth pressure coefficient
K_{pc}	passive earth pressure coefficient due to cohesion

K_{pq}	passive earth pressure coefficient due to surcharge
$K_{p\gamma}$	passive earth pressure coefficient due to weight
L	maximum length of scour
ℓ	length of scour at any instant
L_1	maximum length of surcharged soil
ℓ_1	length of surcharged soil corresponding to l
M	mass of the icebetg
M1	rectangular prismatic model
M2	model M1 with 30° inclined front face attached to it
M3	model M1 with 60° inclined front face attached to it
M4	model M1 with curved front face attached to it
M5	model M1 with cylindrical front shape attached to it
M6	model M1 with triangular wedge shape attached to it
O_s	outer sloping length of scour track
P	soil resistance on the front face of the idealized iceberg
S	initial depth of penetration
S_ℓ	lower bound of S
S_u	upperbound of S
T_s	top width of scour track
V	velocity of the iceberg at any instant
V_0	initial steady state velocity of iceberg (also averaged current velocity
W	weight of soil in the failure wedge
W_0	weight of surcharge piled up in front of model
α	angle of slope of the displaced soil

α_w angle between tangent to failure surface and normal to wall

β angle of slope of the seabed

ϕ angle of internal friction of soil

δ friction angle between soil and model

δ_m mobilized friction angle between soil and model

γ' submerged unit weight of the ocean soil

γ_{exp} experimental density

γ_{max} maximum dry density

γ_{min} minimum dry density

τ shear strength of soil ($\tau = c + \sigma \tan \phi$)

σ normal stress

γ_t saturated unit weight of the ocean soil

θ angle of the failure plane with horizontal

ρ density of sea water

CHAPTER I

INTRODUCTION

1.1 General

Icebergs drifting along the Canadian East Coast have always been of concern to the safety of merchant vessels plying the Northwest Atlantic. Ever since the Titanic disaster in 1912, the International Ice Patrol has been conducting studies and observations of icebergs with the primary objective of avoiding a collision with ships. However, with the recent exploration for hydrocarbons in the iceberg-infested waters off Canada's eastern and northern coasts, and the discovery of the Hibernia oil field, the iceberg problem has become more significant. Icebergs start their journey from Greenland, and drift along the Labrador Coast. Such icebergs are likely to damage offshore structures due to a direct collision or uproot buried structures such as pipelines and wellheads as a result of scouring the seabed. Instances where icebergs damaged blowout preventor stacks of exploratory wells and Transatlantic cables have been reported (Milne 1973, Duval 1975). An estimate of the safe burial depth for seabottom structures is therefore essential. One solution to this problem is to develop an understanding of the soil-iceberg

interaction through theoretical and laboratory models. This has been one of the ongoing research topics at Memorial University of Newfoundland. The present thesis is an extension of the earlier research (Chari 1975, Green 1984) on geotechnical modelling of iceberg scours.

1.2 Scope of this Investigation

Two approaches have been used by researchers to estimate the maximum iceberg scour depth. One method is to conduct side scan surveys and high resolution accoustic profiling for a number of years and establish scouring probabilities of various depths (Lewis and Barrie 1981). This is quite expensive and time consuming. In the second approach the scouring phenomena is physically simulated in the laboratory to help develop theoretical models and predict maximum scour depth from a knowledge of the environmental parameters. The latter approach has been followed in this investigation.

The analytical models proposed earlier for determining maximum scour depth have been reviewed and the energy solution proposed by Chari (1979) is extended to take account of nonlinear velocity of scouring icebergs. Icebergs undergo continuous oblation and degradation during which small chunks of protrusions break off, rendering the berg unstable. Such bergs roll over in order to attain a new

position of equilibrium resulting in a change of the draft which in turn could cause a penetration of the iceberg into the seafloor. An expression has been developed for studying the scouring potential of such icebergs.

The experimental study in this investigation is aimed at studying the influence of iceberg keel shape on the maximum scour depth. Six different idealized shapes of the iceberg were pushed horizontally into a sloping sand bed. The total soil resistance acting on the model and the pressure distribution on the front face of the model were continuously monitored. The component of the soil resistance acting on the front face of the model in the experiment is compared with soil resistance computed from theoretical methods.

1.3 Organization of the Thesis

In chapter II of this thesis, a brief review is given of the origin and distribution of icebergs. A detailed review of the literature is presented on the analytical and experimental modelling of iceberg scours.

In chapter III a detailed description of the mechanics of scouring is given. The extended analytical model is presented and the results thereof discussed.

Chapter IV describes the experimental program of this investigation. Details of experimental facilities, test procedures and instrumentation are presented.

Chapter V contains the results of the experiments, the analysis and a comparison with the theoretical solutions.

Finally, the summary and conclusions of this investigation are presented in chapter VI.

CHAPTER II

LITERATURE REVIEW

2.1 General

The first exploratory well for hydrocarbons on the Canadian East Coast was drilled on the Labrador shelf in 1971. Within a decade, twenty eight other wells were completed on the Labrador and Northeast Newfoundland shelf, many of which have confirmed the presence of oil and gas. For a proper design of the production systems, it is necessary to assess the potential hazards due to icebergs and devise suitable solutions. A summary of the literature related to the iceberg problem is presented in this chapter. The source of icebergs, their general characteristics, and their significance to the operations of the petroleum industry are briefly described. A detailed review of the literature on the analytical and experimental study of the mechanics of scouring is given followed by the presentation of the objectives of this investigation.

2.2 Origin of Icebergs

Most of the general data on icebergs in the Northwest Atlantic have been published by the International Ice Patrol. These have been compiled and comprehensively

reported by Smith (1931), Murray (1969), and Dinsmore (1972) covering the aspects of the origin of icebergs, their size, shape, drift, and deterioration.

About 85 percent of icebergs reaching the Newfoundland coast originate from about twenty one glaciers located between Melville Bugt and Disco Bugt on the west coast of Greenland (Fig. 1). East Greenland glaciers account for ten percent and the remaining five percent are known to come from Northern Ellesmere Island. The glacier flow comes out of the fjords into the sea and 'calving' (i.e. breaking) of the iceberg from the parent glacier occurs due to a combination of gravity and buoyancy forces on the protruding tongue of the glacier (Smith, 1931). The icebergs drift along the West-Greenland and Baffin Island coasts to join the Labrador current and move around the eastern flank of the Grand Banks before they completely disintegrate in the warm Gulf Stream. There are also several branches and deviations to this general drift pattern as shown in Fig. 1. While the number of icebergs calved at their source varies from 15,000 to 40,000 per year, the majority of these are trapped in the bays and coastal indentations and only an average of about 400 bergs reach the Grand Banks off Newfoundland. Fig. 2 illustrates the variation in the number of icebergs detected annually south of the latitude 48°N.

2.3 Physical Characteristics

The size of the iceberg at the time of calving from the parent glacier depends on the mechanism of calving (Smith 1931). Icebergs longer than 1000 meters have been reported around Cape York, West Greenland (Kollemeyer, 1980). The shape of the iceberg is generally irregular and no two icebergs look alike. Even the same iceberg looks different from various angles. The International Ice Patrol has classified icebergs based on the above water dimensions as shown in table 1, and according to the above-water shape as shown in table 2. Assuming the specific gravity of glacier ice as 0.9 and that of seawater as 1.03, the submerged volume of an iceberg would be nearly seven times the above-water volume. However, the draft to height ratio need not be in the same proportion and is a function of the iceberg shape.

Icebergs generally deteriorate in the process of their travel south. The process of melting and erosion at the water line by constant wave action causes the bergs to become unstable and roll. In this process several protrusions of the berg may also be broken off. The draft of the iceberg could increase by as much as 50 percent (Bass and Peters 1984) when they roll and assume a new stable position. This particular phenomenon has a potential consequence in the iceberg scouring process which will be discussed in a later section.

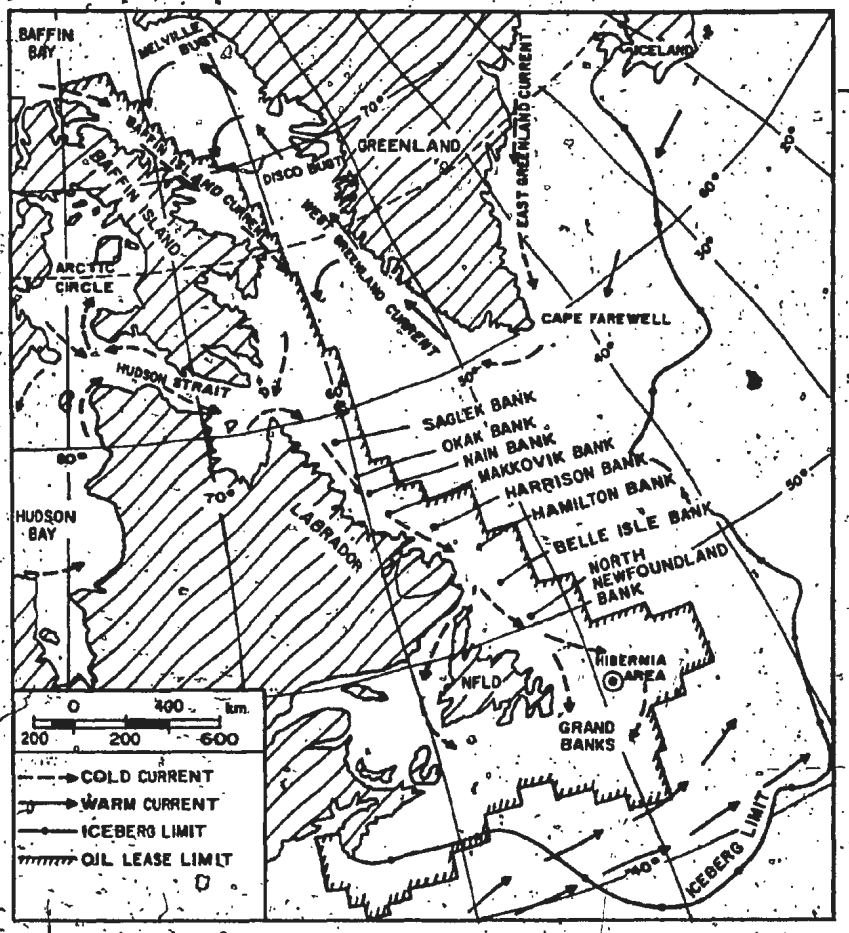

FIGURE 1. REGION OF ICEBERG PROBLEMS

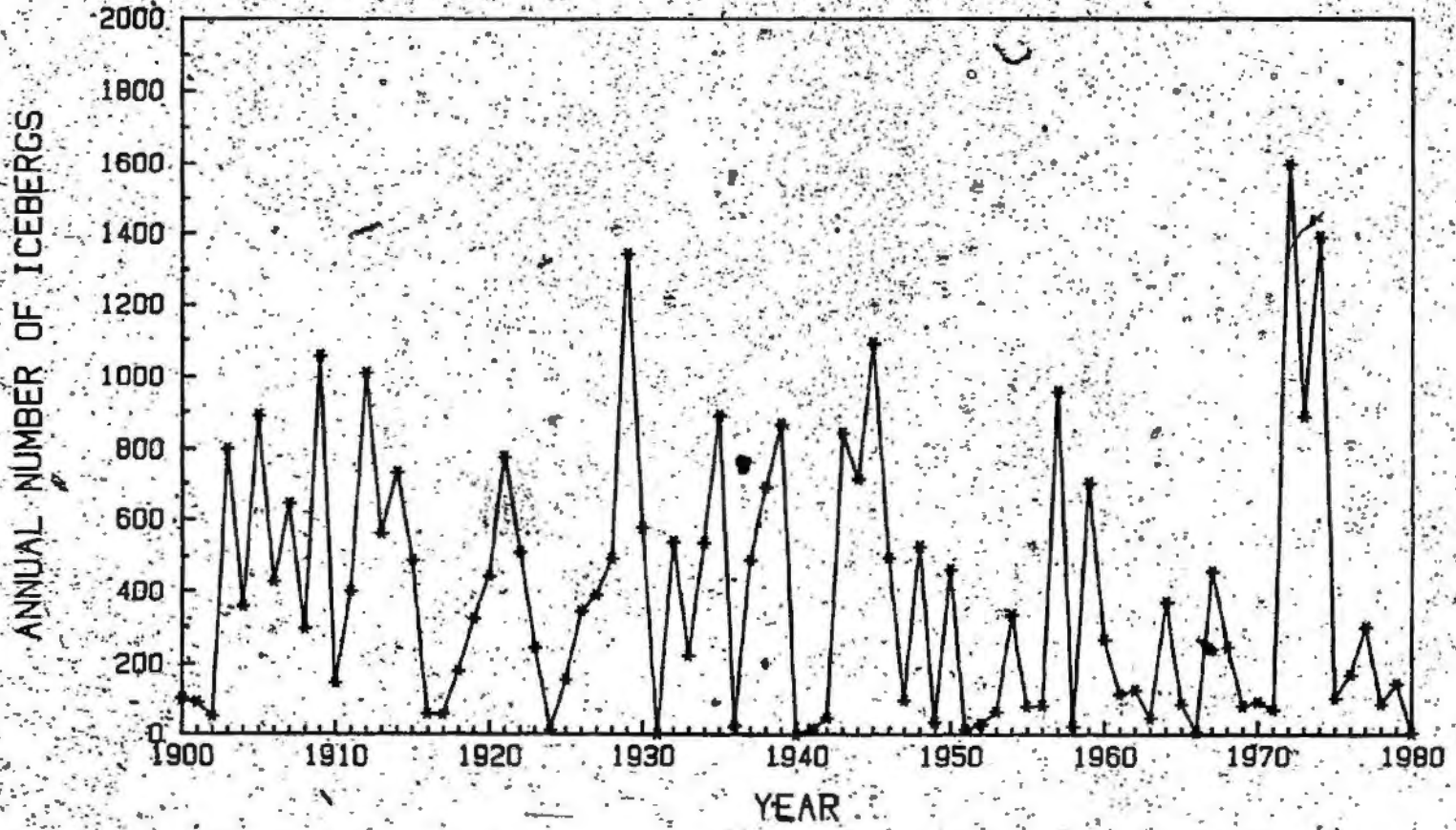

FIGURE 2 ANNUAL NUMBER OF ICEBERGS CROSSING 48°N LATITUDE (INTERNATIONAL ICE PATROL)

TABLE 1 ICEBERG CLASSIFICATION BY SIZE (MURRAY 1969).

Name	Height		Length	
	m	(ft)	m	(ft)
Tabular berg				
S - small	<6	<20	<91	<300
M - medium	6 to 15	20 to 50	91 to 213	300 to 700
L - large	>15	>50	>213	>700
Others				
S - small	<15	<50	<61	<200
M - medium	15 to 46	50 to 150	61 to 122	200 to 400
L - large	46 to 78	150 to 255	122 to 213	400 to 700
VL - very large	>78	>255	>213	>700

TABLE 2 ICEBERG CLASSIFICATION BY SHAPE (MURRAY 1969)

Type	Description
B - blocky	Steep precipitous sides with horizontal or flat top, very solid berg, length/height ratio 5:1.
DK - drydock	Eroded such that a large U-shaped slot is formed with twin columns or pinnacles, slot extends into waterline or close to it.
D - dome	Large smooth rounded top, solid type berg.
P - pinnacled	Large central spire or pyramid of one or more spires dominating the shape, less mass than dome shaped bergs of similar dimensions.
T - tabular	Horizontal or flat topped berg with length to height ratio 5:1
Bergy bit	A mass of glacial ice smaller than a berg, but larger than a growler, about the size of a small cottage, small berg or large growler is preferred usage.
Growler	A mass of glacial ice calved from a berg or is the remains of a berg. Less than 2.5 m high and 6 m long.

2.4 Iceberg Hazards

Because of their huge mass, even while drifting at low velocities icebergs carry enormous kinetic energy. A direct collision of an iceberg with a moving ship or a fixed offshore rig is one hazard that is well known. When the iceberg runs into shallow waters its keel may come in contact with the seabed causing long scours on the seabed. Such features have been mapped and measured extensively (Harris and Jollymore 1974; Lewis and Barrie 1981) on the Canadian Eastern seaboard during the past decade. The ploughing of the seabed by large icebergs is a potential hazard to any buried installation such as pipelines, blow out preventer stacks, and foundations.

Scouring of the seabed could also occur when an iceberg rolls over, penetrates the seabed due to a change in the draft, and then moves along causing a gouged feature on the seabed.

A review of the literature on the engineering evaluation of the problem is given below.

2.5 Iceberg Scours

There are two areas of current interest to the offshore petroleum industry where seabed scouring by moving ice features is a potential hazard. In the Beaufort Sea, gouges of up to 1 m depth have been observed in water depths

up to 20 m (Barnes et al 1978). These gouges are formed by moving ice keels and the predominant propelling force is the wind action on large areas of the ice sheet. In the Labrador sea, iceberg scours have been observed in water depths up to 250 m and scour depths of 6.5 m have been measured (Harris and Jollymore 1974) using side-scan sonars. The major propelling force for icebergs is the drag due to the ocean currents.

There are several similarities between the ice keel scours of the Beaufort Sea and the iceberg scours of the Labrador Sea. However, the energy balance equations are different because of the difference in the type of the driving forces. The models discussed below are with reference to freely floating icebergs. But they can be easily modified for the ice keel scours.

2.6 Methods of Estimating Maximum Scour Depths

One method of evaluating maximum scour depths is to conduct side-scan and high resolution seabed surveys to actually measure the dimensions of the existing features. However, a major uncertainty is whether such features are relict and ancient or caused by recent icebergs. Annual and repetitive surveys of the seafloor is one way to delineate new and fresh scours. The amount of infilling in a scour and the effort required for repetitive surveys of the same area

are the two limitations with this method. The third method which is the scope of this thesis is to develop analytical and physical models. Scour sizes can then be computed using the models for a given set of environmental parameters. The disadvantages with this method are the validation of the model to the real scours, the scale effects, and the accuracy of the input parameters. At this time, it would seem appropriate that all the above methods are to be pursued and attempts made to integrate them in a suitable field program. A flow chart of such an approach (Lewis and Benedict 1981) is shown in Fig. 3.

2.7 Analytical Models

The earliest attempt to analyze the scouring phenomena was by Chari and Allen (1972). They idealized the iceberg as a rectangular prism moving normal to a sloping bed of cohesive sediments of very low strength. The berg was assumed to plough the seabed without uplift, overcoming the passive resistance of the soil developed on the front face and the adhesive resistance on the base and sides. By equating the kinetic energy of the iceberg to the work done in ploughing, an equation was obtained. By knowing the initial kinetic energy, keel width of the iceberg, the slope of the seabed and its average shear strength an estimation of the maximum scour depth can be obtained from this theory.

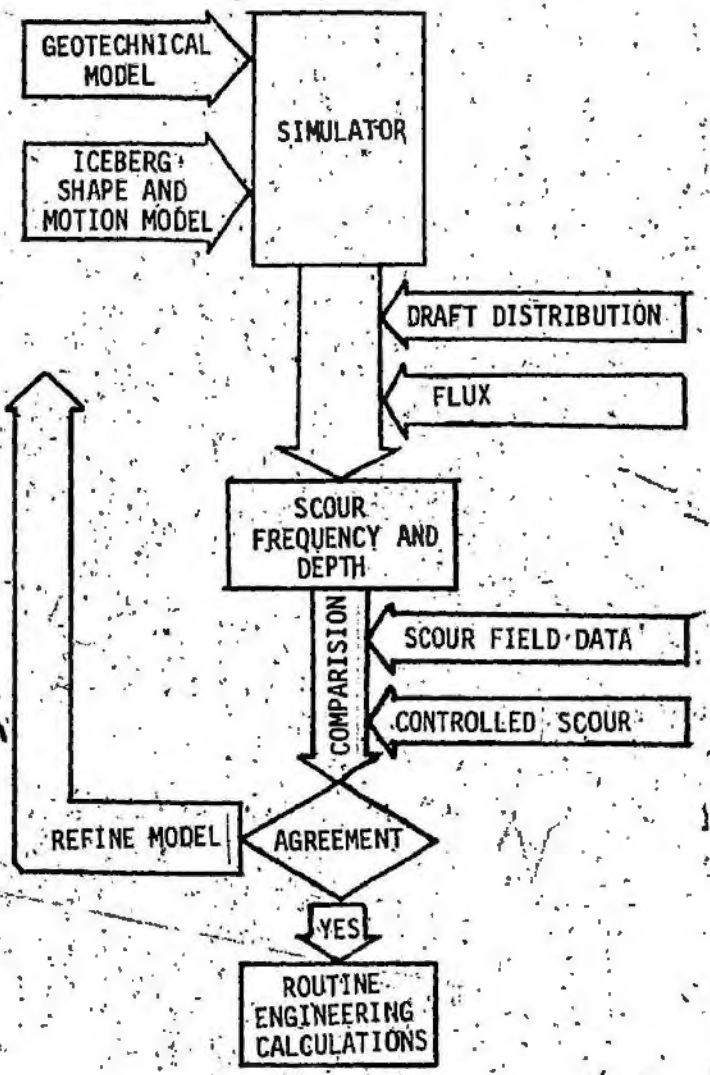

FIGURE 3 INTEGRATED APPROACH TO SCOUR PROBLEM (LEWIS AND BENEDICT 1981)

Refinements to this model have been made by considering the influence of surcharge on the total soil resistance (Chari 1975) and the effect of current drag on the scouring iceberg (Chari and Muthukrishnaiah 1978). Chari and Green (1981) examined the effect of side friction on the iceberg for scours in cohesionless soils.

Lopez et al (1981) formulated a differential equation for the velocity of a scouring iceberg by balancing the forces of inertia and current drag with the soil resistance in order to delineate the hydrodynamic drag effects in the estimation of maximum scour depths. However, for analytical convenience; the soil resistance and the soil model were approximated in this formulation.

Foundation Engineering Company of Canada (FENCO) developed a variety of models for the Arctic Petroleum Operators Association (APOA 69-1, 1975) for different types of ice scours. These models can be classified into two broad categories; estimation of the scour depths due to ice ridges in the shallow water region of the Beaufort Sea and the estimation of scour depths due to large sized ice blocks such as ice islands and icebergs.

The first model designated by FENCO as the Dynamical Solution is a generalized model and can take into account the influence of the initial kinetic energy and environmental forces such as winds, waves, currents, and pack

ice forces on the scouring potential of the ice mass. The ice mass is a rectangular prism floating in water with three degrees of freedom, surge, heave, and pitch. Three equations of motion using three equilibrium equations were formulated considering inertial forces due to motion and hydrodynamic forces, gravity, buoyancy and soil resistance under the influence of the driving forces. From the known initial conditions, these equations were solved using the 4th order Runge-Kutta method. The soil resistance consists of the frontal passive earth pressure, base reaction and the side friction. The base reaction was calculated using elastic, plastic and elasto-plastic methods. Results presented were restricted to Beaufort Sea conditions. This analysis shows that the scour track is very much undulated in contradiction to smooth variations observed in scour surveys. Selection of a proper soil model in determining the base reaction seems to be crucial in obtaining numerical stability of the solution.

The energy solution presented in the APOA report 69-1 (1975) is very similar to that of Chari and Allen (1972). The only minor differences are the inclusion of the side friction of the soil, and the method of determination of the frontal resistance. The sum of external forces due to wind, wave, current and pack ice was equated separately to the total soil resistance of the soil at the end of the scour.

It was concluded that for the Beaufort Sea conditions, the influence of pack ice force predominates and is much larger than the effect of kinetic energy. A good agreement between the results of the energy model and that of the dynamic model was reported for Beaufort Sea conditions. However, none of these models have been verified experimentally.

2.8 Experimental Studies and Physical Models

As mentioned earlier, the basic mechanism in iceberg scouring is the dissipation of the kinetic energy in doing work against the soil resistance and according to well established principles of conservation of energy. However, there are several practical difficulties in physically modelling the phenomenon to laboratory scale. One major problem is to scale the soil strength and other related properties. It has been argued (Chari 1980) that the energy balance needs no physical verification and the only experimental verification required would be for the geotechnical aspect of the analytical model.

Chari (1975) designed a tiltable glass sided tank 3.6 m long, 0.75 m wide and 0.7 m deep to prepare 1:10 slopes of silty clay. Several experiments were conducted using 230 mm wide plexiglass prismatic models. Significant qualitative observations were also made in this study

regarding the failure phenomena of soil and other geotechnical aspects of interest which formed the basis for subsequent and also current investigations. Quantitative measurements included the measurement of the total force necessary to push iceberg models of three different shapes into the sloping bed, the pressure distributions on all the faces of rectangular prismatic models and also at some locations in the soil bed. The influence of velocity of the iceberg on the total soil resistance was examined and found to be negligible. The measured soil resistance was correlated with the calculated static passive soil resistance using Coulomb's trial wedge analysis and correlated with the theoretical scour model.

The Arctic Petroleum Operators Association (APOA) commissioned a project in 1980 on the experimental study of iceberg scours (Abdelnour and Lapp 1980). A total of 110 experiments were conducted using two rectangular prismatic models (widths 520 mm and 260 mm) and an inverted square pyramid with a cone angle of 54 °. These models were pushed at three velocities into saturated flat beds of sand, silt and clay with three different depths. Data on soil resistance in both vertical and horizontal directions of motion, pressure distribution on the model front face and also in the soil, and the shape characteristics of the scour profile were collected. The results were presented in the

dimensionless form proposed by Schuring and Emori (1964). Contrary to the generally accepted theories in geotechnical engineering, it was suggested by Abdelhour and Lapp (1980) that the velocity of the iceberg has an influence on the total soil resistance even in cohesionless soils.

Green (1984) conducted experiments in a 14 m x 3 m x 1 m soil tank with dry sand. Based on the measurements of total soil resistance in the direction of motion and the pressure distributions on the front and sides of a 500 mm wide rectangular prismatic model, it was concluded that the contribution of side friction and base friction to the total soil resistance was negligible. It was also reported that the influence of the iceberg velocity was negligible and the total resistance was proportional to model width. The importance of iceberg keel shape in determining the total soil resistance was demonstrated and further testing with different keel shapes was recommended. Tests were also conducted with a pipeline model of 122 mm diameter. The model was instrumented with pressure transducers and burried at several depths in the sand bed below the maximum scour in order to delineate the zone of sediment movement below the scouring berg.

2.9- Geotechnical Models for Soil-Iceberg Interaction

The purpose of the physical models in iceberg scour studies is to understand the soil-iceberg interaction. The effect of the keel shape is one of the parameters identified in previous investigations. This will be examined further in the experimental work and discussed in Chapter V. Although there are several good publications in the geotechnical literature on passive soil pressure, most of these are for cases of relatively small wall movements and for vertical or nearly vertical surfaces. The geotechnical research topic nearest to the phenomenon of iceberg scours is the movement of bulldozer blades in soils. Even here, there are several differences, such as the sloping soil surface, the large amount of soil surcharge in front of an iceberg, and the three dimensional shape of the berg. Nevertheless, all the relevant and available theoretical methods will be used in analyzing the experimental data. The simple theoretical methods suggested by Coulomb (1776), Terzaghi (1943), Shields and Tolunay (1973), Rosenfarb and Chen (1973), and Harison (1973) are reviewed below.

The limit equilibrium solution of Coulomb assumes a shear plane inside the soil starting from the toe of the retaining wall. By considering horizontal and vertical forces on the wedge (Fig. 4) the force on the wall can be computed. The critical failure plane is that which requires

a minimum horizontal force. The assumption of plane shear surface is not a generalized condition. A large error is associated with the Coulomb's method when the angle of wall friction is greater than one third the angle of internal friction for the soil (Terzaghi 1943). In such cases, a curved surface of failure is to be considered.

The sliding surface can be assumed as a logarithmic spiral (Terzaghi and Peck 1967). In the logarithmic spiral method, (Fig. 5), the spiral starting at the toe smoothly joins the Rankine's failure surface which is inclined at an angle of $45° - \phi/2$ to a major principal stress direction. Within the mass of the soil represented by ad_1c_1 the state of stress is the same as that in a semi-infinite deposit in a general passive Rankine state. The shearing stresses in this zone on planes bisecting the failure planes are zero. Therefore, the passive earth pressure on the plane f_1d_1 can be calculated from the simple Rankine's solution. By the nature of the assumed failure surface, the resultant of the soil resistance F on the portion bd_1 of the failure surface passes through the center of logarithmic spiral. The entire process is to be repeated many times by varying the position of the center of the logarithmic spiral on the line d_1a and its extension. The failure surface which gives the minimum computed resistance is considered as the critical failure surface.

Shields and Tolunay (1973) suggested a procedure to calculate the passive earth pressure coefficients which is similar to the logarithmic spiral method. However, there is no need to search a failure surface in this method. From a knowledge of the stress conditions at the soil-wall interface, the angle of the tangent to failure surface α_w at the toe of the wall can be determined which then gives a specific location for the center of the spiral and hence the entire failure surface. The soil mass to be analyzed is bounded by the vertical wall, the spiral, and the principal plane, which is a vertical passing through the intersection of the logarithmic spiral and Rankine's failure plane. From Mohr's circle of stress at the bottom of the wall, the angle of failure surface α_w was calculated to be:

$$\alpha_w = \frac{1}{2}\left[\text{arc. cos}\left|\cos(\phi' - \delta) - \frac{\sin(\phi' - \delta)}{\tan\phi'}\right| - \phi' - \delta\right] \quad [1]$$

where α_w is the angle between failure surface and the normal to the wall as shown in Fig. 6. The mass to be analyzed was divided into vertical slices and the horizontal and vertical equilibrium of each slice was satisfied. In doing so, it was assumed that all vertical shear force in the zone was concentrated in the slice next to the wall.

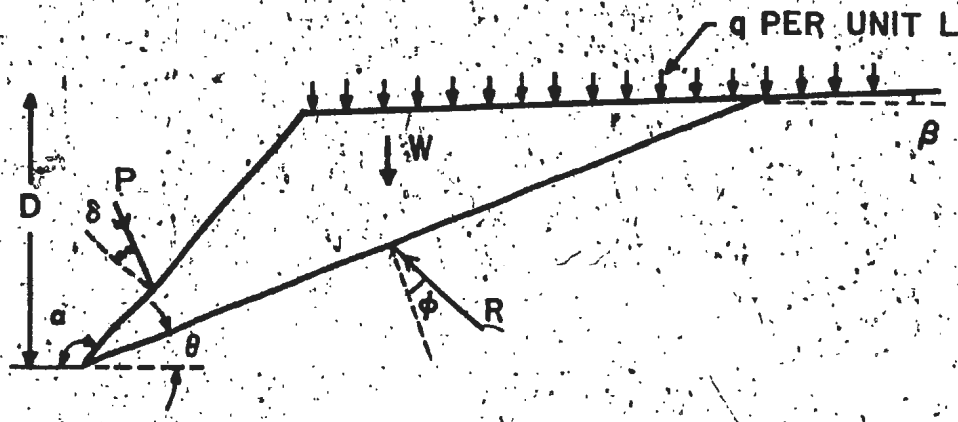

FIGURE 4 COULOMB'S FAILURE WEDGE FOR PASSIVE CONDITION

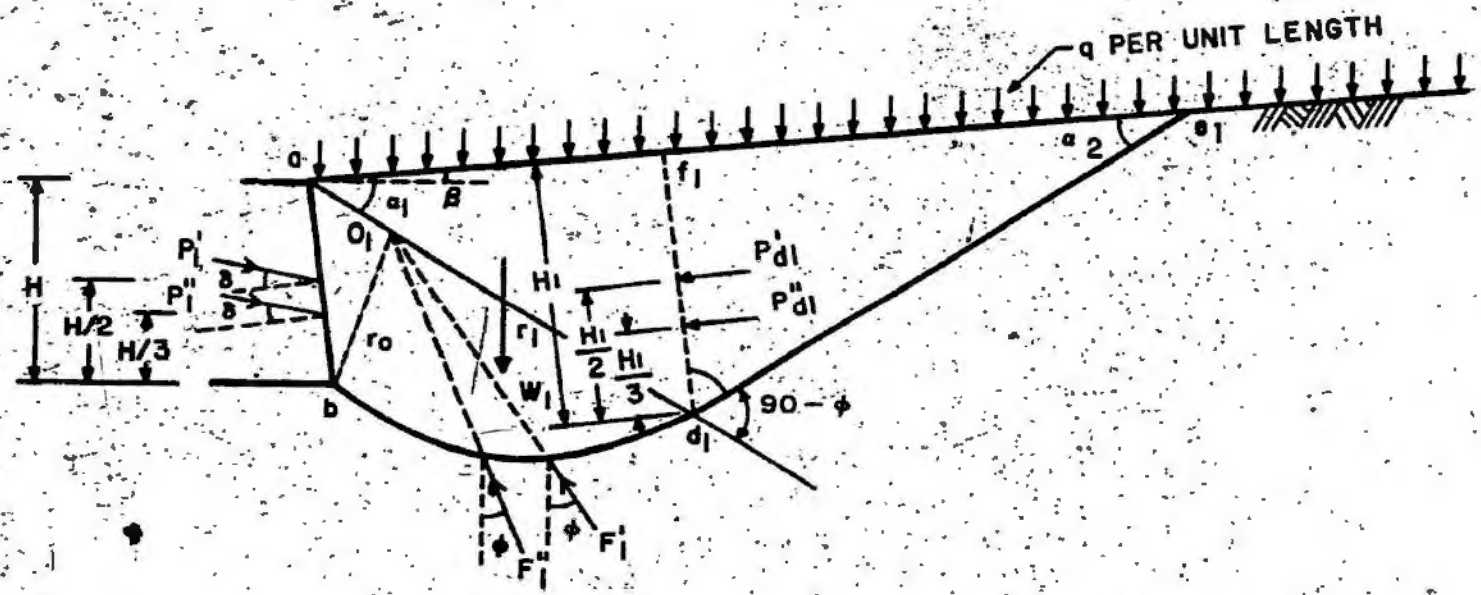

FIGURE 5. LOGARITHMIC SPIRAL FAILURE SURFACE. (TERZAGHI AND PECK 1967)

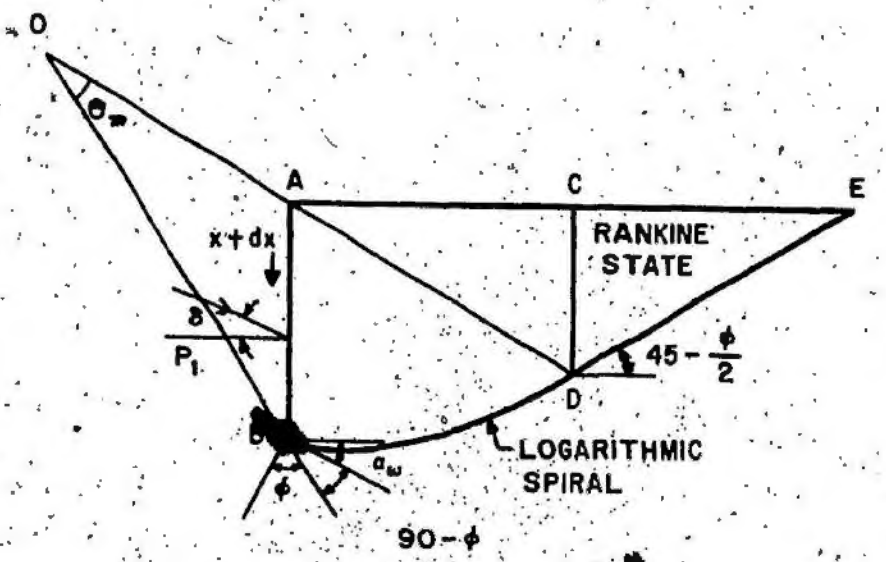

FIGURE 6 FAILURE SURFACE PROPOSED BY SHIELDS AND TOLUNAY (1973)

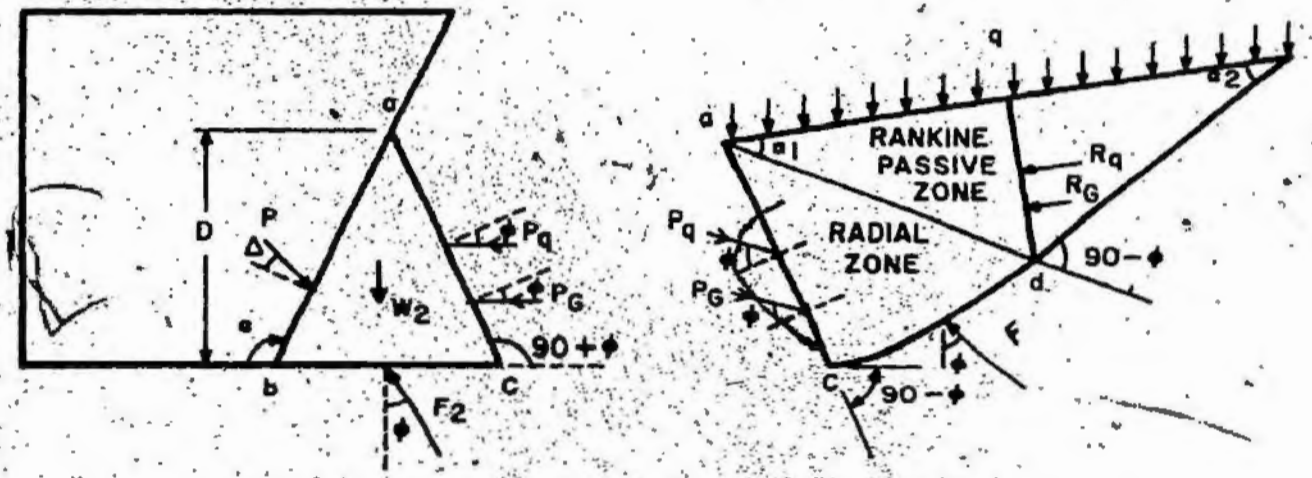

FIGURE 7 FAILURE MECHANISM PROPOSED BY HARRISON (1973)

Harrison (1973) proposed a method to analyze the ultimate load capacity of an inclined rigid interface linearly translating into a soil in a specific direction. Harrison (1973) developed this method basically to analyze the plate grouser problem in agricultural engineering. This method is similar to the Shields and Tolunay (1973) method in the sense that there is no need to locate a failure surface. Shields and Tolunay (1973) assumed that the full angle of friction was mobilized at the moving wall which is justified when large displacements are allowed. The compatible failure surface is determined using Mohr's diagram. Harison (1973) assumed that the direction of the failure surface coincides with the direction of translation of the wall, and the mobilized friction angle would be restricted to maximum soil-structure contact friction. Evidence for this assumption was shown by photographing the failure phenomena when inclined plates were pushed horizontally into the soil. The failure mechanism according to this theory is shown in Fig. (7). The equilibrium wedge abc which forms on the interface ab must move horizontally along with the model and ac becomes the failure plane making the required angles $(90+\phi)$ with the extension of the line bc. The interface ac is treated as a perfectly rough retaining wall and the earth pressure is calculated using the logarithmic spiral method. The pole of the spiral is located at a; ad and ac are the

radii of the spiral. The resultant force thus calculated was used to compute the earth force on the model when the horizontal and vertical equilibrium of the wedge abc were satisfied.

Chen and Rosenfarb (1973) used the upper bound technique of limit analysis to obtain passive limit earth pressures. They followed the method of superposition which states that if a failure mechanism is described by n independent parameters, the passive pressure acting on the rigid wall can be expressed as:

$$P = \frac{1}{2}\gamma H^2 \min K_{p\gamma}(\theta_1, \theta_2 - - - \theta_n) + qH \min K_{pq}(\theta_1, \theta_2 - - - \theta_n) + CH \min K_{pc}(\theta_1, \theta_2 - - - \theta_n) \quad [2]$$

where $K_{p\gamma}$, K_{pq} and K_{pc} are pure numbers representing the effects of weight, surcharge and cohesion respectively. For cohesionless soils the third term is neglected. Closed form expression for earth pressure coefficients can be derived using upper bound technique of limit analysis method in terms of soil parameters and independent parameters of the failure mechanism. When these expressions are minimized with respect to parameters $(\theta_1, \theta_2 - - - \theta_n)$ and used in the above equation, the passive earth resistance P per meter length of the wall can be obtained. Several failure mechanisms

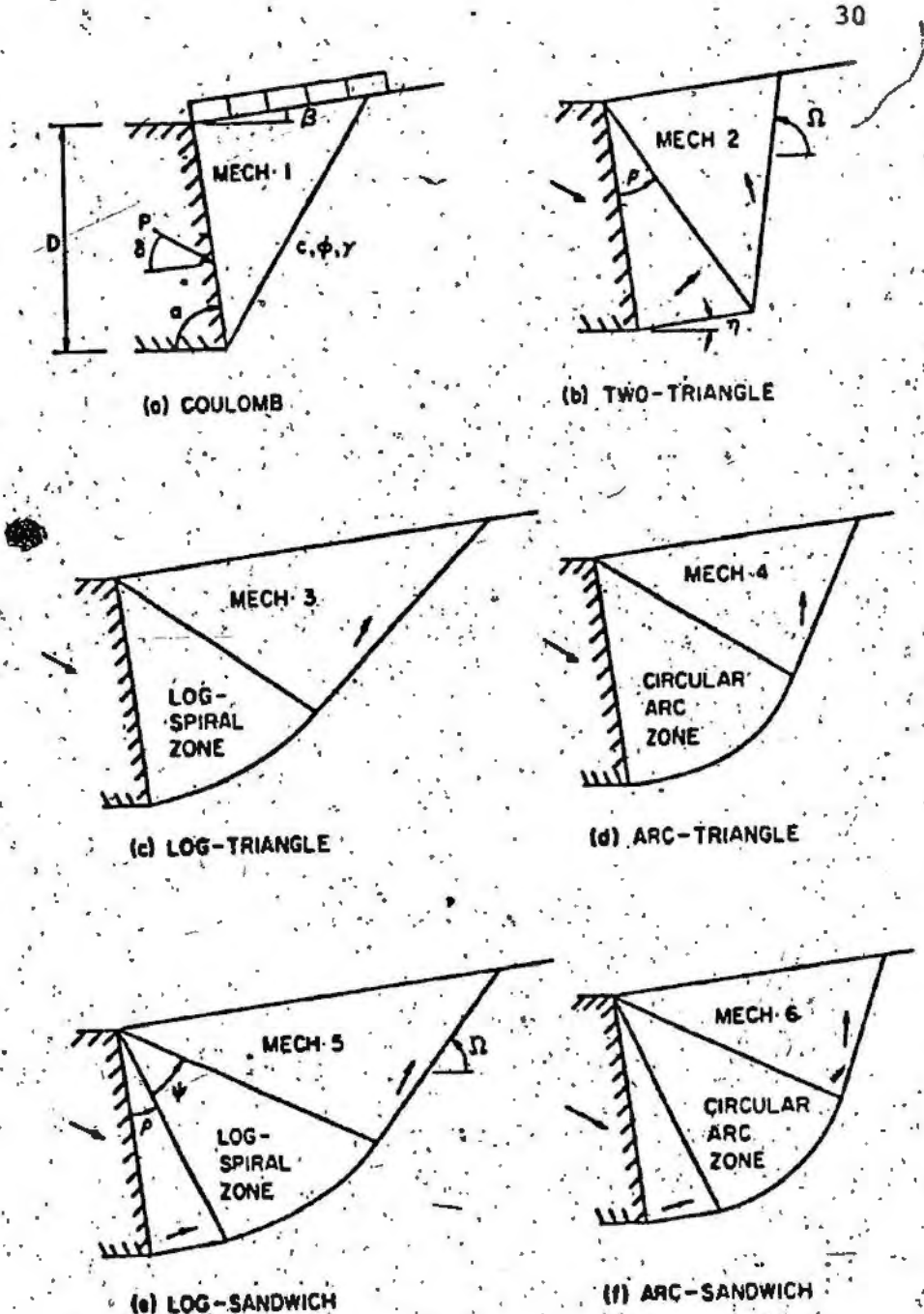

FIGURE 8 FAILURE MECHANISMS CONSIDERED BY CHEN AND ROSENFARB (1973)

TABLE 3. PASSIVE PRESSURE COEFFICIENTS K_{PY} (β=0) FOR VARIOUS FAILURE MECHANISMS

(CHEN AND ROSENFARB 1973)

		Mechanism						Sokolovskii
ϕ	δ	(1)	(2)	(3)	(4)	(5)	(6)	
10	0	1.36	1.36	1.52	1.47	1.36	1.36	1.34
	5	1.45	1.46	1.53	1.50	1.45	1.45	1.46
	10	1.55	1.54	1.54	1.54	1.54	1.54	1.53
20	0	1.75	1.75	2.31	2.01	1.75	1.75	1.71
	10	2.08	2.08	2.36	2.18	2.08	2.08	2.08
	20	2.49	2.44	2.46	2.47	2.44	2.47	2.42
30	0	2.27	2.28	3.86	2.75	2.28	2.30	2.16
	15	3.16	3.16	4.06	3.36	3.16	3.18	3.16
	30	4.76	4.43	4.50	4.76	4.41	4.76	4.30
40	0	3.02	3.02	7.76	3.52	3.02	3.27	2.84
	20	5.34	5.32	8.33	5.39	5.31	5.89	5.32
	40	12.80	10.00	10.10	15.50	9.88	—	9.32
10	0	1.42	1.42	1.68	1.60	1.42	1.42	1.42
	5	1.57	1.56	1.69	1.63	1.56	1.56	1.56
	10	1.73	1.68	1.71	1.68	1.68	1.67	1.66
20	0	2.04	2.04	3.07	2.60	2.04	2.04	2.04
	10	2.64	2.58	3.12	2.82	2.58	2.61	2.55
	20	3.53	3.18	3.27	3.19	3.17	3.19	3.04

Continued on next page...

TABLE 3 PASSIVE PRESSURE COEFFICIENTS $K_{p\gamma}$ (β=0) FOR VARIOUS FAILURE MECHANISMS

(CHEN AND ROSENFARB 1973)

		Mechanism						Sokolovskii
ϕ	δ	(1)	(2)	(3)	(4)	(5)	(6)	
30	0	3.00	3.00	6.38	4.80	3.00	3.01	3.00
	15	4.98	4.71	6.61	5.88	4.71	4.97	4.62
	30	10.10	7.24	7.37	8.31	7.10	8.31	6.55
40	0	4.60	4.61	16.10	15.40	4.50	4.67	4.60
	20	11.80	10.10	17.70	23.60	10.10	12.50	9.69
	40	92.60	22.70	21.70	67.90	20.90	--	18.20
10	0	1.76	1.74	3.10	2.06	1.74	1.74	1.75
	5	1.90	1.83	3.12	1.97	1.96	1.96	1.95
	10	2.04	1.91	2.77	1.90	2.16	2.14	2.10
20	0	2.98	2.91	6.41	4.03	2.91	2.93	2.90
	10	3.78	3.38	6.50	3.85	3.91	3.94	3.80
	20	4.81	3.92	5.22	3.79	5.04	4.95	4.62
30	0	5.34	5.09	15.60	10.20	5.08	5.33	5.06
	15	9.22	6.99	16.10	10.10	8.93	10.20	8.45
	30	72.70	10.10	11.70	11.50	14.40	17.60	12.30
40	0	10.70	9.73	50.30	127.00	9.71	11.40	9.56
	20	89.70	17.60	53.50	141.00	25.50	69.40	22.40
	40	77.40	--	34.90	298.00	56.60	--	44.70

composed of rigid bodies and radial shearing zones were considered. The mechanisms considered by Chen and Rosenfarb (1973) and the variation of the results obtained there are given in Fig. 8 and Table 3. It was concluded that the two-triangle mechanism and log-sandwich mechanism gave better results and also had a limited number a parameters to be minimized.

2.10 Objectives of the Present Investigation

From the literature review, it may be concluded that the energy model is quite simple and offers good correlation with other models. The model assumes that the scour formation is gradual, starting from an initial touch down by the iceberg. It has been reported (Lewis and Barrie 1981) that several pock mark features have been observed in the region of iceberg scours. It has also been shown (Bass and Peters 1984) that the draft of an iceberg could increase as a result of rolling. It is possible that such bergs could pierce the seabed if the water depths were less than the increased draft and cause a local depression on the seafloor. As an extension of the theoretical model of Chari (1979) it was decided to examine the effect of an initial seabed penetration by a rolling iceberg and the resulting shape of the scour track. As part of such a theoretical study, it was

also decided to evaluate the nonlinearity effects of the current drag on a decelerating iceberg during scouring. This part of the study is an extension to that done by Lopez et al (1981).

It has been shown earlier (Chari 1975, Green 1984) that the frontal shape of the iceberg model has an effect on the measured forces. However, the results have not been quantified. As part of this investigation, the experimental study consists of quantifying the influence of the frontal shape of the iceberg on the total soil resistance and hence the computed scour size. The tasks in this investigation can be stated as:

1. To modify the analytical model for estimating the maximum scour depth using the principles of conservation of energy (Chari 1979) and considering the nonlinear velocity of the scouring iceberg (Lopez et al 1981) to account for hydrodynamic drag forces during scouring.
2. To extend the analytical model to compute the scouring potential of an iceberg which penetrates the seabed dus to instability (Bass and Peters 1984).
3. To experimentally verify the effect of the frontal shape of the keel on the soil resistance by horizontally pushing six different shapes into a sloping bed of sand and measuring the total soil resistance and pressure distribution on the front face along the length of scour.

4. To correlate the measured front face soil resistance with computed soil resistance from available theoretical methods.
5. To incorporate the effect of the iceberg keel shape in the analytical model.

CHAPTER III

ANALYTICAL STUDY

3.1 General

The analytical model for iceberg scouring published in the literature is that of Chari (1979) in which the seabed is assumed to be a weak cohesive sediment and the scour depth is obtained using the principle of energy balance. This model will be examined further in this chapter and will be extended to include the effect of nonlinearity of the iceberg deceleration, the presence of frictional soils, and the effect of initial seabed penetration by an iceberg before scouring.

3.2 Mechanics of Scouring

The drift of an iceberg, particularly those with large drafts, is primarily due to ocean currents. Under steady-state conditions, the drift velocity can be taken as the velocity of the current averaged over the draft of the iceberg. There is no net hydrodynamic drag under such steady-state conditions. For purposes of analysis, iceberg scouring may be visualized as one of the variations or combinations shown in Fig. 9. In the first case, the bottom of the iceberg touches the seabed and rides along a hard

surface, grounding in a short distance due to the transformation of kinetic energy into potential energy. No visible scour marks are likely to be left on the seabed in this process. In the second mode, which represents another extreme condition, the iceberg comes in contact with very weak seabed soil and scours the seabed through a horizontal ploughing action. A long and deep scour mark is likely to be left on the sea floor. The third mode shown in Fig. 9c is a combination of the above two modes in which the iceberg forms a scour track and is also subjected to an uplift.

Icebergs are known to become extremely unstable due to the process of continuous melting and frequent breaking of portions of the iceberg. It is very common for icebergs to rotate due to this instability and to assume a new position of equilibrium with a different draft. It has been suggested by Bass and Peters (1984) that iceberg drafts could increase by as much as 50% when they roll and reorient to a more stable position. During such a process, it is possible that the iceberg could penetrate the seabed and then cause a long scour (Fig. 9d). This phenomenon, which was not considered in previous research, is now examined and discussed in this thesis.

3.3 Iceberg Scour Model

When an iceberg scours into a gentle slope, the soil scooped out will initially pile up in front of the iceberg. As the scouring continues, ridges will be formed on either side of the track. The idealized concept of iceberg scouring (Chari 1979) is shown in Fig. 10, in which it is assumed that the friction between the iceberg and the soil can be neglected because of the low strength of soil and the presence of a thin film of melt water around the iceberg. Thus the resistance to iceberg movement is primarily the frontal resistance on the scouring face. For icebergs scouring in soft and weak seabed sediments, the energy of the iceberg was equated to the work done by soil resistance in ploughing action and the resulting equation of energy balance was expressed (Chari 1979) in the form:

$$\frac{1}{2} MV_o^2 + \int_0^L F_d \, dl = \int_0^L P \, dl \qquad [3]$$

where:

M = mass of the iceberg

V_o = initial steady-state velocity of the iceberg (also velocity of currents)

F_d = drag force on a decelerating iceberg

l = length of scour at any instant

L = maximum length of scour

P = soil resistance on the front face of idealized berg

For cohesive soils, the soil resistance P at any instant can be expressed as:

$$P = \frac{\gamma' (h+d)^2 B}{2} + 2\, cdB + \sqrt{2}\, cd^2 \qquad [4]$$

where:

γ' = submerged unit weight of soil

h = height of surcharged soil at any instant during scouring (obtained from geometry of scour trench)

d = depth of scour at any instant

B = width of idealized iceberg

c = shear strength of cohesive soil

The soil shear strength c varies over a wide range for terrestrial soils and the variation is even greater for sea floor soils. Published data of shear strength for marine soils (Andersen 1976) show a range of values from nearly zero up to about 500 kPa in the 5 m depth zone below the mudline. At the Hibernia site and its vicinity, the surficial sediments are medium dense to dense sand and a shear strength in the range of 100 kPa has been genetally used (Russell and Muggeridge 1981) as the typical value for purposes of computations. A range of 25 - 100 kPa for shear strength of the seabed has been used in this thesis.

On the left side of Eq. [3], the first term is the steady-state kinetic energy of the iceberg when it is moving without any relative velocity between the ocean currents and

the scouring iceberg. The second term of Eq. [3] represents the energy due to the effect of the currents on the iceberg during the scouring process. The drag force on a decelerating iceberg can be expressed as:

$$F_d = \frac{1}{2} C_d \rho A |V_o - V| (V_o - V) \qquad [5]$$

where:

C_d = drag coefficient

ρ = density of water

A = projected area of the submerged iceberg normal to the propelling current

V = instantaneous velocity of iceberg

and the other terms as already defined.

In the above expression, the coefficient C_d can vary from 0.5 to 2.0 depending on the shape of the floating body (Bureau Veritas 1975) and for bodies in contact with the seabed, C_d may be multiplied by 1.4. Banke and Smith (1974) measured drag coefficients of 1.2 during actual towing of small icebergs. Mountain (1980) has used a drag coefficient of 1.5 for icebergs of all sizes and shapes. Shirasawa et al (1984) measured drag coefficients varying from 0.63 to 0.91 in laboratory models. If a drag coefficient of 1.0 is assumed as a typical value for purposes of discussion, the corresponding kinetic energy due to the added mass component will be in the order of 4.5 (Prasad and Chari 1984). The

consequent influence due to the effect of this added mass on the scour depth computation is negligible and hence not identified separately in Eq. [5].

From Eqs. [3], [4], and [5], the maximum scour depth and length in cohesive soils has been expressed as:

$$\frac{MV_o^2}{2} + \frac{C_d \rho A L V_o^2}{6} = \frac{\gamma'(H+D)^2 BL}{6} + cDLB + \frac{\sqrt{2}}{3} cD^2 B \qquad [6]$$

$$D = L \tan \beta \qquad [7]$$

where:

D = maximum scour depth corresponding to maximum scour length L

β = slope angle of the seabed

and the other terms as already defined.

The above equations were derived on the assumption that the iceberg velocity decreases linearly from a maximum of V_o at the commencement of scouring and theoretical curves of maximum scour depth were developed (Chari 1979). A parametric analysis of the effect of different variables was presented by Chari and Peters (1981). Equation [6] will be examined further in the following sections.

3.4 Iceberg Velocity During Deceleration

Lopez et al (1981) examined the hydrodynamic drag on decelerating icebergs during grounding and concluded that the effect is an important component in the propulsion of

icebergs during scouring and in computing the maximum scour depths. It was also concluded that the gouge length would be overestimated by 11% at worst, by assuming a linear velocity during deceleration. The conclusions are valid for the simplified soil model assumed by Lopez et al (1981) in which the soil resistance was assumed to be directly proportional to the square of the depth. It may be seen from Eq. [6] that several factors such as the density, soil strength, depth of penetration, and seabed slope influence the soil resistance. The effect of these factors are to be taken into consideration in calculating the soil resistance.

The velocity variation of decelerating icebergs can be obtained numerically in incremental steps instead of considering a continuous function as done by Lopez et al (1981). The residual kinetic energy of the iceberg (E_{net}) at any instant may be obtained knowing the initial kinetic energy of the iceberg (KE), the cumulative energy expended in overcoming the soil resistance (E_s) and the cumulative energy added due to the hydrodynamic drag (E_{drg}). This can be expressed as:

$$E_{net} = KE - E_s + E_{drg} \qquad [8]$$

$$\frac{MV^2}{2} = \frac{MV_o^2}{2} - \int_o^{\ell} P \, d\ell + \int_o^{\ell} \frac{C_d \rho A |V_o - V| (V_o - V)}{2} d\ell \qquad [9]$$

Equation [9] can be solved in steps till the velocity V is nearly zero indicating that the iceberg has

come to rest and the gouging process has been completed. Figure 11 is the flow chart for the computer programme (Appendix A). The velocity profile obtained from this iceberg motion as given by Eqs. [3] and [8] is a better representation than the assumption of a linear velocity variation. For the purpose of the parametric analysis, ranges of values were assumed as shown in Table 4 and the results are discussed below.

Figure 12 shows the velocity variation for an iceberg of 10 x 10^9 kg (10 million tons) during grounding as obtained using Eq. [8] and [9]. The cumulative energy driving the iceberg into the soil, the work done by the soil resistance, and the convergence of these two at the end of the scour are also shown in the figure. It is obvious that the computed velocity profile deviates from the straight line. The estimates of scour length using the nonlinear velocity profile are greater by about 12% for the values of the parameters shown in Fig. 12.

The velocity profile and the drag force were computed for a typical 10 x 10^9 kg (10 million ton) iceberg for different drag coefficients and the results are shown in Fig. 13. The nonlinearity in the velocity variation is more pronounced for lower drag coefficients and the variation tends to be linear for higher drag coefficients. A similar effect noticed for the drag force is also shown in the figure.

Fig. 14 shows the effect of shear strength on the computed maximum scour depths. The maximum scour depth decreases with increasing shear strength which is to be expected and the results are similar to those published earlier (Chari and Peters 1981). However, the assumption of a linear profile for the velocity will result in an underestimation of the scour depth in the order of 11% for a 10×10^9 kg (10 million ton) iceberg.

A similar comparison for the effect of the varying seabed slope (Fig. 15) shows that the assumption of linear velocity would overestimate the scour depth for a steeper seabed and will underestimate the value in flatter slopes. The difference in the computed results would be about 23% at worst. It may be observed that the seabed slope has virtually no effect on the scour depth computations for larger icebergs when the nonlinear velocity variation is considered.

The analysis of the effect of the coefficient of drag (Fig. 16) on the scour depth computations shows that the calculated scour depths are more sensitive to the variation in the drag coefficient than previously reported by Chari and Peters (1981). It can be seen that the assumption of linear velocity variation results in an overestimation for lower drag coefficients and an underestimation at higher drag coefficients.

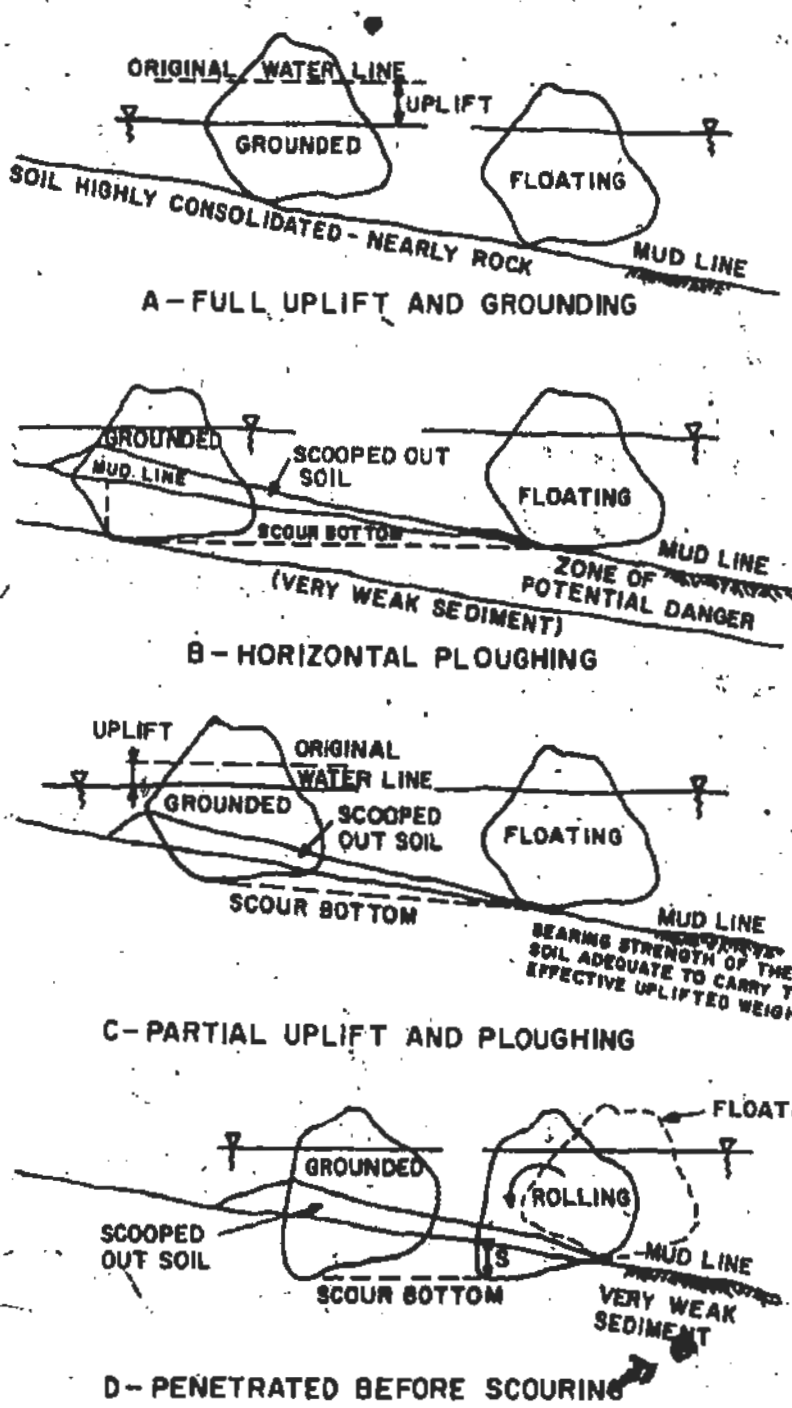

FIGURE 9 GENERALIZED CONCEPTS OF ICEBERG SCOUR

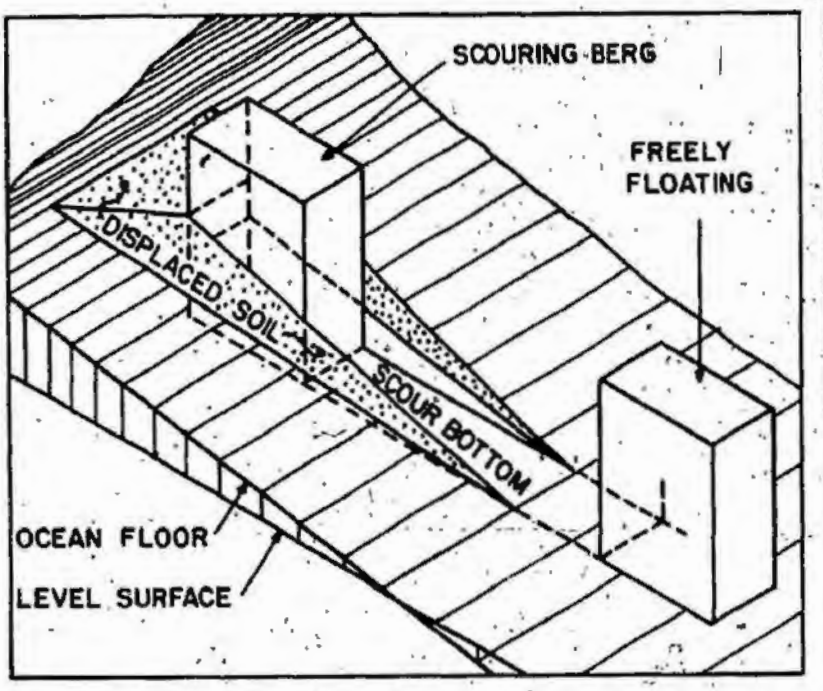

FIGURE 10 IDEALIZED THEORETICAL CONCEPT (CHARI 1979)

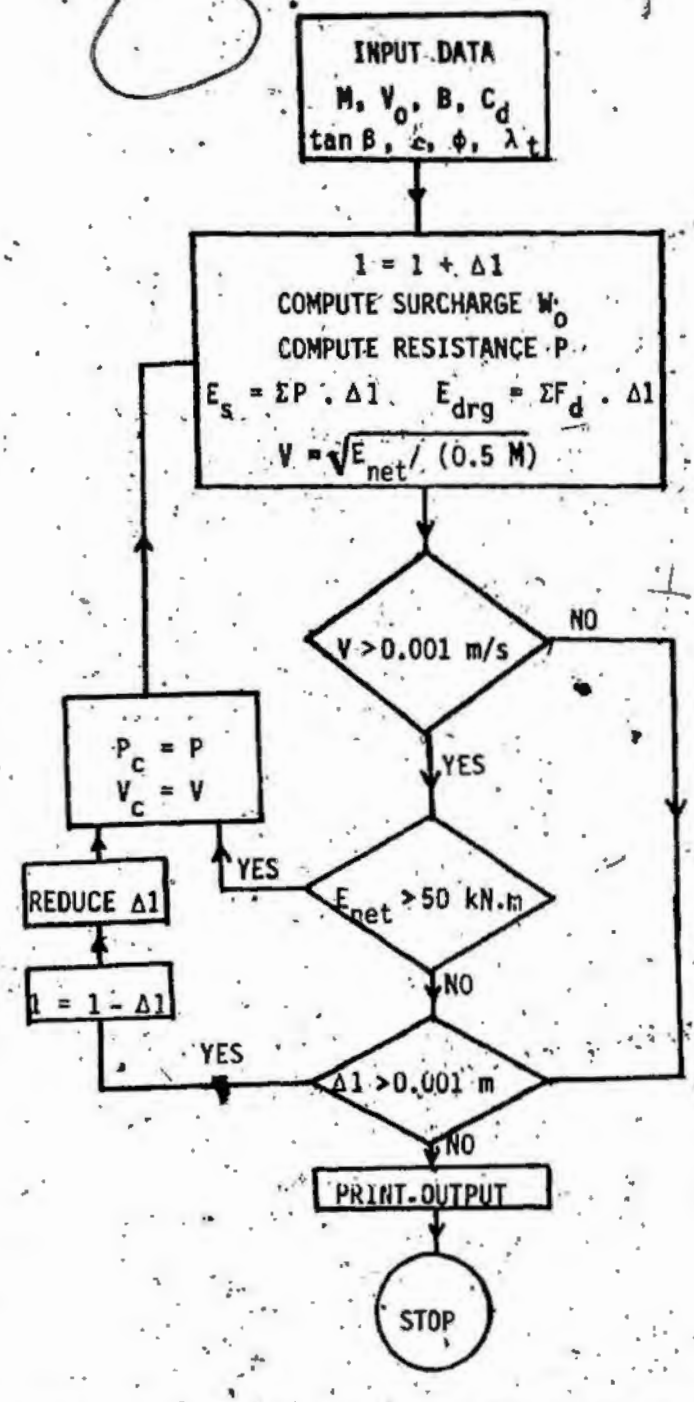

FIGURE 11 FLOW CHART FOR COMPUTING MAXIMUM SCOUR DEPTH

TABLE 4 RANGE OF PARAMETER VARIATION

PARAMETER	STANDARD REFERENCE VALUE	RANGE OF VARIATION
Iceberg Mass (M)	10×10^9 kg	$10^9 - 25 \times 10^9$ kg
Drift Velocity (V_o)	1.0 m/sec	0.2 - 1.0 m/sec
Keel Width (B)	20 m	10 - 30 m
Drag Coefficient (C_d)	1.0	0.5 - 2.0
Seabed Slope (Tan β)	1:500	1:100 - 1:1000
Soil Shear Strength (τ)	100 kPa	25 - 100 kPa
Angle of Internal Friction (ϕ)	--	20° - 40°
Unit Weight of Soil (γ_t)	15 kN/m^3	--

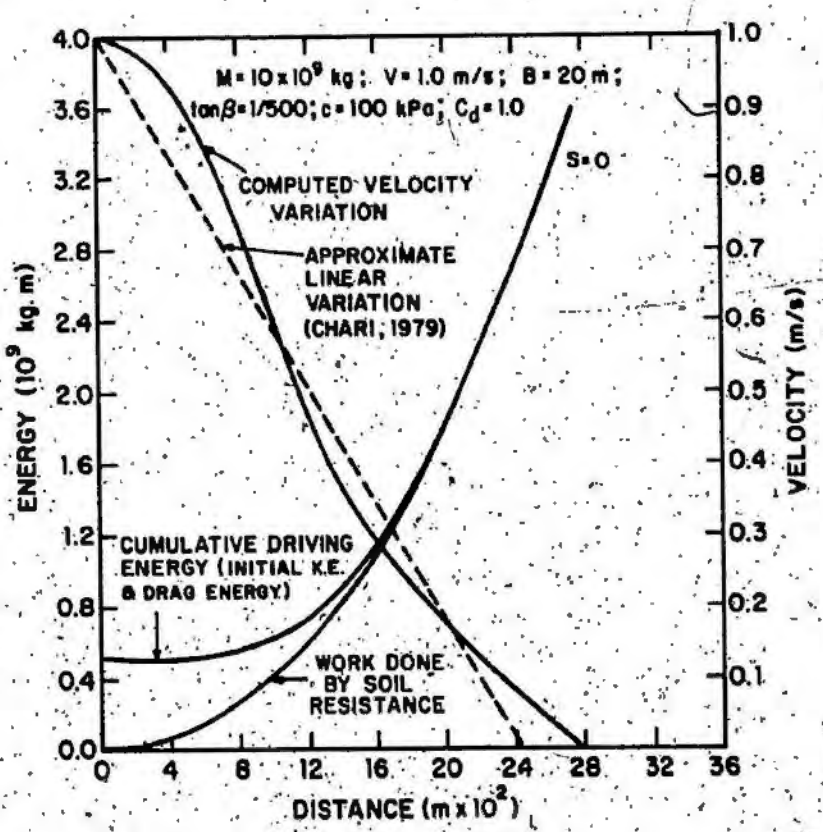

FIGURE 12 ENERGY AND VELOCITY VARIATION WITH SCOUR LENGTH

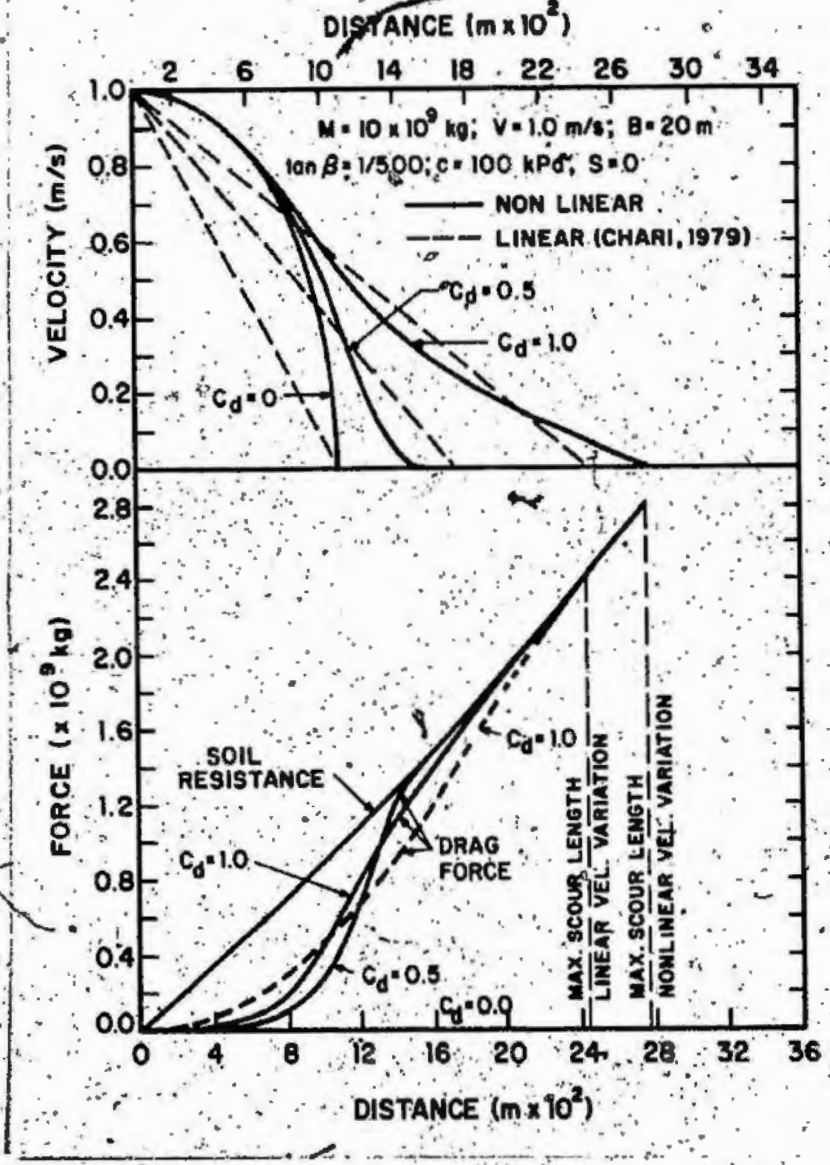

FIGURE 13 VARIATION OF VELOCITY AND DRAG FORCE WITH DRAG COEFFICIENT

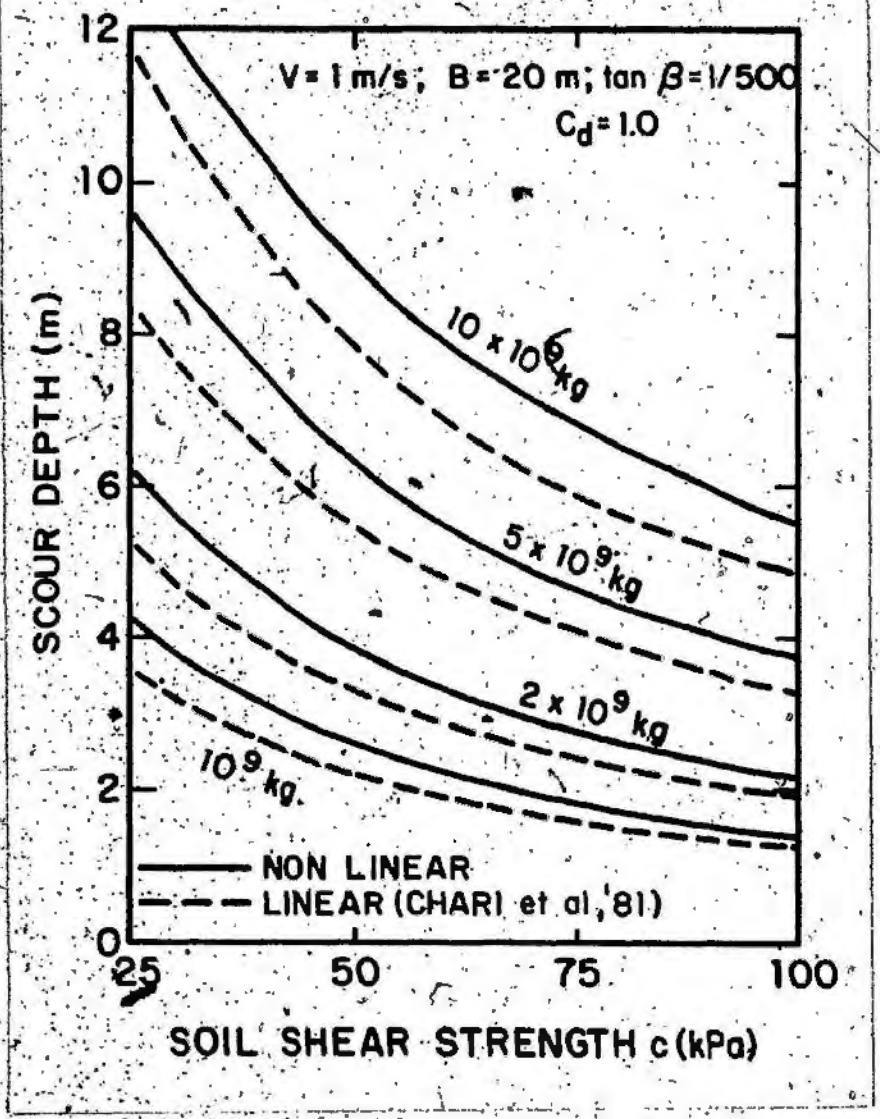

FIGURE 14 VARIATION OF SCOUR DEPTH WITH SOIL SHEAR STRENGTH

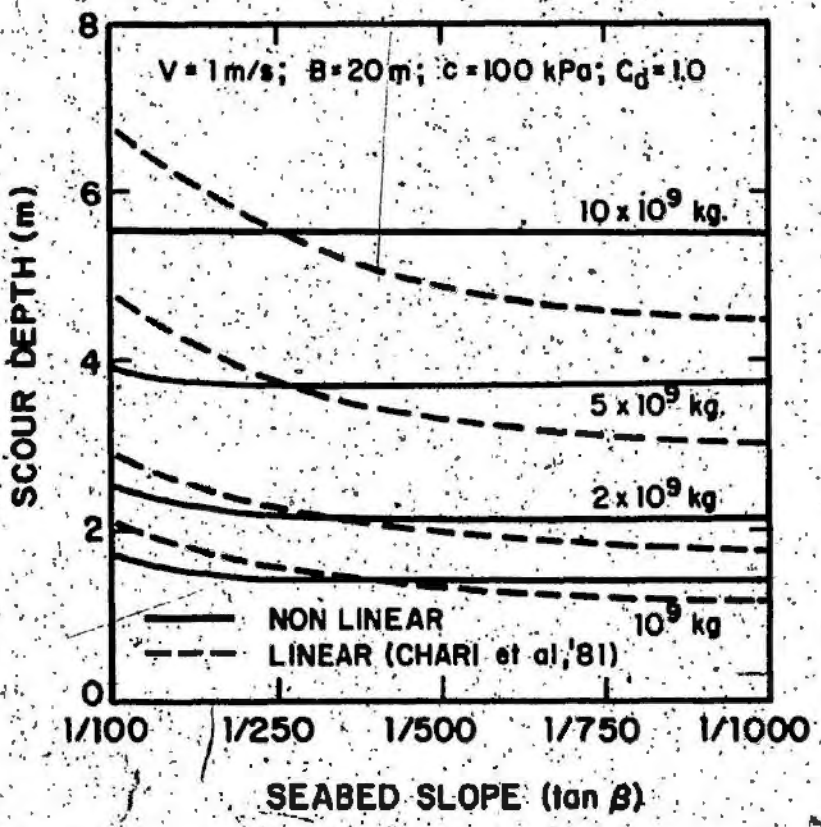

FIGURE 15 EFFECT OF SEABED SLOPE ON SCOUR DEPTH

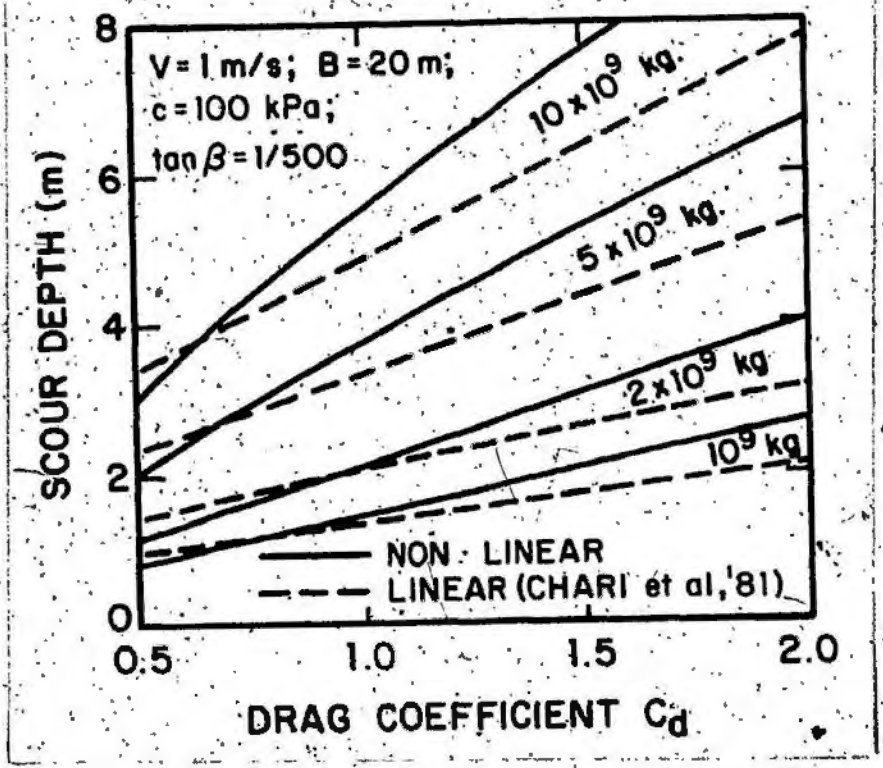

FIGURE 16 EFFECT OF DRAG COEFFICIENT ON SCOUR DEPTH

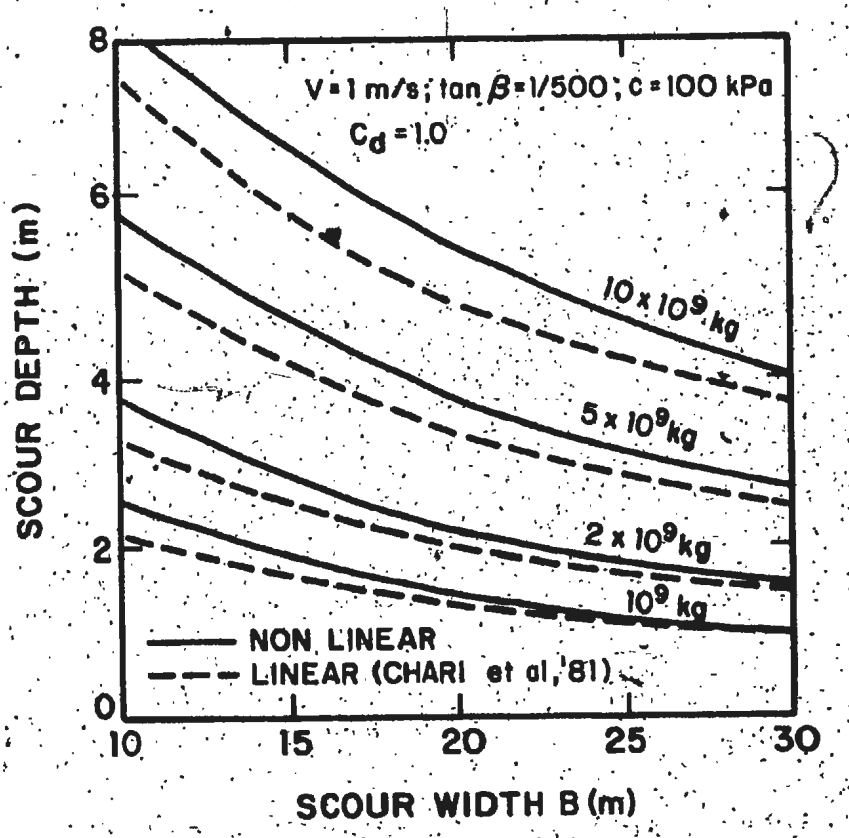

FIGURE 17 EFFECT OF SCOUR WIDTH ON SCOUR DEPTH

A similar comparison is made in Fig. 17 for the effect of varying scour width on the sensitivity of gouge depth computations. The extended model gives scour depths which are up to 16% higher than earlier computations. It is thus concluded that while the assumption of a linear velocity variation during scouring is a good first approximation, the true velocity profile is nonlinear. The actual deviation in the computation of scour depth is dependent on the combination of the other environmental variables.

3.5 Effect of Soil Type

Generally, surficial seabed sediments are cohesive and underconsolidated and the first attempt in modelling iceberg scours was for such soils. However, the surficial sediments are not universally the same. For example, in the Grand Banks region where the Hibernia oil field is situated the seabed is made up of predominantly sand and gravel. For a general soil with cohesion and friction, the soil resistance P as given by Eq. [4] has to be modified by considering Coulomb's trial wedge (Fig. 18). The force P can be expresses as:

$$P = \frac{(W_o + W)\sin(\theta + \phi) + (F + 2F')\cos\phi}{\cos(\delta + \phi + \theta)} \cos\delta \quad [10]$$

where:

W_o = weight of surcharge at any instant

$$W = \gamma' B \frac{1}{2} \frac{d^2 \cos\beta \cos\theta}{\sin(\theta - \beta)}$$

F = shear resistance on the bottom of wedge

$$= \frac{B\, d \cos\beta}{\sin(\theta - \beta)}\, c$$

F' = shear resistance on each side of the wedge (negligible for icebergs of larger widths)

$$= \left[\frac{1}{2} d^2 \frac{\cos\beta \cos\theta}{\sin(\theta - \beta)}\right] \left[c + K_o \left\{\frac{\gamma' d}{3} + \frac{W_o \sin(\theta - \beta)}{B\, d \cos\theta}\right\} \tan\phi\right]$$

K_o = coefficient of earth pressure at rest

$= 1 - \sin\phi$ (Jaky 1948)

and the other terms are as defined earlier.

A critical angle θ of the failure wedge is obtained by minimizing P with respect to θ. The approximation in assuming a plane failure surface is justified as long as $\delta < \phi/3$ (Terzaghi 1943). The friction at the soil-iceberg interface may be assumed to be a minimum because of the continuous pressnce of the meltwater. The value of P as obtained from Eq. [10] can be incorporated in the enetgy balance Eq. [3] and thus the scour dimensions can be computed for any type of seabed soil. This is an extension to the solution proposed earlier by Chari (1979) for purely cohesive materials.

The influence of the angle of internal friction of the soil on the scour depth computations is shown in Fig. 19. By comparing Fig. 14 and Fig. 19 it can be seen that the maximum scour depths obtained in cohesionless materials with friction angles in the range of 25° - 40°, are somewhat similar to those computed for purely cohesive soils with undrained shear strengths in the range of 25 - 100 kPa. Kivisild et al (1982) have given an energy solution for ice keel grounding which is compared with the present solution. The scour depths obtained using the model proposed here are higher (Fig. 20). This is due to the additional hydrodynamic effect duting scouring which is considered in the present model and also the different techniquss for computing the soil resistance.

3.6 Effect of Initial Seabed Penetration

Icebergs are subjected to continuous ablation in the process of which they gain equilibrium. In such a condition even a very small perturbation such as the initial contact of the iceberg with the seabed or the breaking of a small protrusion of the iceberg would cause it to roll with the poesibility of penetration into the seabed due to an increased draft (Fig. 9d). Assuming that the iceberg will then plough horizontally, the volume of the scooped out soil may be equated to the volume spread out. The length of the frontal surcharge at any instant can be obtained from Fig. 21

and expressed as:

$$2K_1^2 l_1^4 + 4K_1^2 l l_1^3 + (2K_1^2 l^2 + 3K_1 l B \tan\alpha)\, l_1^2 - 3l^3 B \tan\alpha \tan\beta - 6l^2 BS \tan\alpha = 0 \qquad [11]$$

where:

$K_1 = l_1(\tan\alpha + \tan\beta)$

l_1 = length of front surcharge at any instant

α, β = slopes of surcharged soil and seabed respectively

S = initial depth of penetration

and all other terms as already defined

The above equation is similar to that derived by Chari (1975) except that the scour trench in this case has an initial depth. At any scour length l, the front face soil resistance in cohesive soils can be obtained by slightly modifying Eqn. 4 and written as:

$$P = \frac{\gamma'(h + S + l\tan\beta)^2 B}{2} + 2C(S + l\tan\beta)B + \sqrt{2}\,C(S + l\tan\beta)^2 \qquad [12]$$

all the terms are as defined earlier

An equation of energy balance similar to Eq. [7] can be obtained as:

$$\frac{MV_0^2}{2} - \frac{C_d \rho A L V_0^2}{6} = \frac{\gamma'(H+S+L\tan\beta)^2}{6}\frac{(S+L\tan\beta)}{\tan\beta}B + \frac{cB[S+L\tan\beta]^2}{\tan\beta} + \frac{\sqrt{2}}{3}\frac{c(S+L\tan\beta)^3}{\tan\beta} - \gamma'\frac{(K_2 S+S)^2 SB}{6\tan\beta} - \frac{cB\,S^2}{\tan\beta} - \frac{\sqrt{2}}{3}c\frac{S^3}{\tan\beta} \qquad [13]$$

where:

$$K_2 = \frac{l_1(\tan\alpha + \tan\beta)}{S + L\tan\beta}$$

and all other terms as already defined

Equation [13] was evaluated numerically and the scour dimensions computed for different values of the environmental parameters.

Figure 22 is a typical result for the standard reference values shown in Table 4. It is seen that there is an upper bound S_u for the initial penetration depth corresponding to each iceberg size for a given set of parameters. From the figure, it may be seen that the iceberg will gouge the sea floor after piercing, if and only if the initial penetration is less than this upper bound. If the penetration is greater than this S_u, there will be no perceptible further scouring. In such a case, there is likely to be a pockmark formed on the seabed. This phenomenon is consistent with the observation of Lewis and Barrie (1981) wherein actual pockmarks have been noticed on the ocean floor. The upper bound may be identified in Fig. 22 by locating the points where the curves of initial penetration tend to become horizontal.

It may also be seen from Fig. 22 that the maximum scour depth is not affected by initial penetrations less than a certain lower bound S_l. For initial penetration below this bound, the maximum scour depth will be as if there were no such initial penetration. Envelopes of these upper and lower bounds are shown in Fig. 22. Such envelopes may be established for any given set of parameters.

With increasing initial depths of penetration, the contribution of energy due to hydrodynamic drag effect is reduced. This may also be deduced intuitively as the soil resistance soon after penetration is directly proportional to the penetration depth. Thus, with increasing initial penetration, the iceberg will come to a stop after a shorter travel.

The above effect on the computed scour depths is shown in Fig. 23 from a slightly different perspective. It is seen that increased shear strength decreases the maximum scour depth which is to be anticipated. However, the magnitude of the soil shear strength has no influence when the initial depth of penetration is larger than the critical depth. Similarly, if the soil shear strength is less than a certain value corresponding to a given initial penetration, the depth of penetration has no influence on the maximum scour depth. The existence of such critical depths is also demonstrated in Fig. 24 in which the effect of iceberg drift velocity is shown. The upper and lower bound penetration depths are thus unique to a given iceberg.

From an extension of the analytical model, it has been shown that the velocity of an iceberg during seabed gouging is nonlinear. However, its effect on the accuracy of the computations depends on the other parameters. It has been shown that one can establish upper and lower bounds for

initial penetration of the seabed by capsizing icebergs for purposes of computing further scouring of the seafloor.

The related physical model tests and results are discussed in the following chapters.

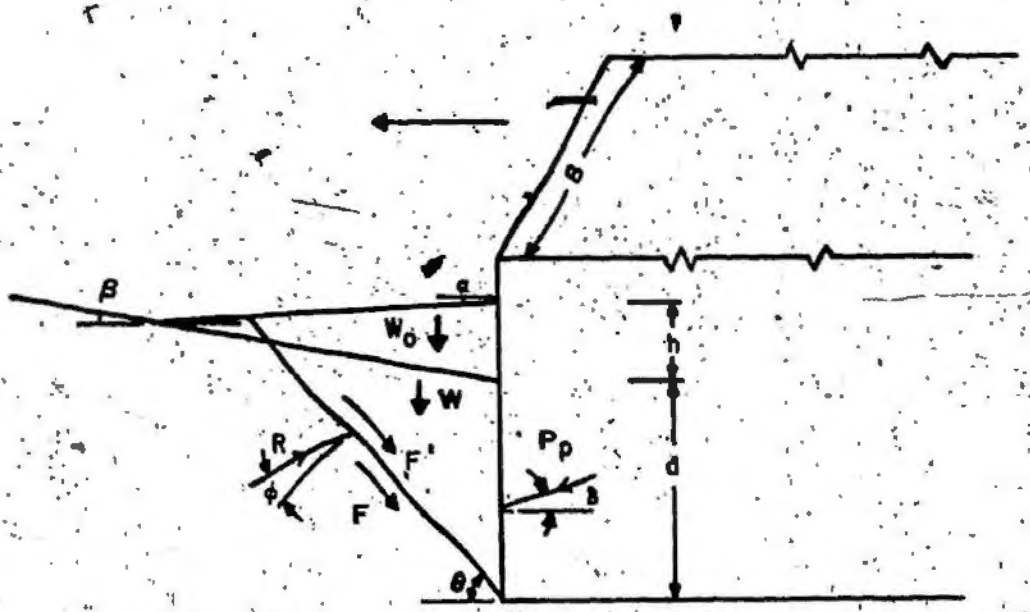

FIGURE 18 SYSTEM OF FORCES ACTING ON A FAILURE WEDGE IN FRICTIONAL SOILS

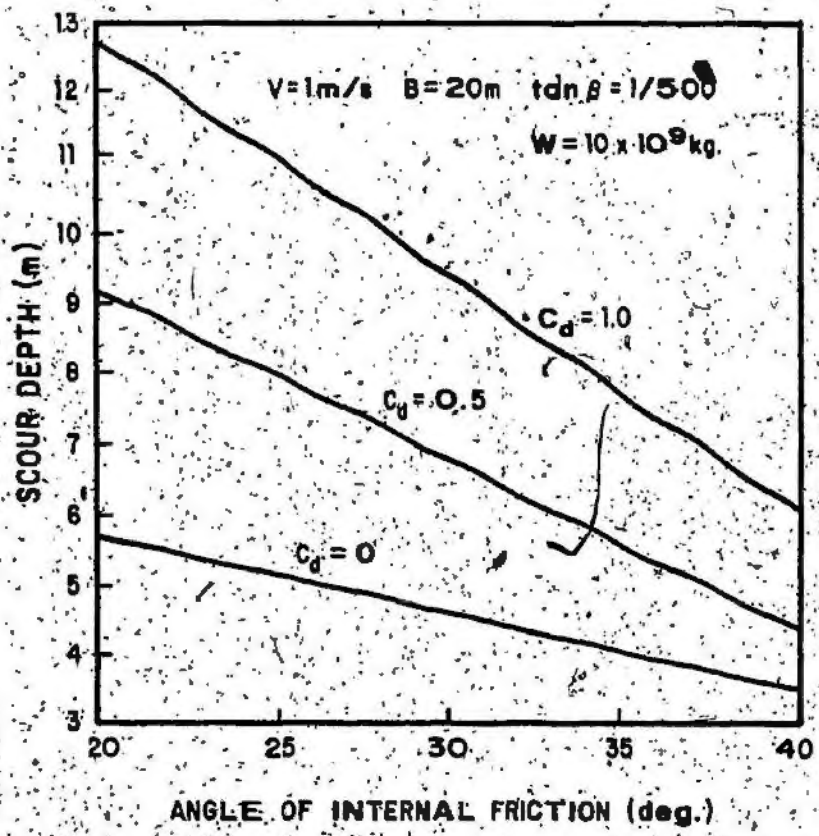

FIGURE 19 VARIATION OF SCOUR DEPTH WITH ANGLE OF INTERNAL FRICTION.

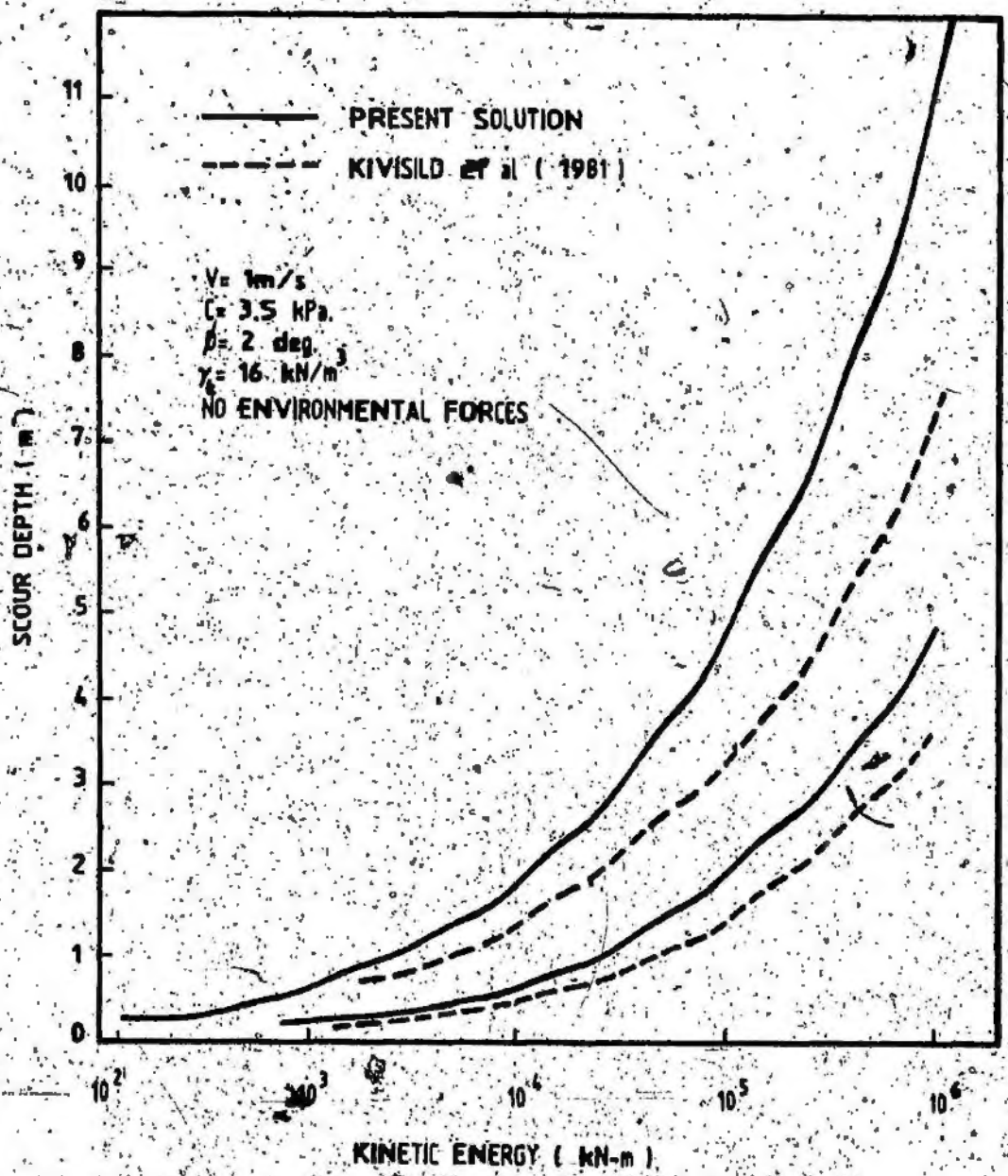

FIGURE 20 COMPARISON OF PRESENT SOLUTION WITH THAT OF KIVISILD ET AL.

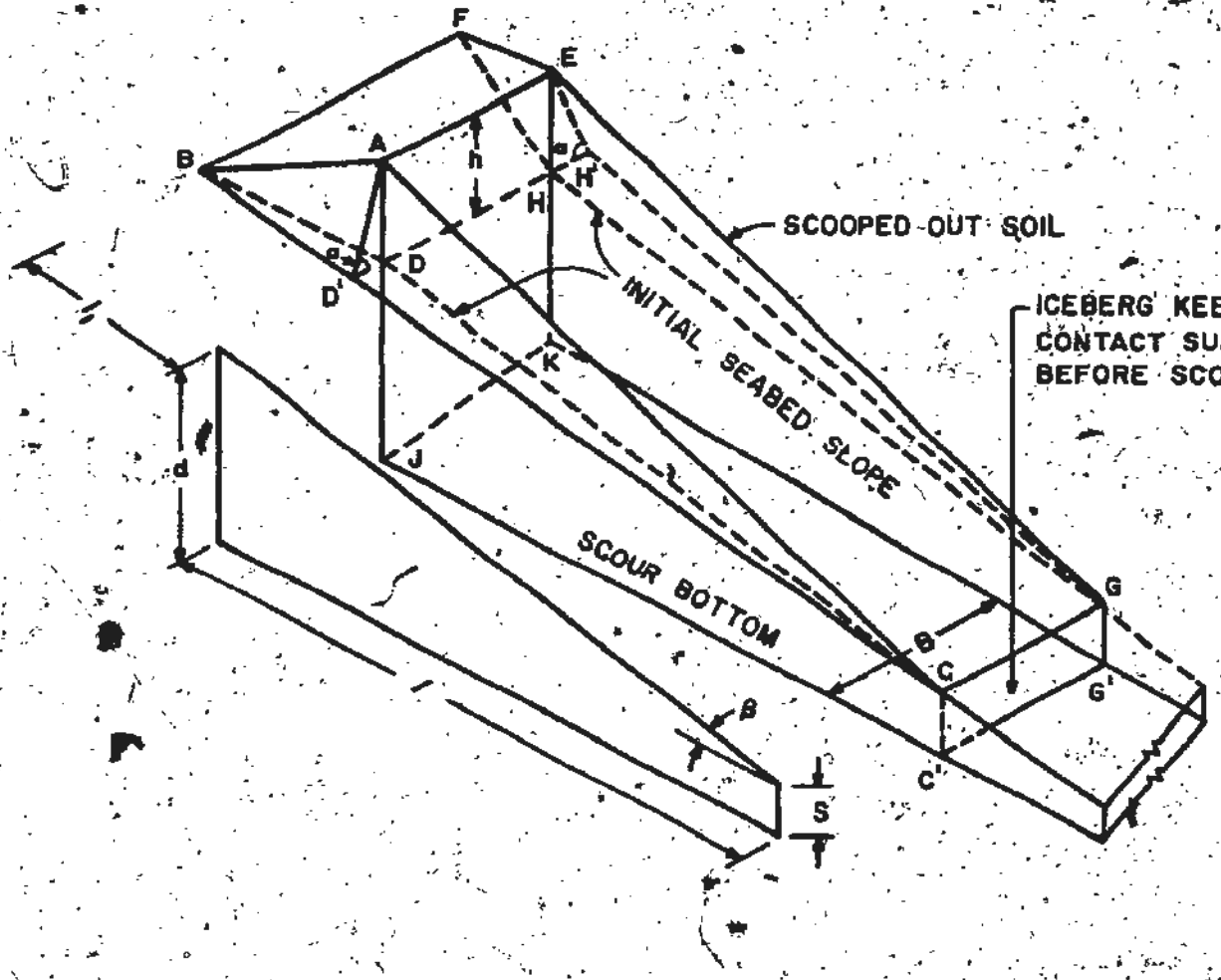

FIGURE 21 EXTENDED MODEL WITH INITIAL SEABED PENETRATION

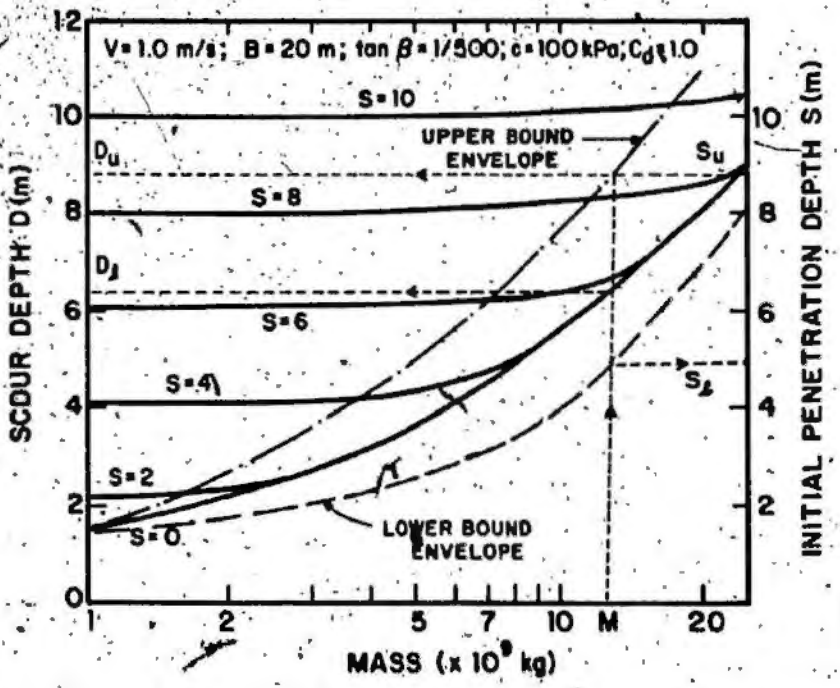

FIGURE 22 SCOUR DEPTH FOR DIFFERENT ICEBERG SIZES AND INITIAL SEABED PENETRATIONS

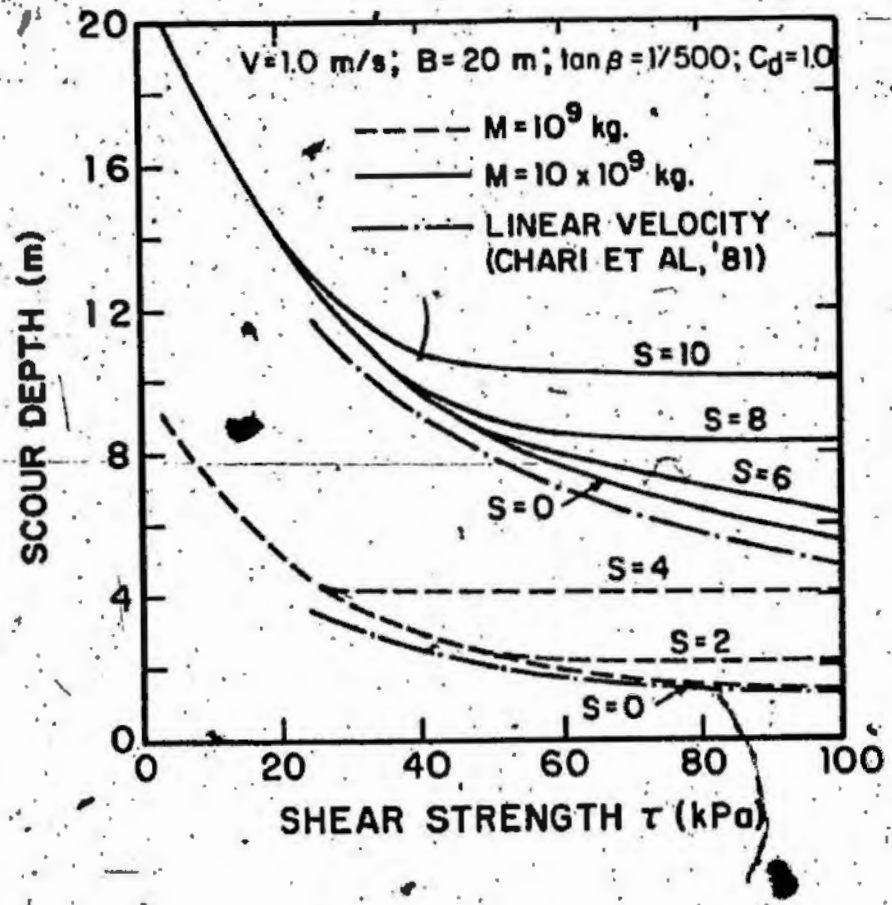

FIGURE 23. VARIATION OF SCOUR DEPTH WITH SHEAR STRENGTH FOR VARIOUS INITIAL SEABED PENETRATIONS

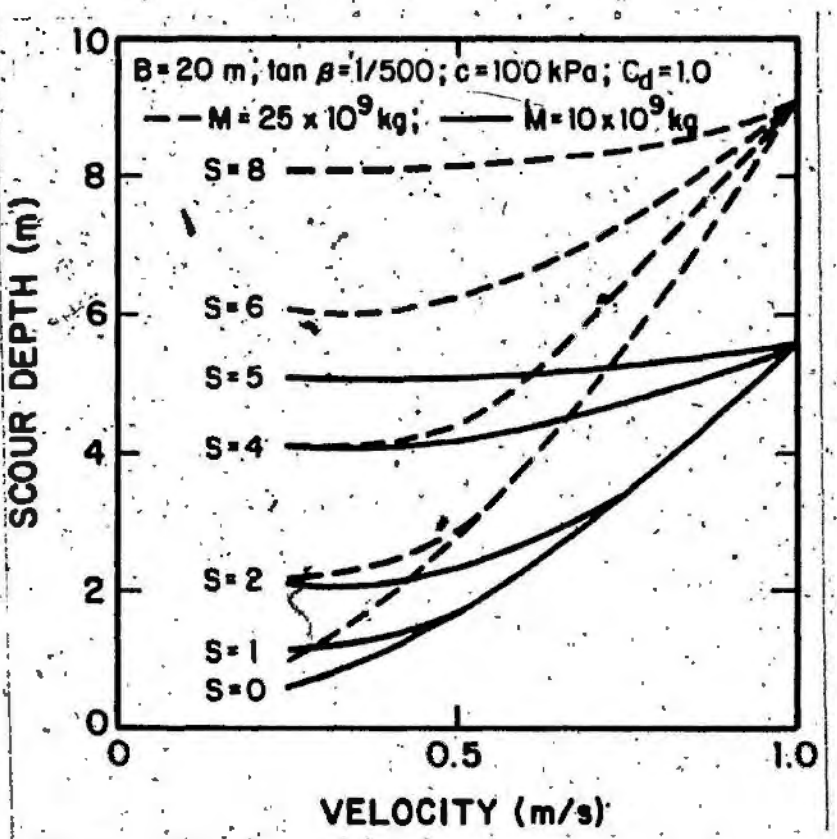

FIGURE 24 VARIATION OF SCOUR DEPTH WITH VELOCITY AND INITIAL SEABED PENETRATION

CHAPTER IV

EXPERIMENTAL ORGANIZATION AND TEST PROCEDURE

4.1 General

The analytical model described in the previous chapter cannot be duplicated in its entirety in the laboratory due to limitations in scaling the soil grain size and shear strength (Chari 1975). The analytical model is based on two main principles; energy balance and soil-iceberg interaction. The concept of energy balance needs no verification in the laboratory. The analytical model would be fully verified if the soil-iceberg interaction can be physically modelled. Any physical modelling of iceberg scours will thus be a partial, nevertheless a valid model.

The earlier studies by Chari (1975) were conducted in a tiltable, glass-sided flume with 23 cm (9") wide plexiglass instrumented models and in clays of 1:10 slope. Green (1984), conducted tests in medium sand with 1:35 slopes and 500 mm wide models. The present investigation is an extension of those model tests.

4.2 Experimental Facilities

4.2.1 Towing Tank

The towing tank is 14 m long, 6 m wide and 0.8 m deep and has a central longitudinal dividing wall as shown in

Fig. 25 and 26. The towing carriage is fabricated out of two parallel hollow rectangular beams over 6 m in length and spaced at a clear distance of about 1.3 m with suitable cross beams. The beams are ballasted with steel reinforcing bars to provide a counter-weight of 14 kN in order to resist the overturning moment while scouring. The area between the two beams is covered by metal grillage and the area serves as working space for the instrumentation. A variable speed 7.5 H.P electric motor transmits power through a torque converter to a 62 mm diameter shaft spanning the length of the carriage. The sprockets at each end of the driving shaft are connected to the sprockets of the supporting wheels by a chain. The carriage movement is controlled by press type switches for both forward and reverse directions. In addition to these, limit switches are provided at the two ends of the carriage rails to automatically stop the carriage at a safe distance from either end of the tank.

4.2.2 Iceberg Models

Most of the earlier experimental studies (Chari 1975, Abdelnour and Lapp 1980, Green 1984) have been with prismatic models with some limited testing of non-prismatic shapes. These studies have shown that the shape has an effect on the total soil resistance and recommendations have been made to further investigate the shape effect.

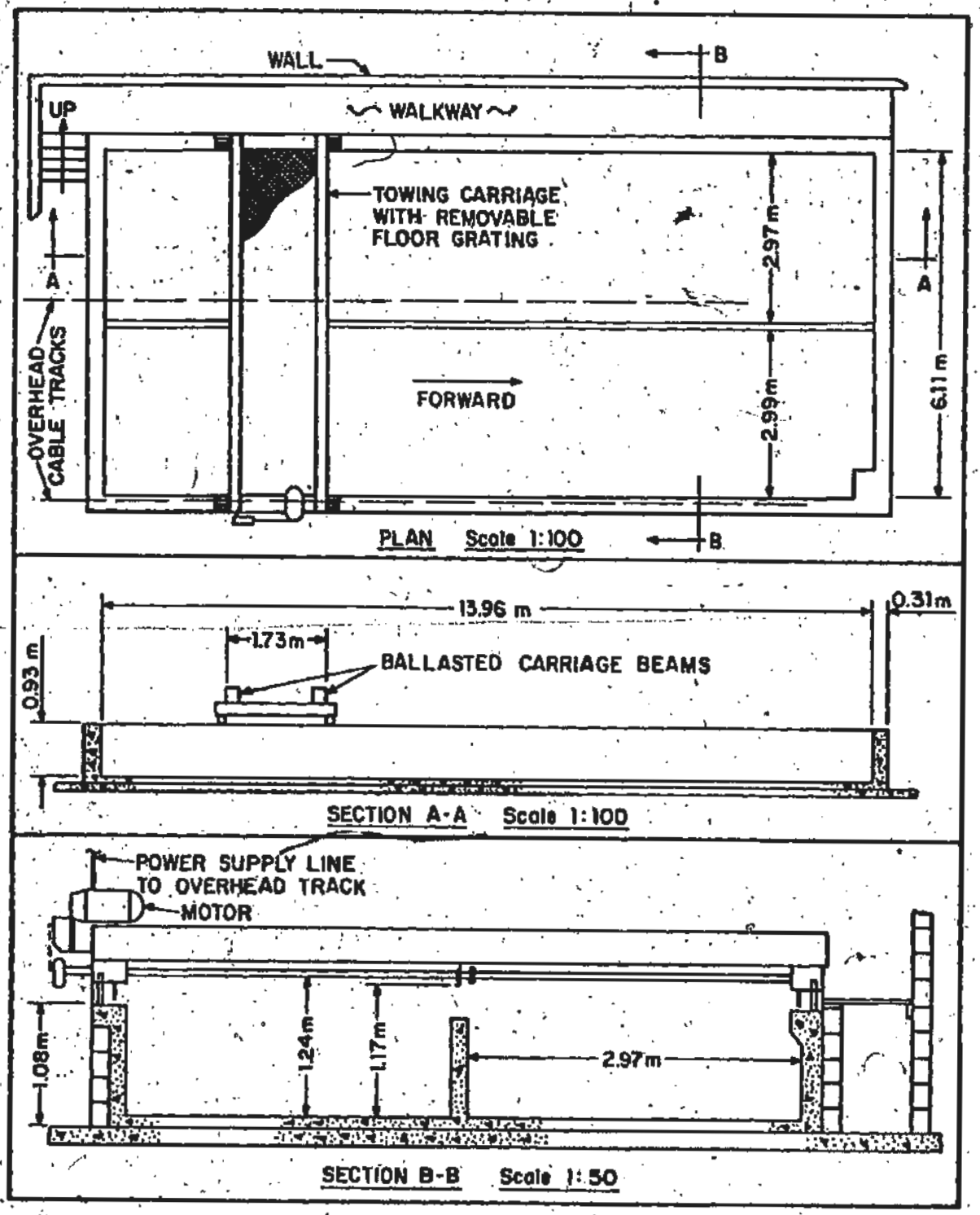

FIGURE 25 PLAN AND CROSS SECTION OF TOWING TANK (GREEN 1984)

FIGURE 26 A GENERAL VIEW OF THE TOWING TANK, CARRIAGE AND MODEL

REFERENCE	DESCRIPTION	SIDE VIEW (mm)	TOP VIEW (mm)
M 1	RECTANGULAR PRISM	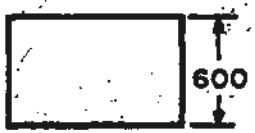	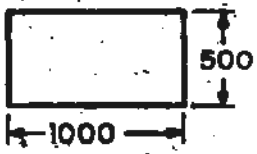
M 2	RECTANGULAR PRISM WITH 30° INCLINED PROFILE		
M 3	RECTANGULAR PRISM WITH 60° INCLINED PROFILE		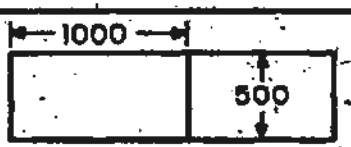
M 4	RECTANGULAR PRISM WITH CURVED-PROFILE	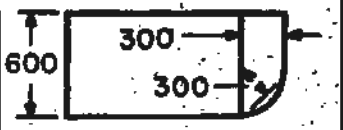	
M 5	RECTANGULAR PRISM WITH CYLINDRICAL FRONT SHAPE		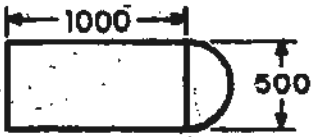
M 6	RECTANGULAR PRISM WITH WEDGE TYPE FRONT FACE	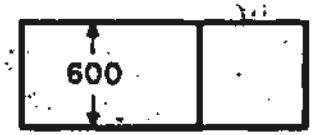	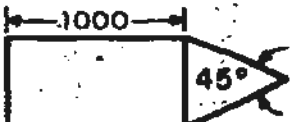

FIGURE 27 VARIOUS SHPAES OF THE ICEBERG MODELS TESTED

FIGURE 28A RECTANGULAR PRISMATIC MODEL

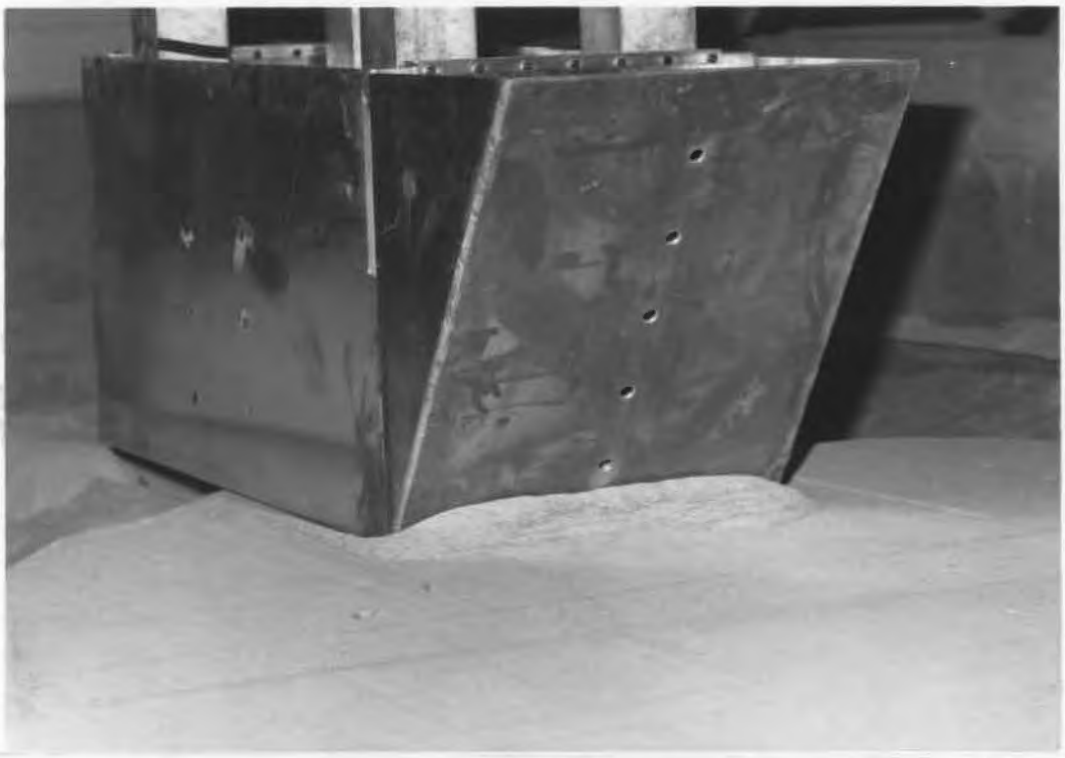

FIGURE 28B MODEL WITH A KEEL SLOPING AT 30°

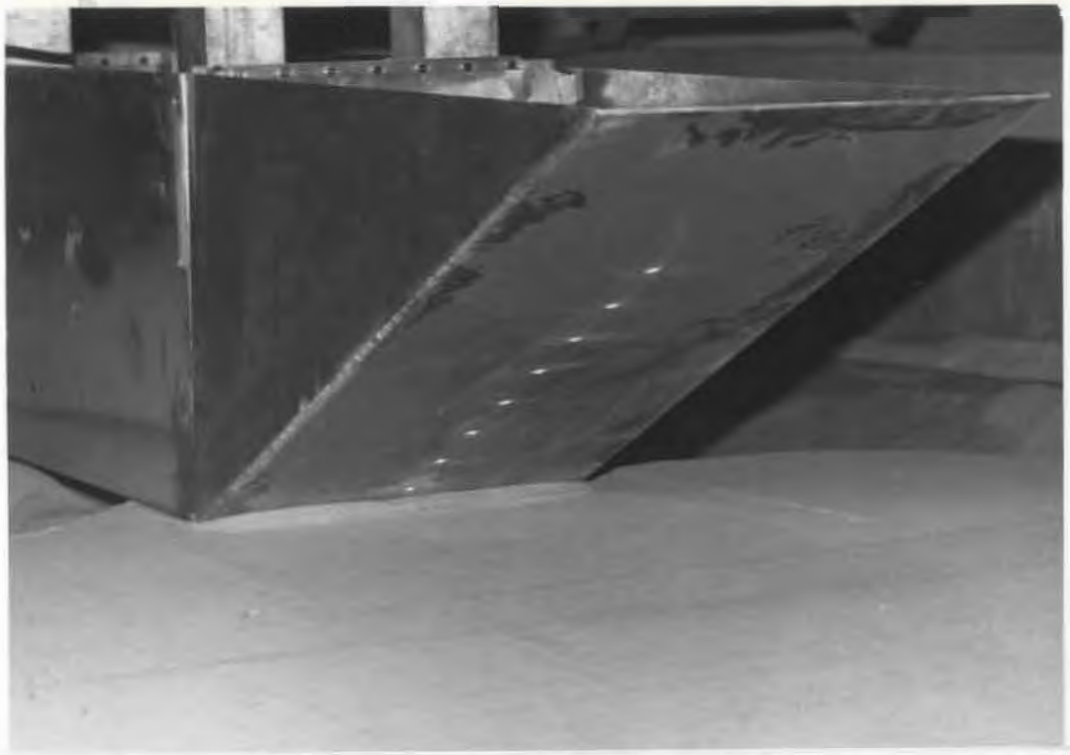

FIGURE 28C MODEL WITH A KEEL SLOPING AT 60°

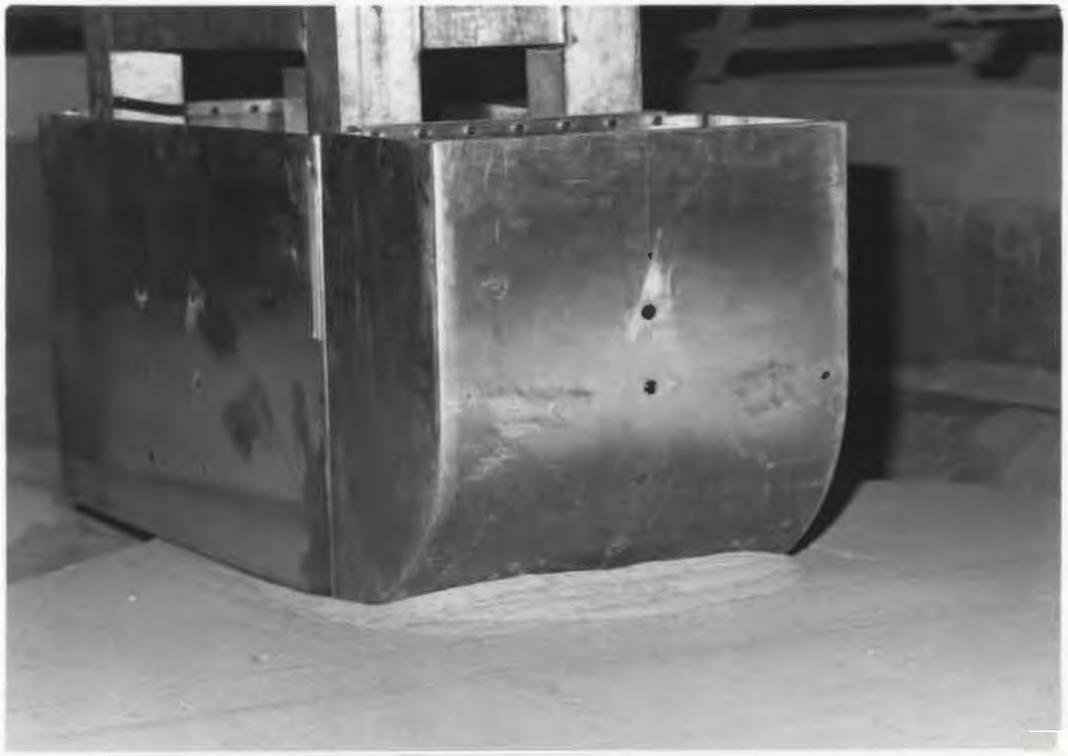

FIGURE 28D MODEL WITH A CURVED KEEL

FIGURE 28E MODEL WITH A CURVED KEEL DURING SCOURING

FIGURE 28F MODEL WITH A CYCLINDRICAL SHAPE DURING SCOURING

FIGURE 28F WEDGE-SHAPED MODEL

FIGURE 28H MODEL WITH A RANDOM SHAPE

FIGURE 28I MODEL WITH A RANDOM SHAPE (NOTE THE FAILURE WEDGES, SIMILAR TO THOSE FOR THE RECTANGULAR SHAPE)

FIGURE 28J SHAPE OF THE SCOUR TRENCH AND RAISED SHOULDERS

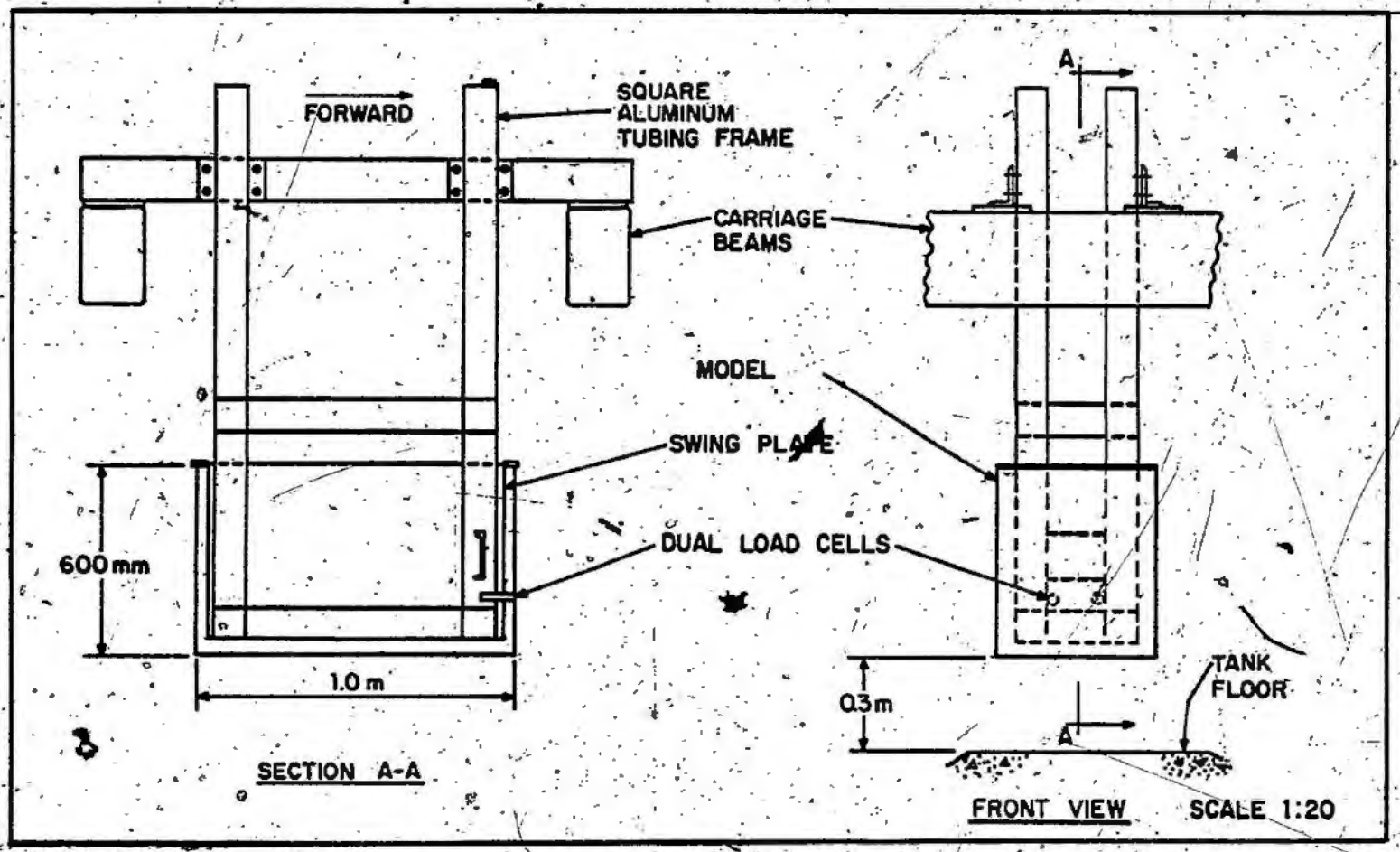

FIGURE 29 MOUNTING FRAME FOR ICEBERG MODELS (GREEN 1984)

In addition to the rectangular prismatic model, five other different shapes were used in this investigation. These are shown in Fig. 27 and 28. The various frontal keel shapes were fabricated with 6 mm aluminium sheets and bolted to the front face of the existing rectangular model.

The rectangular model is connected to a rigid mounting frame (Fig. 29) by means of thin swing plates with a width slightly less than 500 mm. The mounting frame, together with the iceberg model, can be lifted with a pulley block hanging from the roof and placed at any desired elevation relative to the sand bed. Before starting the tests, two load cell holders were screwed into the threaded holes of the mounting frame such that the horizontal force exerted on the iceberg model is transmitted to the two load cells. When the load cells are positioned there is no relative displacement between model, frame and tow carriage. The swing plates were strong enough to eliminate the rotation of the model under an uplift force and also flexible enough to transmit all the horizontal force to the two load cells.

4.2.3 Soil Bed

As briefly mentioned in the literature review, published data on geotechnical properties of sea floor sediments on the Canadian East coast are very scarce. However, from the limited information available, it can be seen that the seabed material in the scoured areas can vary

from soft cohesive soils to sand and boulders. Chari (1975) conducted model tests in saturated silty clay slopes of 1:10. Green (1984) used dry cohesionless sand of 1:35 slopes for tests with the 500 mm wide models. Abdelnour & Lapp (1980) used level soil surfaces of clay, silt, and sand under saturated conditions. However, tests in sand do not necessarily have to be under saturated conditions because of the easy drainage in cohesionless soils. From considerations of ease of handling, experiments for this investigation were conducted in dry sand. The use of dry sand offers the additional advantage of exposing the surcharge, the failure surface, and the scour track all of which can be visually observed and measured. About 18 m^3 of dry cohesionless sand with grain size distribution shown in Fig. 30 and the properties listed in Table 5 was laid at a slope of 1:35. The maximum grain size of the sand is 4 mm which compares well with the 11 mm diameter pressure transducer surface. The method of preparing a consistently uniform sand bed and density calibration will be described in a later section.

4.3 Instrumentation

One of the objectives of this investigation is to measure the total load necessary to tow the iceberg model and the pressure distribution on the front face of the iceberg model. The schematic of the instrumentation is shown in

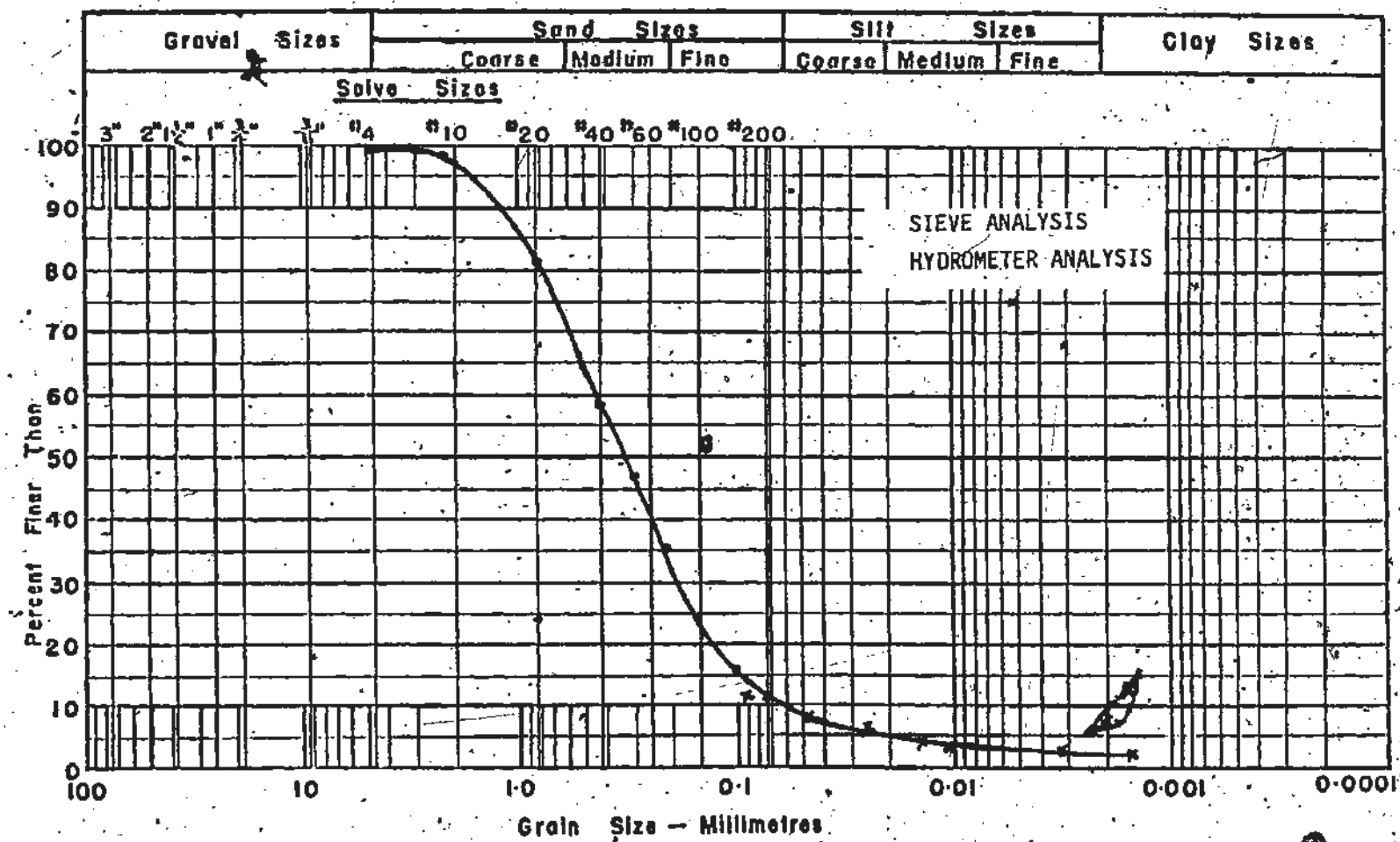

FIGURE 30 GRAIN SIZE DISTRIBUTION CURVE FOR THE SOIL USED IN THE EXPERIMENTS

TABLE 5. PHYSICAL PROPERTIES OF SOIL

Soil Type	Brown, Well Graded Sand with Traces of Silt
Maximum Grain Size	4.75 mm
Effective grain size	0.065 mm
Coefficient of Uniformity	6.9
Coefficient of Curvature	1.23
Relative Density of Grains	2.68
Minimum Dry Density	1706 kg/m^3
Maximum Dry Density	2049 kg/m^3
Experimental Density	1733 kg/m^3 ±2%
Density Index	0.13
Angle of Repose	37° ± 2°
Moisture Content	0.22% (Air Dry)
Angle of Internal Friction	35.5°
Soil-Model Friction Angle	23°

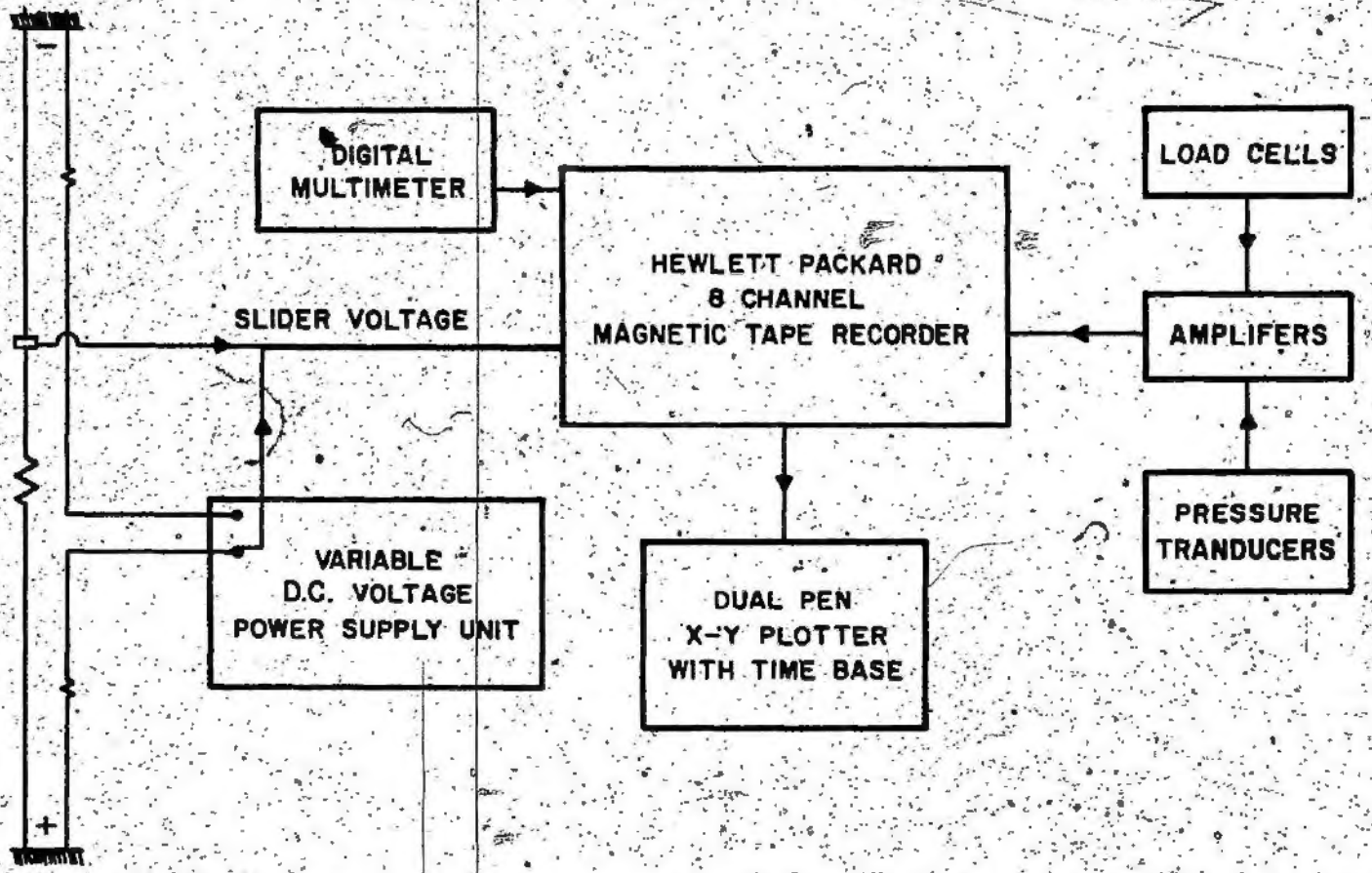

FIGURE 31 SCHEMATIC OF THE INSTRUMENTATION USED IN THE EXPERIMENTS

Fig. 31. Quartz piezo-electric load cells and pressure transducers were used in this investigation. The manufacturer's specifications for the sensors and their re-calibration procedures are given in Appendix B.

The pressure transducers and the load cells were connected to Dual-mode amplifiers (Model 504E, Kistler Instrument Company) through low noise transducer cables. The D.C. voltage output from the amplifier was fed as an input to 8 channel Hewlett Packard Magnetic Tape Recorder.

To locate the relative position of the carriage at any instant during the test, a metal wire was stretched along the length of the tank by the side of a fixed meter tape and, a D.C. voltage of 3 volts was applied at its ends. The potential difference measured between one end of the wire and an aluminium slider fixed to the carriage was continuously measured and recorded as the carriage moved from one end to the other. The reading on the meter tape at the beginning and the end of the scour provided a cross check on the length of the scour. A two pen X-Y plotter was used to play back the recorded readings.

All the recording instruments were placed on custom built work benches on the top of the carriage and suitably protected from dust.

4.4 Test Procedure

The complete test procedure can be divided into four parts. A major portion of the test was devoted to the preparation of the sloping sand bed. The second part was cleaning of the instruments and connecting them together. After these pre test preparations, running the test and retrieving the data was routine. Post scour observations included density verification, measurement of scour dimensions and surcharge build up. Each process is described in detail in the following paragraphs.

4.4.1 Preparation of the Sloping Sand Bed

The volume of the sand involved in this test is about 18 cubic meters. When the volume of the sand involved is small, techniques such as a raining method, vibro-floatation, fluidization are normally used to obtain a test sample of uniform and consistent density. In view of the large quantity of sand involved in this experiment, after trying several methods, it was decided to adopt a simple raking technique to prepare the sand bed everytime. After studying different sizes of rakers, (Green 1984) suggested a simple four pronged rake of about 500 mm width that can be attached to the tow carriage (Fig. 32). Abdelnour and Lapp (1980) used a rake similar to a farmer's harrow.

The method used by Green (1984) was used in this study with some slight modifications. Air dry sand was placed in the tank at an approximate slope of 1:35 with a thickness of about 0.2 m near one end of tank increasing to about 0.6 m at the other end. Two angle sections were fixed to the side walls of the tank on the inside at a slope of 1:35 as a guide to form the surface of the sloping sand bed.

Before starting the soil preparation, the iceberg model, along with the mounting frame was unbolted from the towing carriage with the help of the pulley block, and the model was placed at a higher elevation on wooden blocks resting on the carriage. This avoided the interference of the iceberg model with the sand bed while it was being raked.

Preparation of the sand bed started with shovelling the sand and forming an approximate sloping surface. The towing carriage was then positioned as near to the start of the tank as possible, and a trench of about 300 mm was dug just in front of the forward carriage beam. After moving the rake supports to the prelaid paint markings, the rake was bolted to the studs. Running the tow carriage up and down the tank mixed about a 0.6 m wide track of the soil along the length of the tank. The rake was then moved to the next position and the procedure was repeated until the entire upper layer was mixed leaving a strip of 0.3 m width on both sides of the bed which served as a working space. The level

of the raker was then brought down to the lowest pair of bolts on the rake supports and the bottom most layer was raked. This resulted in a thorough mixing of upper layers which were subjected to more disturbance due to scouring in earlier experiments and reasonable mixture at the bottom layers where least disturbance is expected. In total, the tow carriage was moved twelve times up and down the length of tank for complete mixing of the sand bed. After raking, a wooden bar was placed across the width of the tank, on the sloping guide beams fixed to the inside of the walls. Any soil required in the central portion of the width was supplied with a shovel from the shoulders and the excess material was removed by dragging the wooden bar on the sloping guide beams along the length of tank thus obtaining a smooth bed of reasonably uniform density. This procedure was consistently followed throughout this investigation. The undisturbed average density of this bed was obtained with a hand penetrometer which was calibrated using the same sand rained at different densities in a drum.

4.4.2 Data Recording

The process of preparing the soil bed raises lot of dust and some effort was needed to clean the working area on the tow carriage as the piezo-electric sensors, charge amplifiers and microdot connectors are sensitive to dust. The tow carriage was placed at the end of the tank, and the

iceberg model, along with the mounting frame was lowered to align with the holes in the mounting frame and bolted rigidly. The bottom of the iceberg model was generally about 300 mm from the tank floor so that the rigid floor of the scouring tank did not influence the results obtained.

All the instruments were turned on 30 minutes before each test to allow a warm up period. The caps of the piezo-electric sensors were removed, cleaned with cotton swabs, dipped in Tuner Degreaser and recapped each time they were mounted through the brass holder on the iceberg model. Great care was taken in connecting the microdot connectors to the pressure transducer and amplifier as the slightest amount of dirt or humidity near the connection or a twist in the connector produced a drifting output voltage. The outputs from the charge amplifiers were fed to the precalibrated input plugs of the tape recorder. The variable D.C. power supply unit which applied a potential difference of 3.0 volts at the ends of the steel wire, along the length of the tank was calibrated each time, using a multimeter. The reference line voltage was connected to one of the input channels of the tape recorder. A typical experiment should measure eight parameters, two load cells, five pressure transducers, and the carriage reference voltage. When all the instruments were ready to operate, the tow carriage was moved in small incremental distances such that the bottom of the iceberg

model just touched the sloping sand bed. At this stage, the carriage reference voltage, the position of the slider on the meter tape, and the initial footage of the tape recorder were observed and recorded. All the instruments were tutned on 30 min. before starting the test, the readings were recorded as the scouting continued, and until the model reached the limit switch. At the end of the scour, the counter reading on the tape recorder, carriage reference voltage, and the reading on the meter tape at the carriage slider were noted. Recorded observations from each channel, together with carriage reference voltage were plotted on 300 x 200 mm paper using a two pen X-Y plotter.

4.4.3 Post Scour Observations

In order to check the repeatability of the results, each parameter was measured at least five times under similar conditions or until reasonably consistent values (±10%) were obtained. In general, there was a very good consistency in the total load measured for all the models whereas several repetitions were needed for pressure measurements indicating the variation of local densities integrated to be neglegible. In order to check the uniformity and consistency of the soil density in all tests, a hand penetrometer was used to measure the resistance offered by the soil at several locations on the sand bed. Penetrometer readings were taken at 1 m intervals both inside and outside the scour track up to a depth of 400 mm.

In some experiments, the scour track formed by the model was measured. The measured dimensions included base width of the scour (B_s), top width of the scour (T_s), the inside depth (D_s), and sloping lengths (I_s, O_s) of the scoured cross sections.

In addition to the above observations, for purposes of theoretical calculations, it was necessary to measure the surcharge dimensions in front and at the sides of the model as the scouring proceeded. For this purpose, separate experiments were conducted for each model, in which the tow carriage was stopped at intermittant points, and measurements were made. This procedure was also used successfully by Green (1984). A typical scour track and surcharge dimensions are shown in Fig. 33.

The results of the experiments and the analysis are discussed in the next chapter.

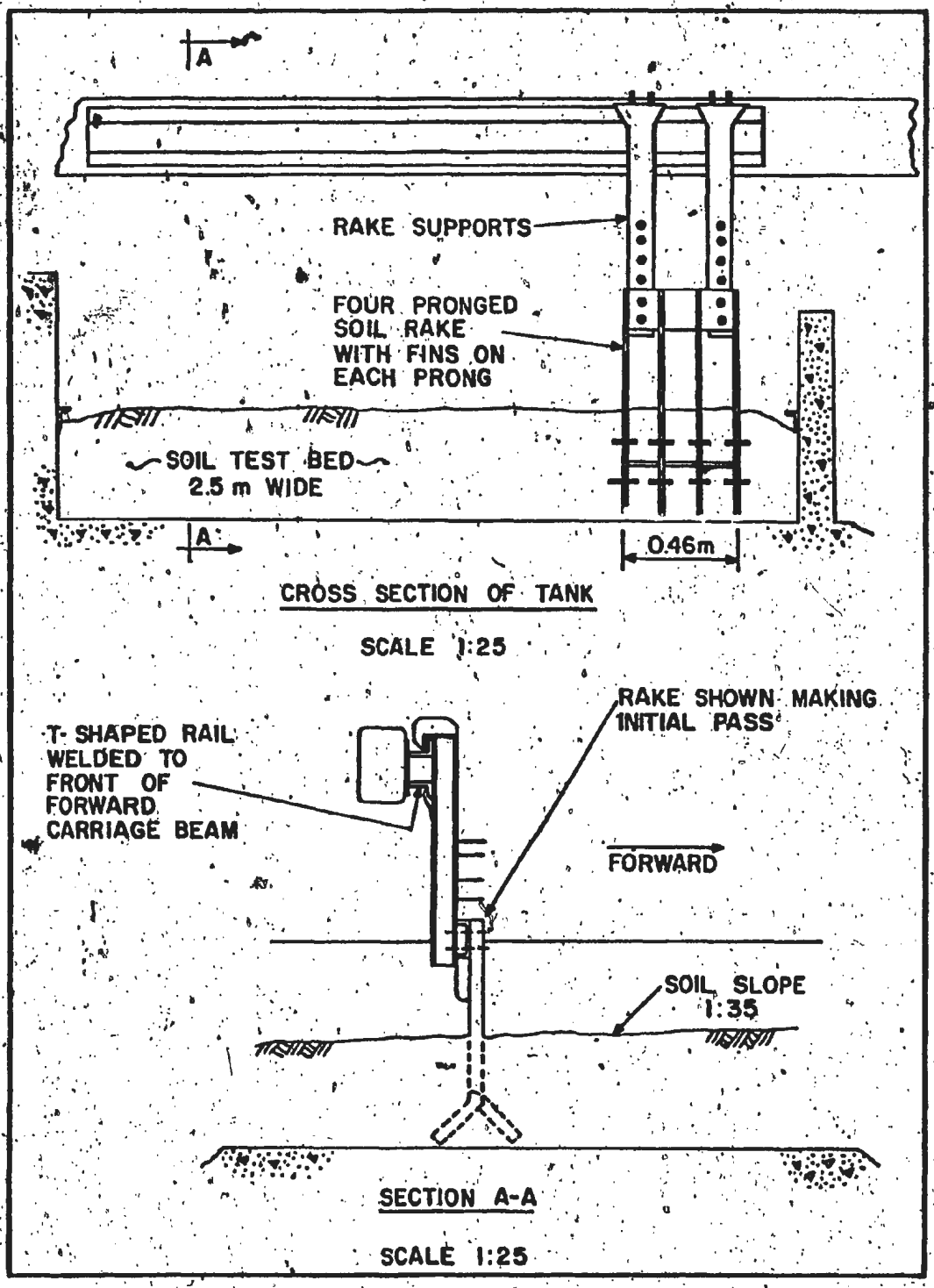

FIGURE 32 THE RAKE SYSTEM FOR THE SOIL TEST BED PREPARATION (GREEN 1984)

FIGURE 33 TYPICAL SCOUR TRACK AND MEASURED SURCHARGE DIMENSIONS

CHAPTER V

EXPERIMENTAL RESULTS AND DISCUSSION

5.1 General

This chapter is organized into three major sections. The first part is a discussion of the scour dimensions and shape. In the second part, the types of the experiments conducted are described and a correlation is made between the force required to push various models into the sloping sand bed and the corresponding pressure distribution on the front face. In the last part, the experimental results are compared with appropriate theoretical methods. Finally, an attempt is made to normalize the scour computations for various keel shapes with reference to the idealized model.

The limitations of modelling iceberg scours in the laboratory and the scope of such models were discussed earlier. The experimental work is limited to verifying the soil-iceberg interaction. Aspects of the problem such as the effect of velocity on the soil resistance and the model size have been studied and discussed by Green (1984). In the experimental part of this investigation, it was decided to investigate the effect of the keel shape on the resistance of the iceberg to ploughing and take this into account in the theoretical model.

After preparing the soil test bed as described in the previous chapter, the iceberg model was positioned, the instruments connected, and the model was towed at a speed of 95 mm/sec. The total soil resistance was measured by the two load cells. A typical force record is shown in Fig. 34. The output from the two load cells was manually added to obtain the total soil resistance. It may be seen that the load cell records are similar to those reported by Siemens (1963), Chari (1975), and Green (1984) in which the development of successive failure planes (Fig. 35) is depicted by the saw tooth pattern of the record. A similar phenomenon was observed in the load cell records of all iceberg models.

5.2 Scour Profiles and Surcharge Dimensions

In the analytical model discussed in Chapter III, the iceberg shape was idealized as a rectangular prismatic shape. The surcharge in front of the iceberg was calculated on the assumption that the volume of the soil scooped out by the iceberg is equal to the sum of the volumes of the soil piled up on the sides and in front of the iceberg. In the attempts to compute the front face soil resistance Chari (1975) measured the surcharge height at the end of scour and assumed a linear variation of it along the length of scour. Green (1984) used different techniques to measure surcharge

dimensions and concluded that stopping the iceberg model at intermediate points along the length of scour did not affect the scour dimensions. Experiments were conducted exclusively to determine the scour dimensions without measuring the loads or pressures. The iceberg model was stopped at several intermediate points and the surcharge was measured at these points and a profile of the surcharge was obtained. The same technique was followed in this investigation. In addition to the front surcharge dimensions, the dimensions of the soil on the sides of the iceberg model were also measured to compute the side friction.

The scour profile at the back of the iceberg model was also measured at the end of the test for each model. From the measurements of scour profiles for each model, it was found that irrespective of the front shape of the iceberg, the form of the scour profile was exactly same. However, depending on the total length of the model, the scour profile at the back of the model was different. From the measured surcharge dimensions, the total volume of the soil in front (V_f) of the iceberg was calculated. These volumes for the different models are shown in Fig. 36. In addition to this, the volume of the soil on the sides of the iceberg model (V_s), and the volume of the soil on the sides of the scour track (inclusive of the infilled soil) (V_b) were calculated.

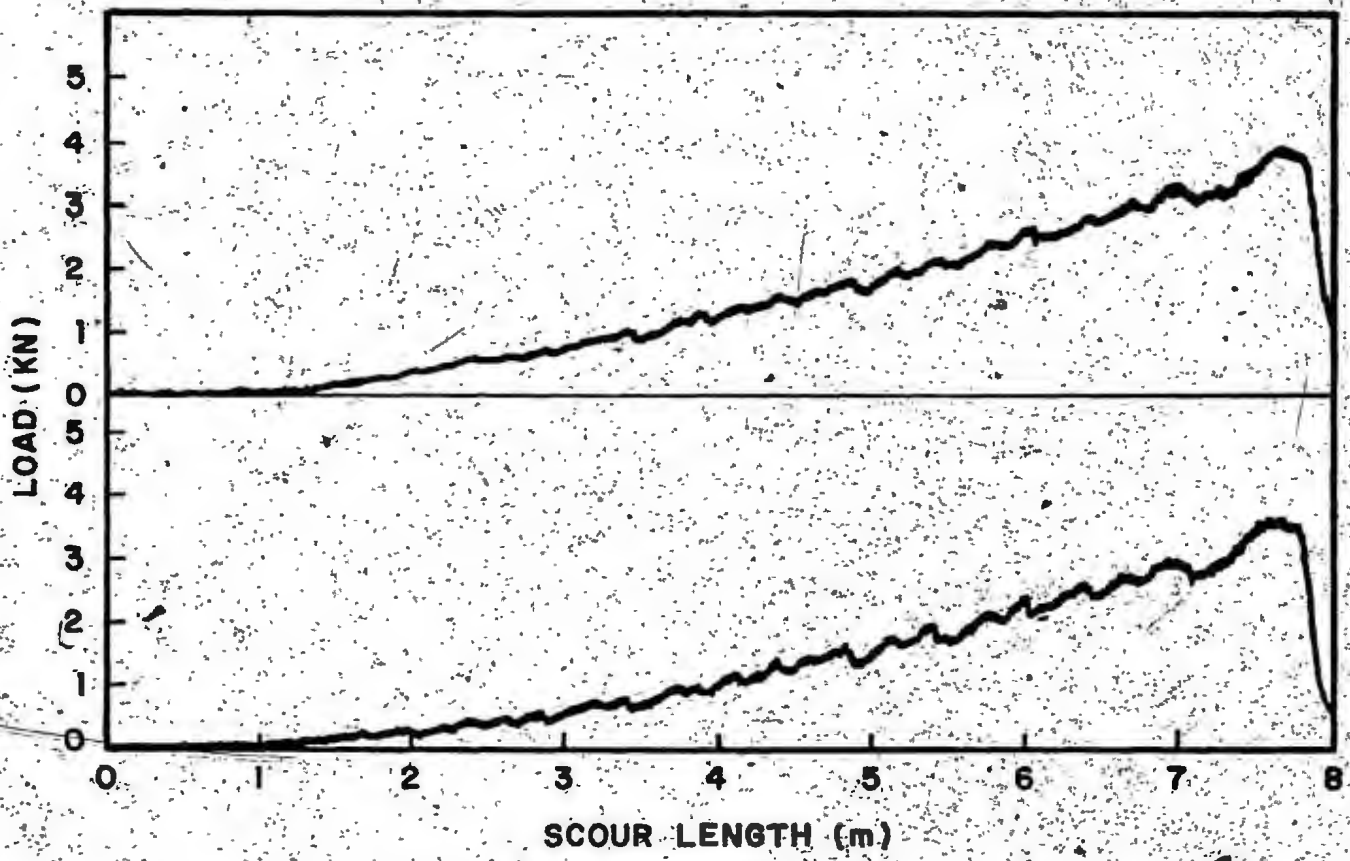

FIGURE 34 TYPICAL RAW OUTPUT OF DUAL LOAD CELLS

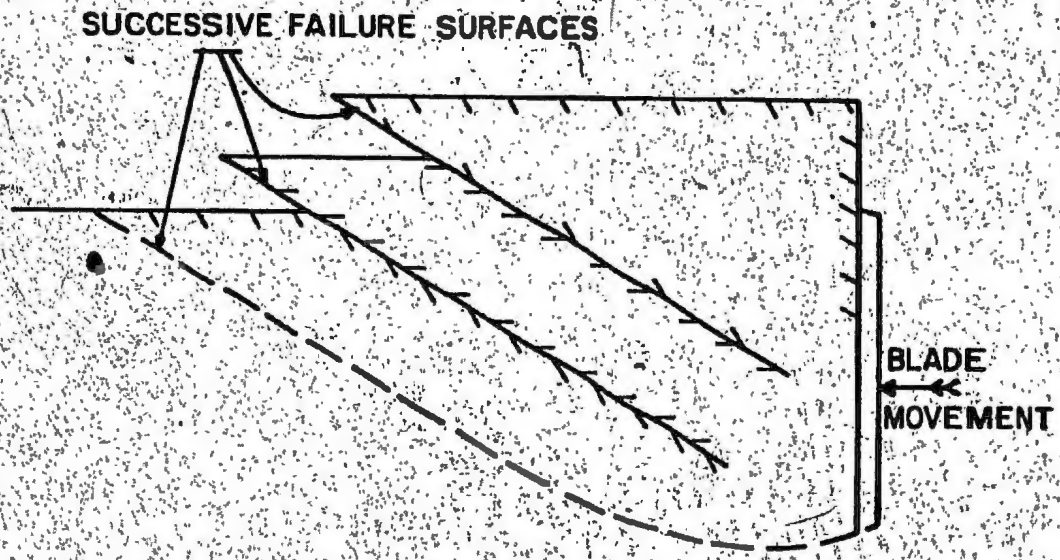

FIGURE 35 SOIL FAILURE ALONG SUCCESSIVE SHEAR PLANES IN FRONT OF EARTHMOVING MACHINES (SIEMENS 1963)

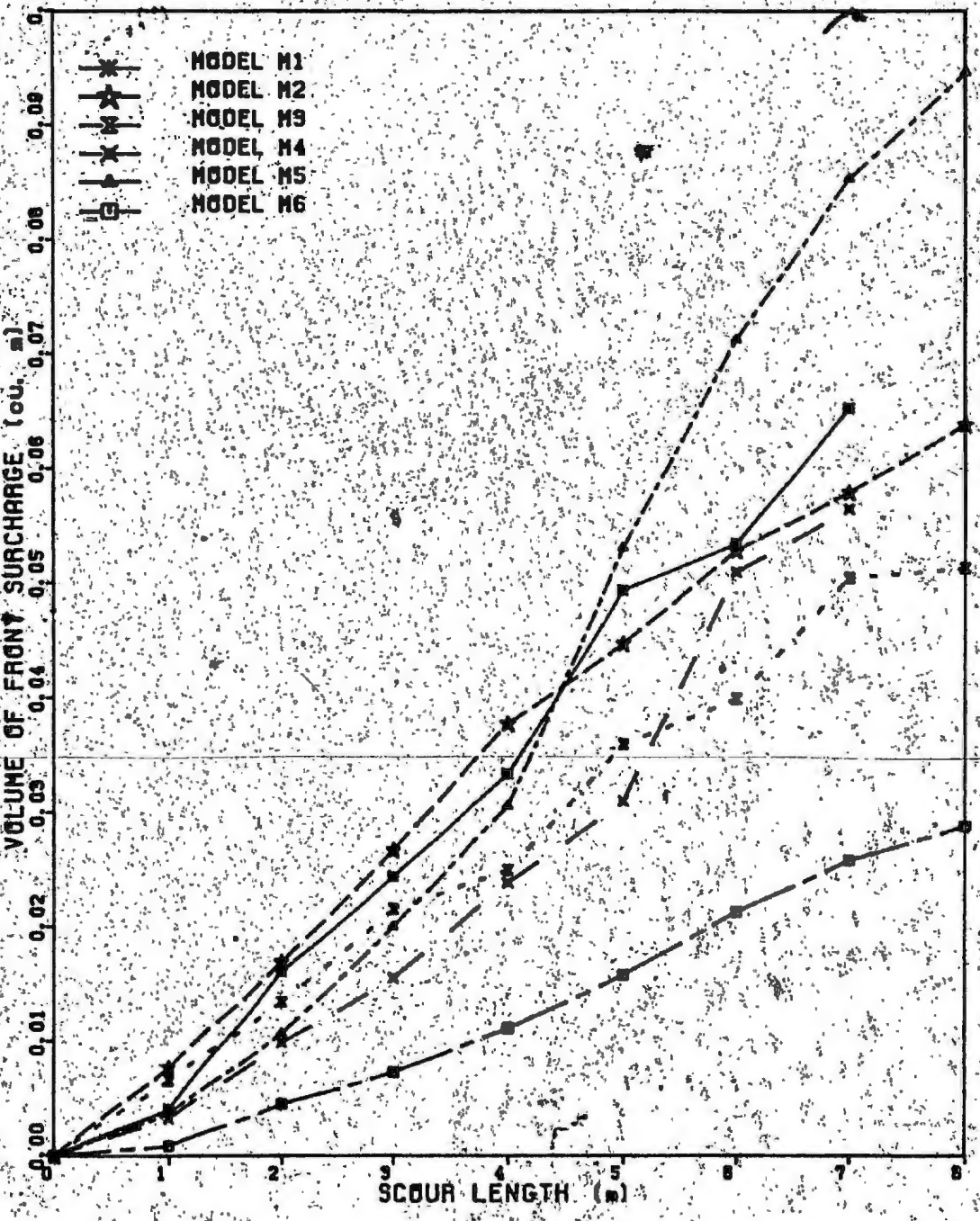

FIGURE 36 VOLUME OF FRONT SURCHARGE FOR DIFFERENT KEEL SHAPES

5.3 Soil-Model Friction

The total soil resistance on the iceberg is the sum of the front face resistance, frictional resistance on the sides and the base friction. In the theoretical model, it was suggested (Chari 1980) that the frictional component of the total resistance may be neglected because of the presence of a thin film of melt water around the iceberg. However, this is not true in the laboratory experiments. Therefore, it is necessary to identify and evaluate the frictional resistance on the sides and base of the model. From a knowledge of the total resistance and the frictional resistance, the force on the front face alone can be obtained and correlated with the pressure measurements.

As mentioned earlier, iceberg models of different keel shapes were pushed horizontally into the sloping sand bed. Theoretically, there should be no base reaction nor base friction since the model moves into a trench pre-cut to its width by the advancing front face. However, because of the development of the frontal surcharge, a situation occurs somewhat similar to the bearing capacity of shallow footing, creating a reaction between the soil and the front end of the base. Base pressure and friction was measured in earlier investigations by Chari (1975), Green (1984), and Abdelnour et al (1980). Attempts were made earlier (Chari, 1975 and Green 1984) to evaluate the frictional component by measuring

the pressure distribution on the sides and the base of the iceberg model. The resistance due to friction was obtained by multiplying the averaged pressure, area of contact, and the coefficient of friction. Abdelnour and Lapp (1980) directly measured the load acting on the sides and base along with the total soil resistance. Chari (1975) reported that the pressures on the sides and base did not contribute significant resistance to forward motion of the model for tests in the underconsolidated clays. For similar studies in dry sand, Green (1984) reported the frictional resistance of the base and sides, as a percentage of total load, to be of the order of 10% and 5% respectively.

In this investigation, a different approach was adopted for estimating the base friction. Two series of tests were conducted; one by towing the iceberg model as it was and another with a thin strip welded to the front bottom edge of the rectangular prismatic model thus eliminating any contact between the base and the soil. The difference between the two tests would thus give the resistance due to base friction. The results obtained by this method are more direct and accurate than those obtained from the method of measuring the pressures. This is confirmed by the fact that in a series of test repetitions, the measured total resistances were more consistent than the measured pressures. For the tests with different frontal keel shapes (models M2,

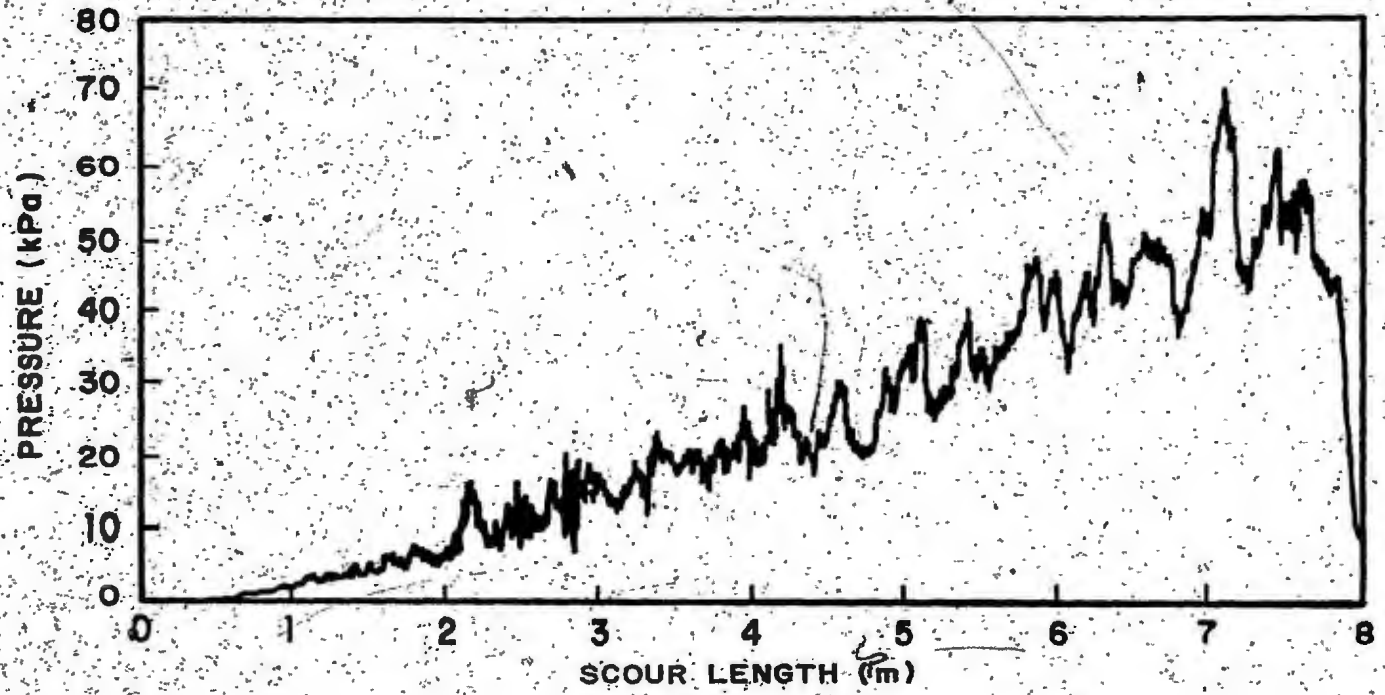

FIGURE 37 TYPICAL PRESSURE TRANSDUCER OUTPUT

M3, and M4), bottom friction was eliminated by attaching the keels with a slight protrusion below the base level. For the curved and wedge shaped models (M5 and M6), two series of tests were conducted, with and without a thin strip welded to the leading bottom edge.

The resistance due to side friction was calculated from measured surcharge dimensions and the active earth pressure coefficient as suggested by Chari and Green (1981).

By subtracting the sum of base friction and side friction from the total resistance measured by the load cells, the soil resistance acting on the front face alone was determined and these results will be discussed later.

5.4 Pressure Distribution on the Front Face

The soil resistance on the front face of the model was also obtained by measuring the pressure distribution using flush-mounted pressure transducers. These front face forces were also subsequently correlated with the various theories of passive earth pressure. The typical output of the pressure transducer during a test is shown in Fig. 37. The locations of pressure transducers on the front face of the models are indicated in Figs. 38 and 39. Fig. 40 shows the pressure distribution on the front face of the rectangular prismatic model (M1) at scour lengths of 2, 4, 6, and 8 m. Pressures on the front face were measured in both

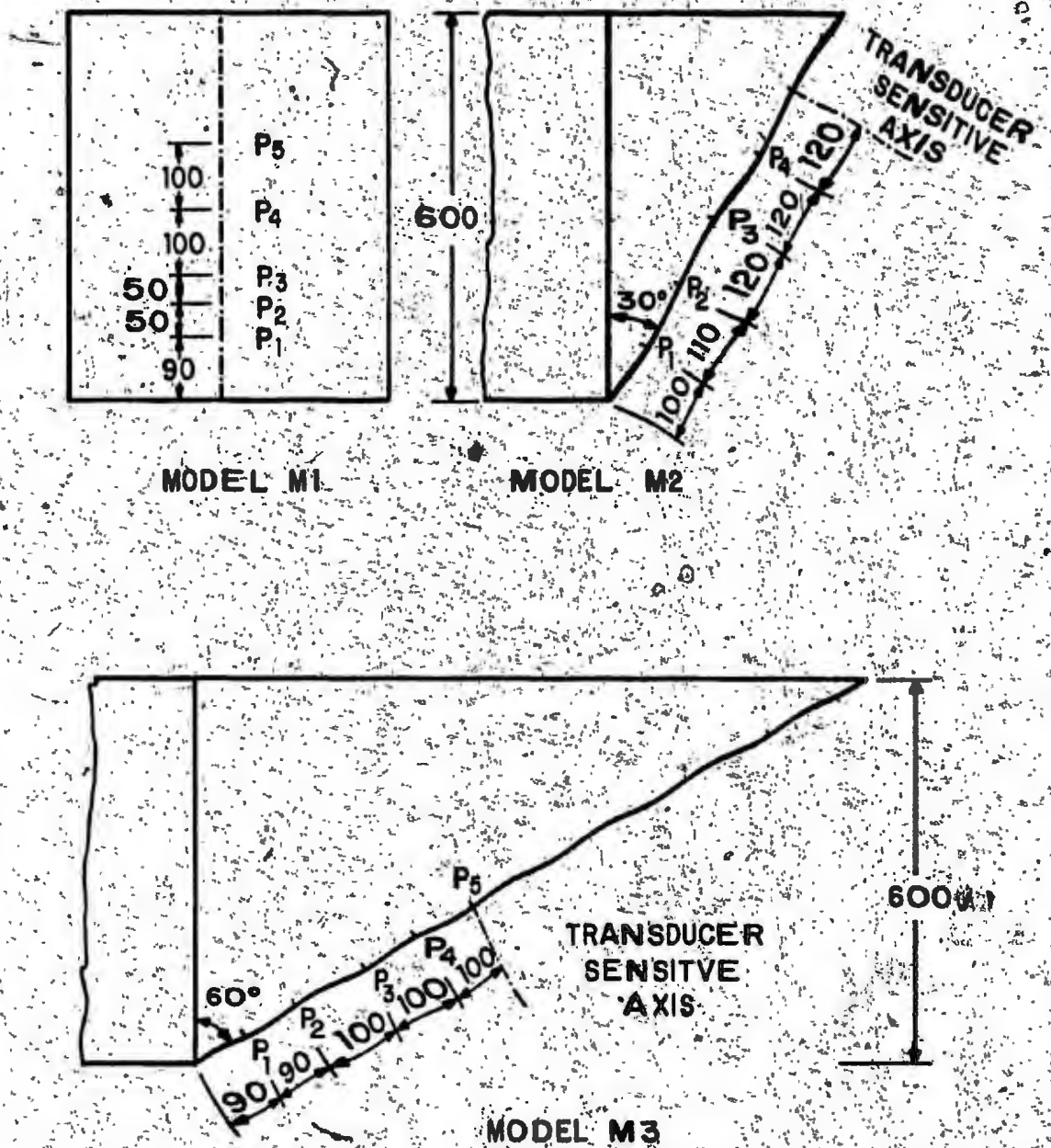

FIGURE 38 PRESSURE TRANSDUCER LOCATIONS FOR MODELS M1, M2, and M3 (ALL DIMENSIONS ARE IN mm)

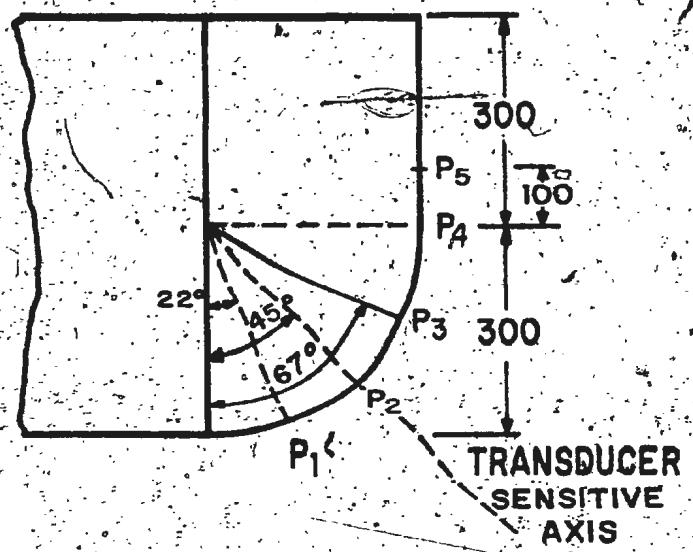

(a) MODEL M4

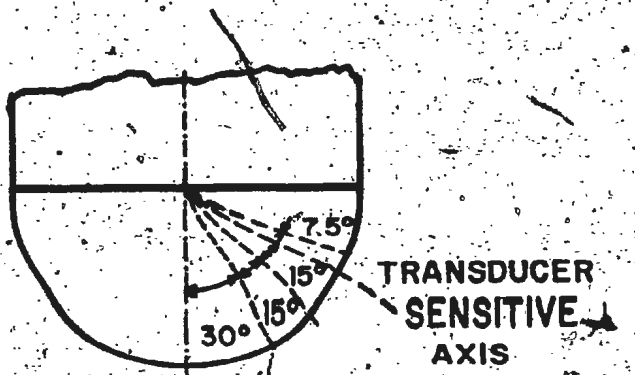

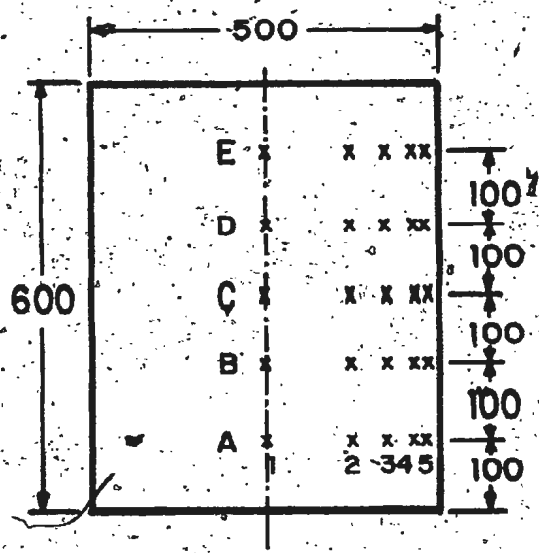

(b) MODEL M5

FIGURE 39 PRESSURE TRANSDUCER LOCATIONS FOR MODELS M4 and M5

(ALL DIMENSIONS ARE IN mm)

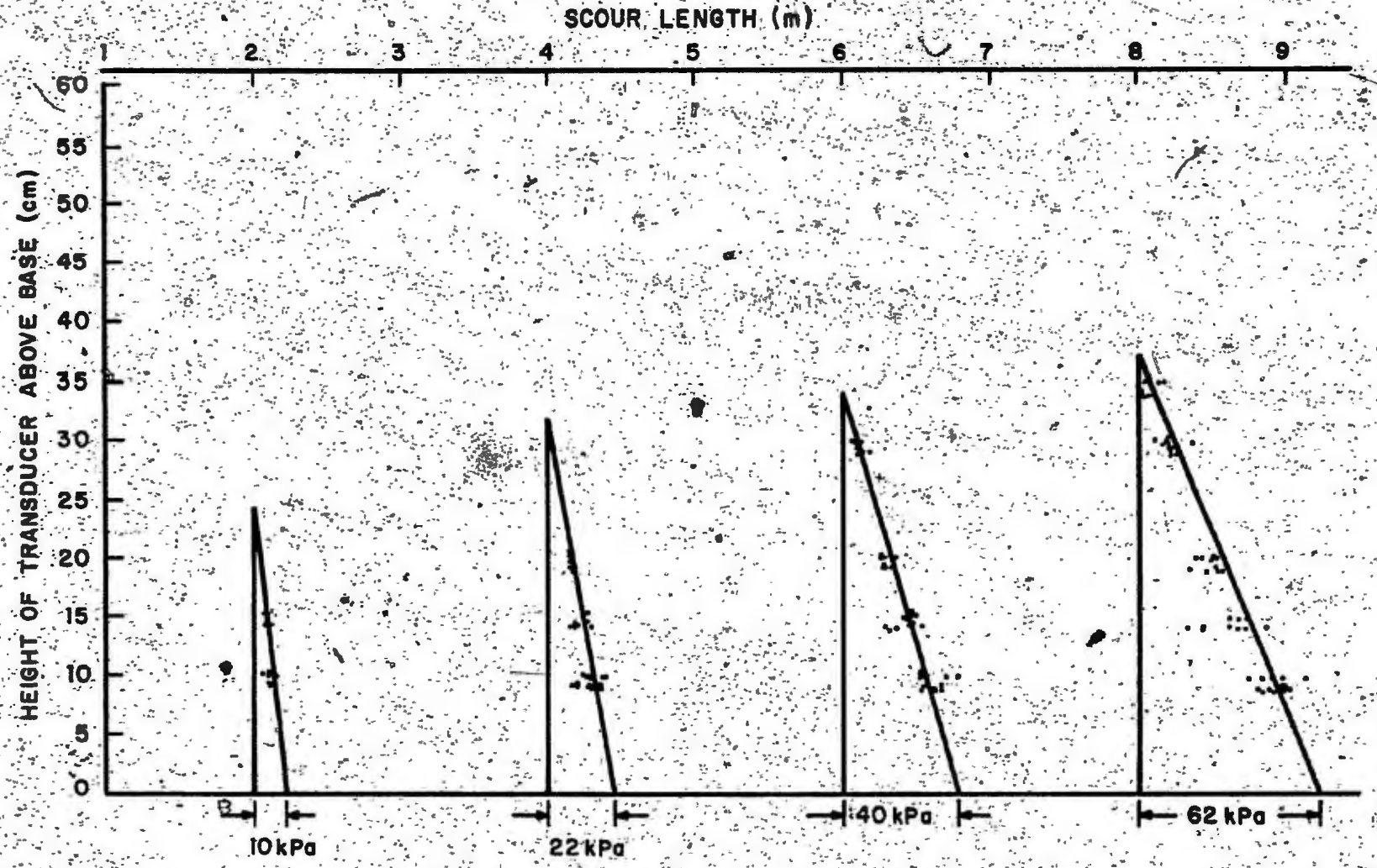

FIGURE 40 PRESSURE DISTRIBUTION ON THE FRONT FACE OF RECTANGULAR PRISMATIC MODEL (M1)

series of tests, with the base in contact with the soil and with base friction excluded. The total force on the front face was obtained by integrating the pressure, which was then compared with the total soil resistance measured by load cell as shown in Fig. 41. The integrated pressures represents the total force acting only on the front face of the model. The total measured resistance comprises of the front face passive resistance, the frictional force on the sides, and the base friction. The frictional force on sides can be computed from the measured surcharge of the excavated soil, using the active earth pressure coefficients and the coefficient of friction between the model and sand. The computed frictional force was found to be in the order of 4% of the measured total resistance. This compares well with the side friction of 5% reported by Green (1984). The base friction obtained from the two series of tests ranges from 36% of the total resistance at the beginning of the scour to about 20% at the end of scour. This is slightly higher than that reported by Green (1984). By deducting the sum of base friction and side friction from the total resistance, the force on the front face alone is obtained and compared with integrated pressures in Fig. 41. There is a good correlation between the two types of computation and the small difference between the two curves is attributed to the variation in pressure readings and the limited number of pressure transducers used on the front face.

Figure 42 shows the pressure distribution on the front face of the model M2 which has a 30° inclination. The horizontal component of the front face normal force face was obtained from the measured pressures, the total resistance measured by load cell, and the computed side friction are shown in Fig. 43. It may be noted that the base friction was not computed as the lower edge of the front keel was located slightly lower than the base of the model. The normal force on the front face was obtained from the measured pressures. However, the magnitude of the horizontal component of this force depends on the wall friction mobilized between the model and the soil. Figure 43 shows the horizontal component of the normal force for two values of δ_m, $\phi/2$ and $2\phi/3$, where δ_m is the mobilized friction and ϕ the angle of shear resistance of the soil. There is a good correlation between pressure measurements and front face resistance. A similar comparison is shown in Figs 44 and 45 for the model M3, which has a front face inclination of 60°. It has to be noted that the angle of shear resistance ϕ is not constant as is commonly assumed. There is likely to be slight increase in the value of ϕ with increasing depth of cut of the scour trench. Thus the value of δ_m is also not constant and the effect of the variation of δ_m is seen in the correlations in Fig. 45. A comparison of pressure distribution on the front

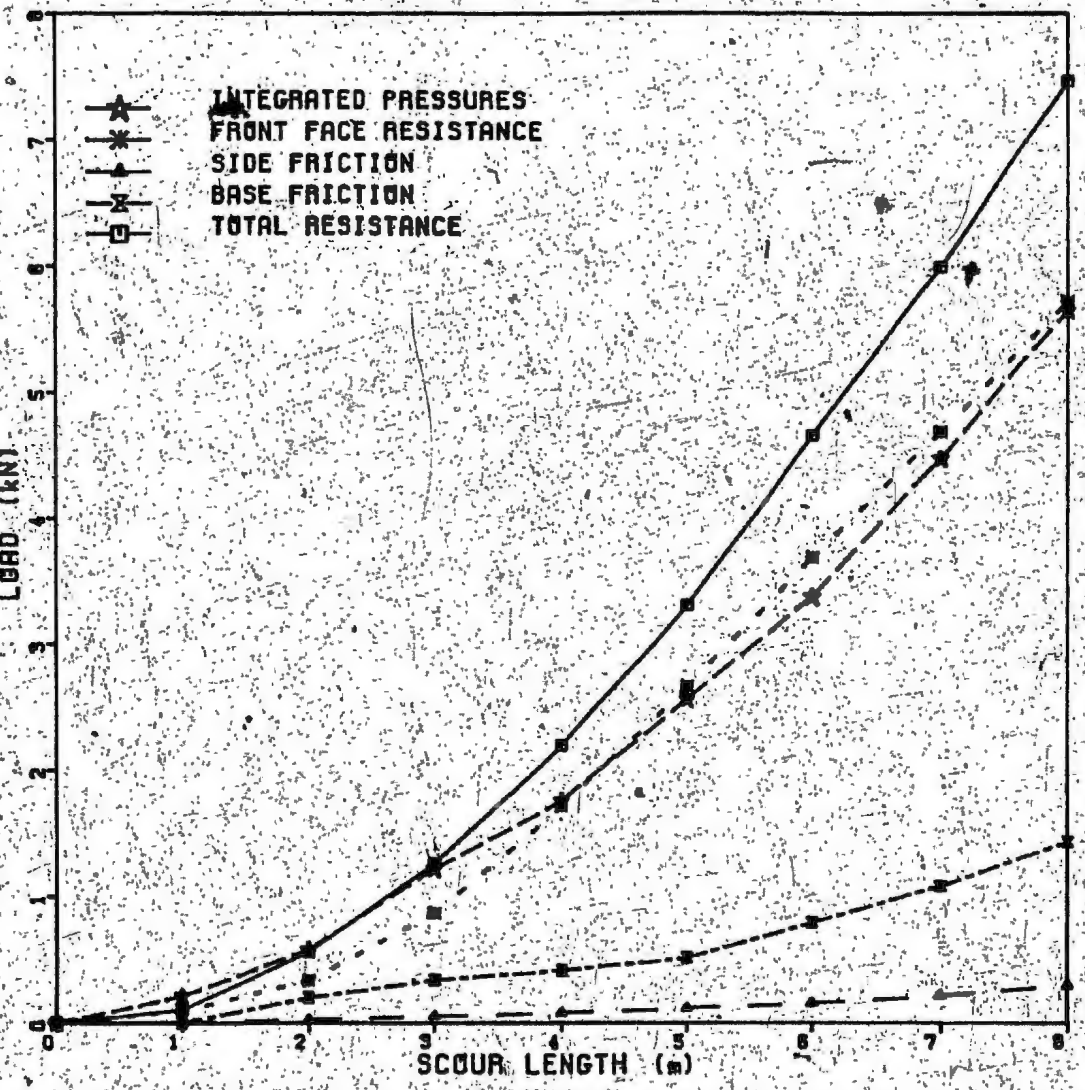

FIGURE 41 COMPARISON OF INTEGRATED PRESSURES WITH FRONT FACE RESISTANCE FOR MODEL M1

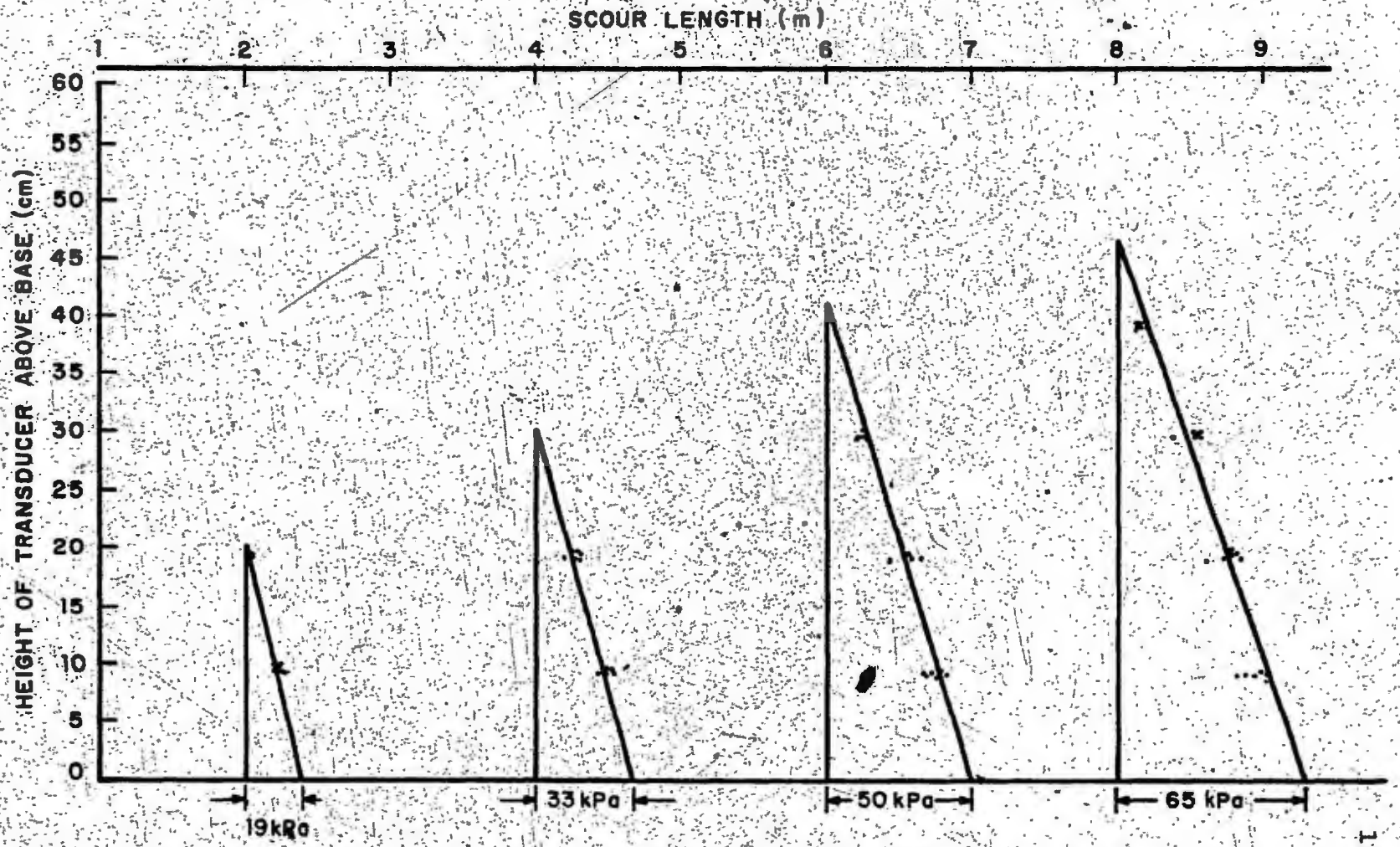

FIGURE 42 NORMAL PRESSURE DISTRIBUTION ON THE FRONT FACE OF 30° INCLINED PROFILE (M2)

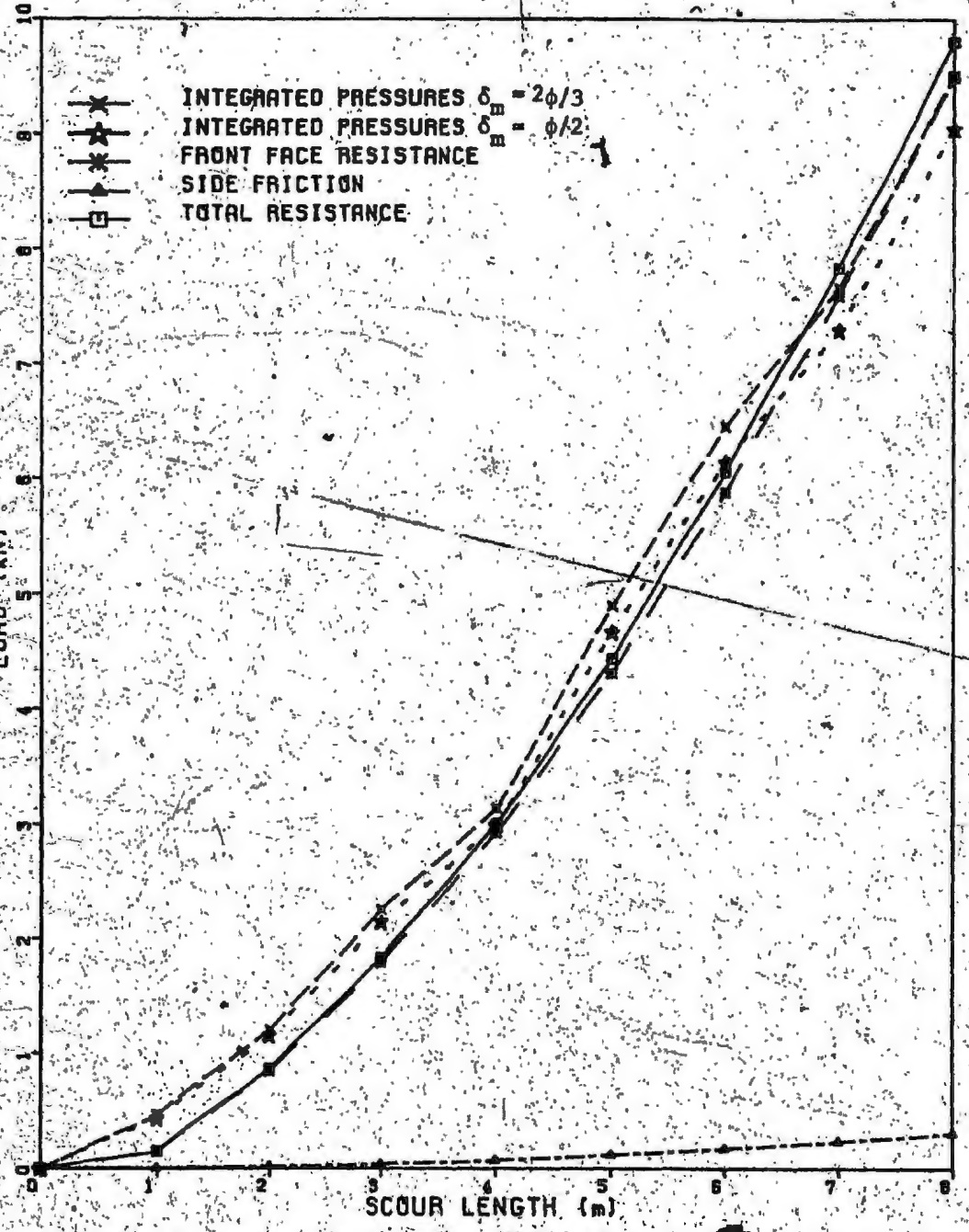

FIGURE 43 : COMPARISON OF INTEGRATED PRESSURES WITH FRONT FACE RESISTANCE FOR MODEL M2

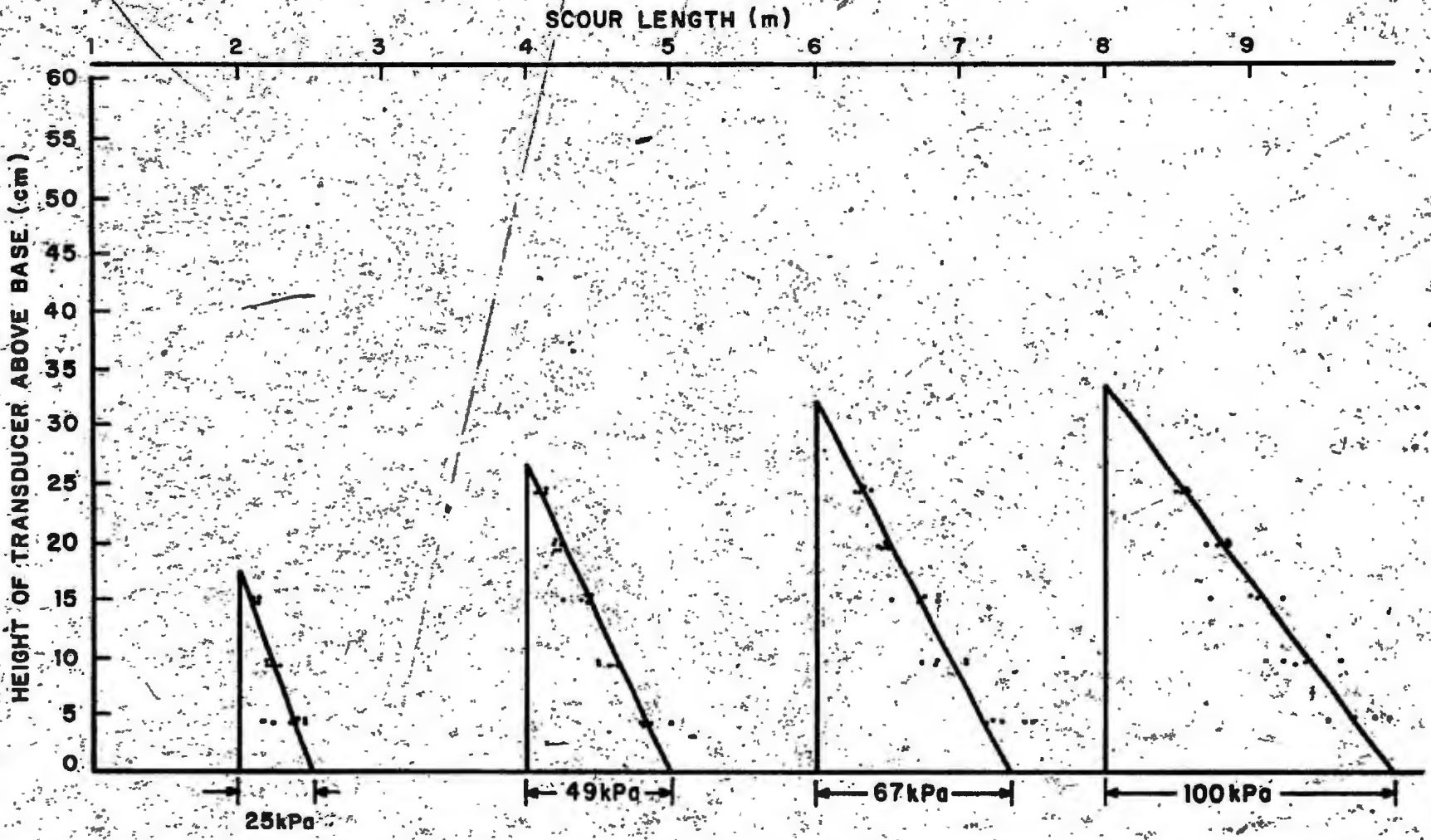

FIGURE 44 NORMAL PRESSURE DISTRIBUTION ON THE FRONT FACE OF 60° INCLINED PROFILE (M3)

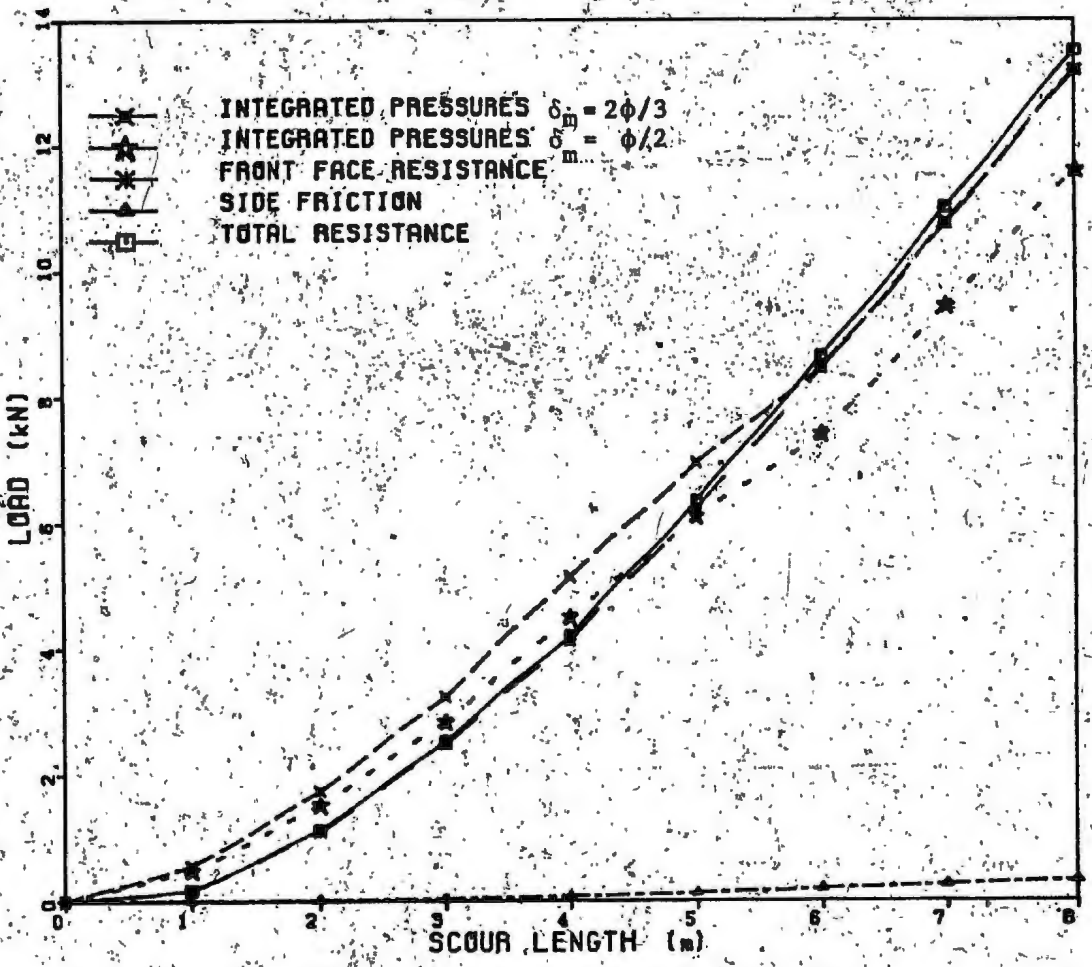

FIGURE 45 COMPARISON OF INTEGRATED PRESSURES WITH FRONT FACE RESISTANCE FOR MODEL M3

face for models M1, M2, and M3 (Figs. 40, 42, and 44) indicates that the front face pressures may be approximated as a hydrostatic distribution even for the inclined surfaces. Also, it can be seen that the measured pressures increase with the inclination of the front face. This is to be expected because when the inclined surface is given a lateral displacement, the displacement normal to the face has two components one vertical and other horizontal. The vertical subgrade reaction is higher than the horizontal subgrade reaction and therefore the pressure increases with increased inclination of the front face. Further, for the same vertical depth of cut, the area of contact between soil and model increases with increasing inclination. The front face pressure distribution on model M4 with a curved keel is shown in Fig. 46. For this model the pressures were also measured normal to the surface. While the pressure distribution was linear for the plane surfaces of models M1, M2, and M3, for the curved model M4, the pressure distribution is non-linear. This is consistent with the earlier observation that the soil pressure not only increases with depth, but is also influenced by the inclination of the keel, which for the cutved surface increases gradually with the depth. The pressure at the leading edge (Fig. 46) was assumed to be zero. However, as discussed earlier, there is likely to be some upward pressure at this edge and ideally, it would have

been desirable to measure its magnitude. In fact, Chari (1975) and Green (1984) measured it for the rectangular model in clay and sand respectively. Assuming the distribution shown in Fig. 46, the horizontal component of the force on the front face was computed for the maximum mobilized wall friction and compared with the measured total soil resistance as shown in Fig. 47. There is a relatively large difference (20%) between the integrated pressures and the resistance obtained from load cell measurements. This is in accordance with the foregoing discussion about the pressure between the leading edge of the model and the first point of pressure measurement. Back calculations were made from the comparison made in Fig. 47 and the most likely pressure distribution on the bottom section of the keel is also shown in Fig. 46. This is realistic and in conformity with the earlier reports of Chari (1975) and Green (1984). The problem of earth pressures on curved surfaces such as the model M4 is not well documented in the geotechnical literature. This is an area of potential further theoretical and experimental research.

The pressure distribution on the model M5 which is cylindrical in plan is shown in Fig. 48. This model is somewhat similar to a cylindrical pile. The variation of pressure at four scour lenghts (2, 4, 6, and 8 m) for the four rows of pressure transducers is shown in the figure.

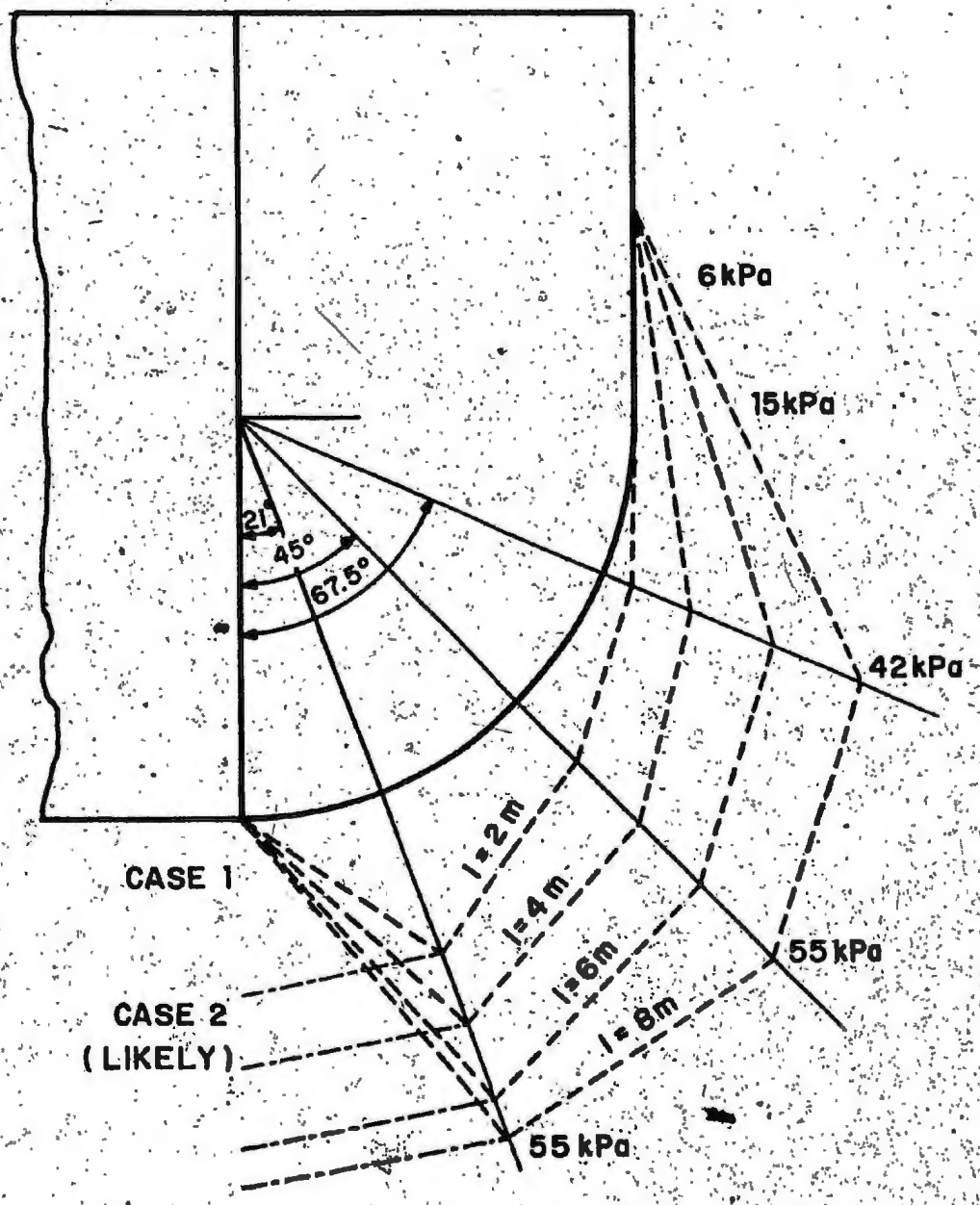

FIGURE 46 NORMAL PRESSURE DISTRIBUTION ON THE FRONT FACE OF CURVED PROFILE (M4)

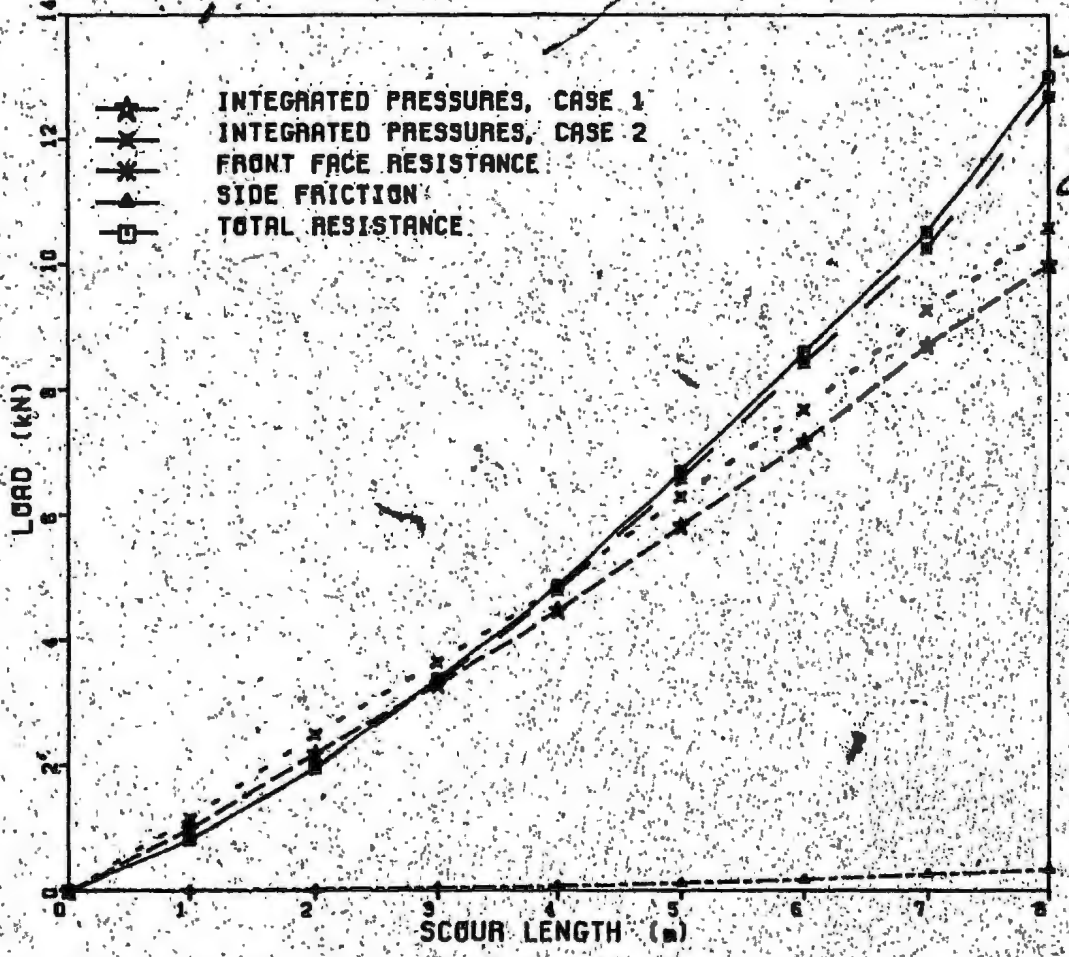

FIGURE 47 COMPARISON OF INTEGRATED PRESSURES WITH FRONT FACE RESISTANCE FOR MODEL M4

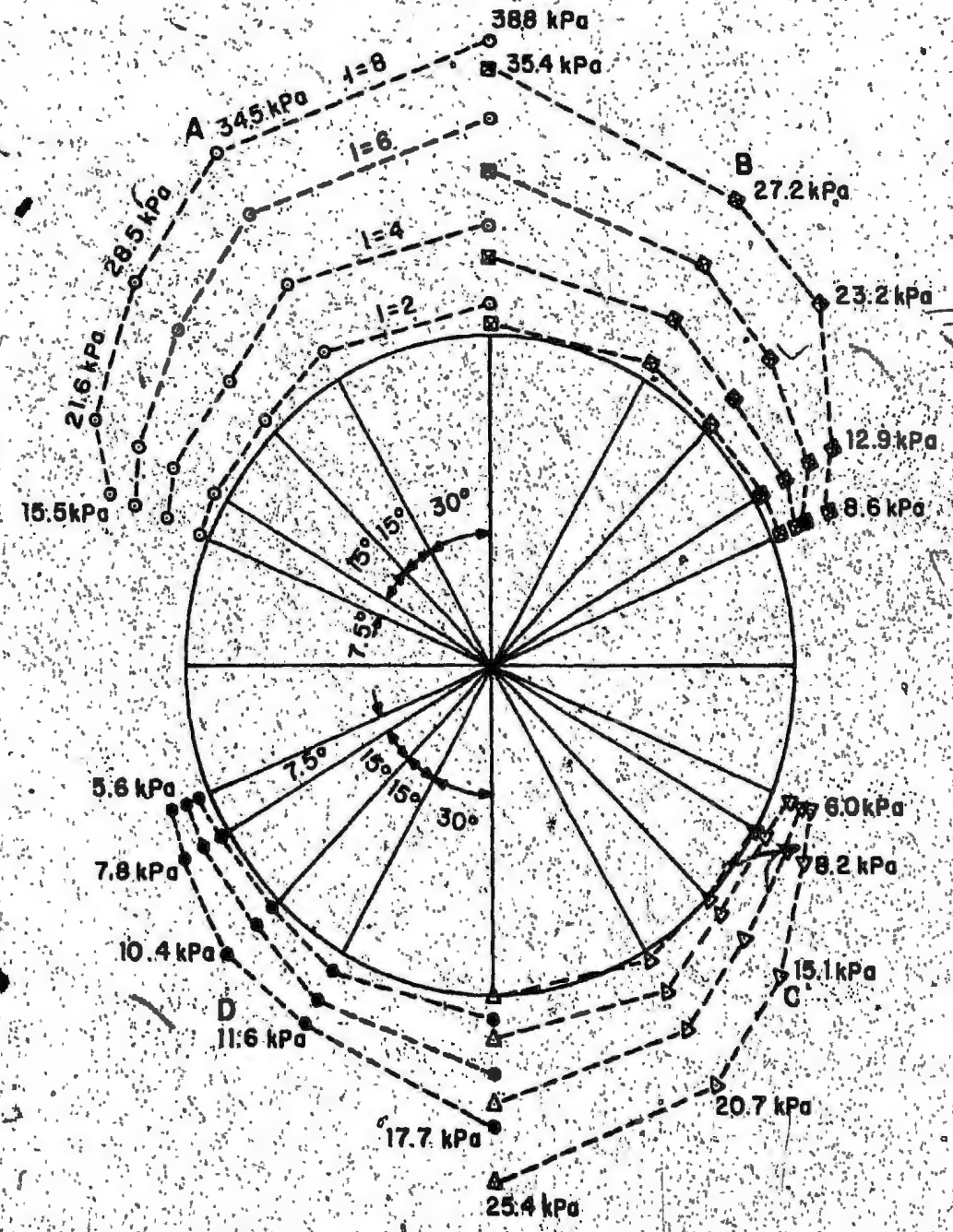

FIGURE 48. NORMAL PRESSURE DISTRIBUTION ON THE FRONT FACE OF CYLINDRICAL MODEL (M5)

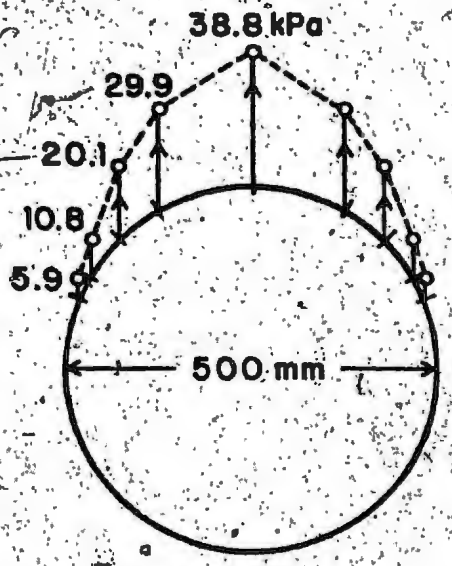

(a) IN THE DIRECTION OF MOVEMENT

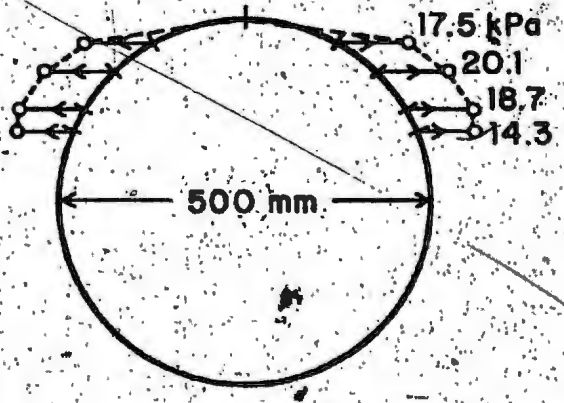

(b) NORMAL TO THE DIRECTION OF MOVEMENT

FIGURE 49 COMPONENTS OF NORMAL PRESSURE ON THE CYLINDRICAL MODEL (M5)

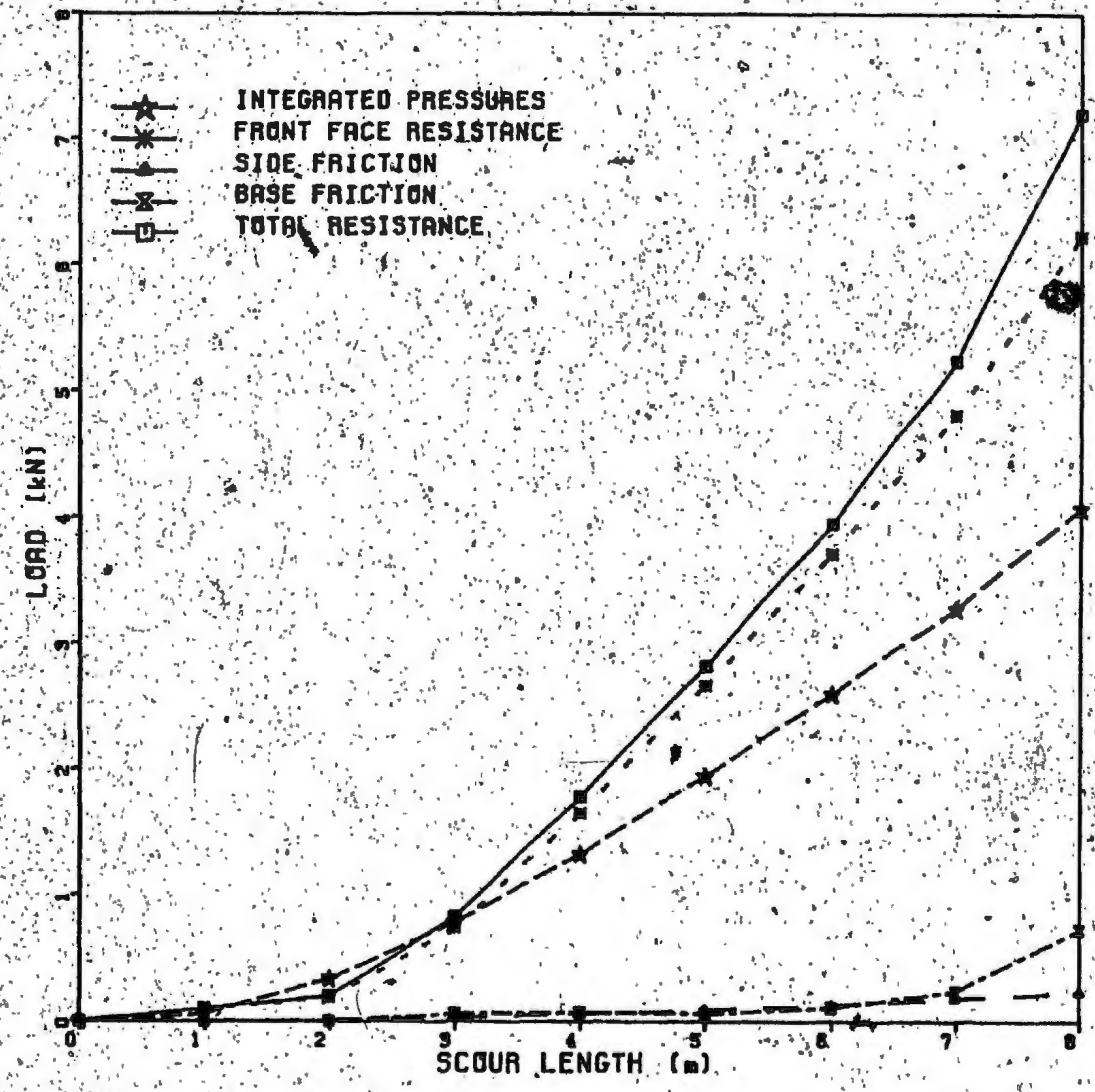

FIGURE 50 COMPARISON OF INTEGRATED PRESSURES WITH FRONT FACE RESISTANCE FOR MODEL M5

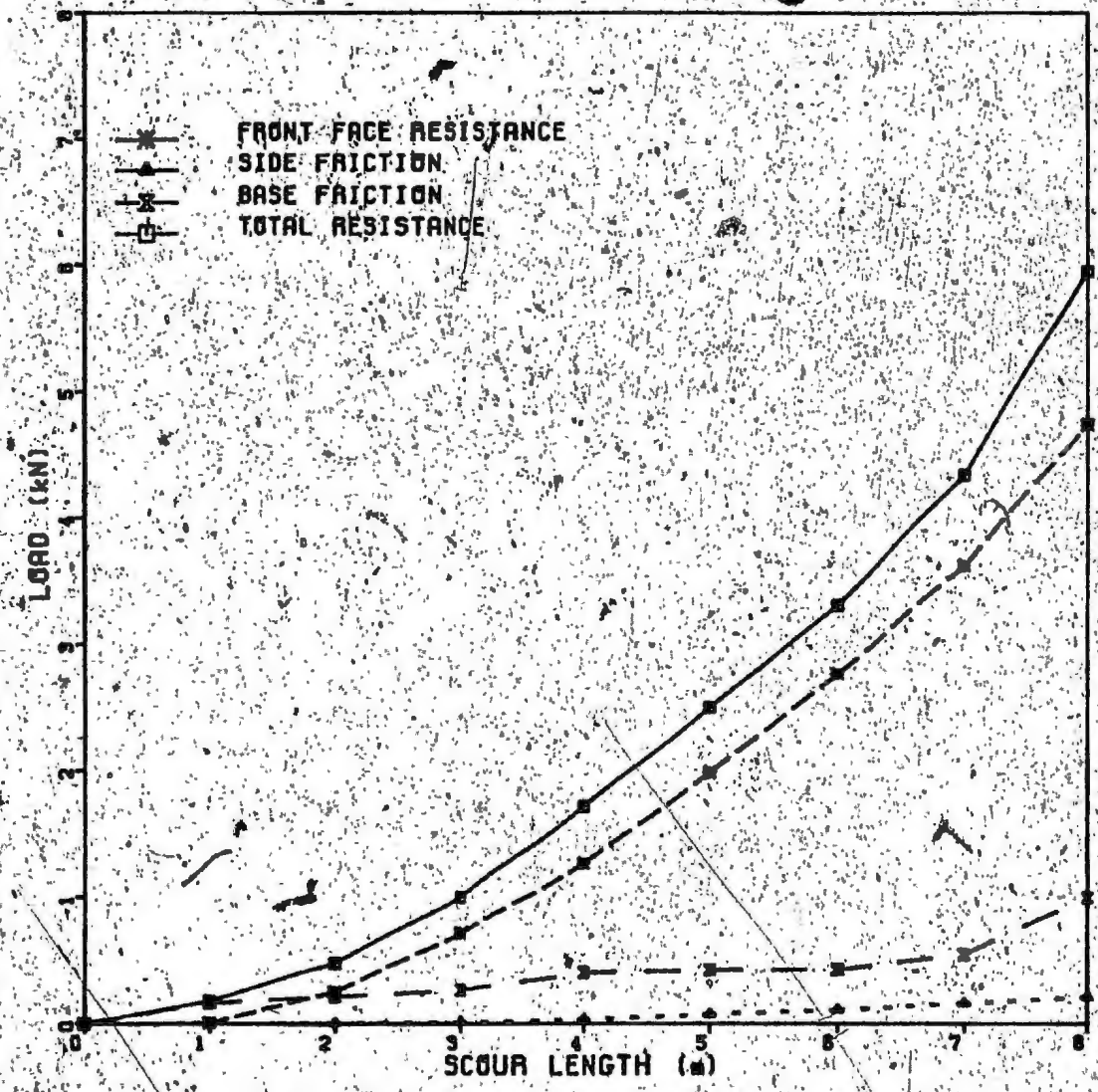

FIGURE 51 SEPARATION OF FRONT FACE RESISTANCE FROM TOTAL RESISTANCE FOR WEDGE SHAPED MODEL (M6)

The pressure is a maximum at the apex of the cylinder and gradually reduces towards the ends of the diameter. Figure 49 shows the pressure distribution in the two reference directions, parallel and normal to the direction of movement of the model. The pressure distribution is somewhat similar to that reported for laterally loaded short piles (Joo 1985). The total force on the model was computed from the measured pressures and compared with the load cell readings as was done for the other models. The results are shown in Fig. 50.

Tests were conducted with the wedge shaped model (M6), but the pressures on the front wedge could not be obtained with consistency due to instrumentation problems. However, the total force on the model, the base friction and side friction are shown in Fig. 51. It can be seen from this figure that base friction was rather high in the initial portion of the scour length because of the wedge shape and the relatively large base area in contact with the soil during the initial portion of the test.

The average unit base friction was calculated for the different models and was found to be 2.9, 2.4 and 2.8 kPa for the models M1, M5, and M6 respectively, which indicates some uniformity.

5.5 Correlation with Theoretical Methods

In the previous sections, the iceberg-soil interaction was verified experimentally. Before incorporating the shape effects in the analytical model, it was first decided to correlate the measured pressures with the available theories of passive earth pressure. Conventional earth pressure theories consider plane surfaces and limited soil deformations such as those occuring in foundations and earth retaining structures. However, some of the recent research on agricultural tillage equipment and earth moving machines has some similarities with iceberg scouring. The results of Harrison (1973) are supported by experiments. But the surcharge is not large nor is the soil on a slope in tillage experiments. Thus, any theoretical correlation of the iceberg scour experiments require further modifications of existing theories.

The dimensional analysis used in agricultural engineering research, even though simple, is not used here because the variables such as unit weight, internal soil friction and wall friction angle were not changed in this investigation. All the theories currently available and used in the present analysis are applicable to plane strain conditions. A review of these was given in Chapter II.

The results for the idealized prismatic model with the vertical front are shown in Fig. 52. The figure also shows the theoretical results using the various theories discussed in Chapter II. All theories give somewhat similar results but the Coulomb's theory is closest to the experimental results. Coulomb's method with a plane failure surface is generally known to overestimate the passive resistance when the wall friction is high; this effect is seen in the initial portion of the tests. However, the agreement is better in the later part of the experiments when the soil surcharge is greater than the weight of the failure soil wedge. The results from the other theories are within 20% of the experimental values. A similar comparison for models M2 and M3 is shown in Fig. 53 and 54. It can be seen that for the models with a sloping keel, the results are in the general range of values obtained by various theories and no particular theory can be said to be in good agreement with the experimental results.

For the curved profile of model M4, the nearest theory which can be used for the analysis is that of Harrison (1973). For this model, the slope of the contact surface changes with increasing depth of scour. Terzaghi and Peck (1967) and Shields and Tolunay (1973) assume that the angle of wall friction is fully mobilized and passive earth resistance generally acts in the direction suggested by

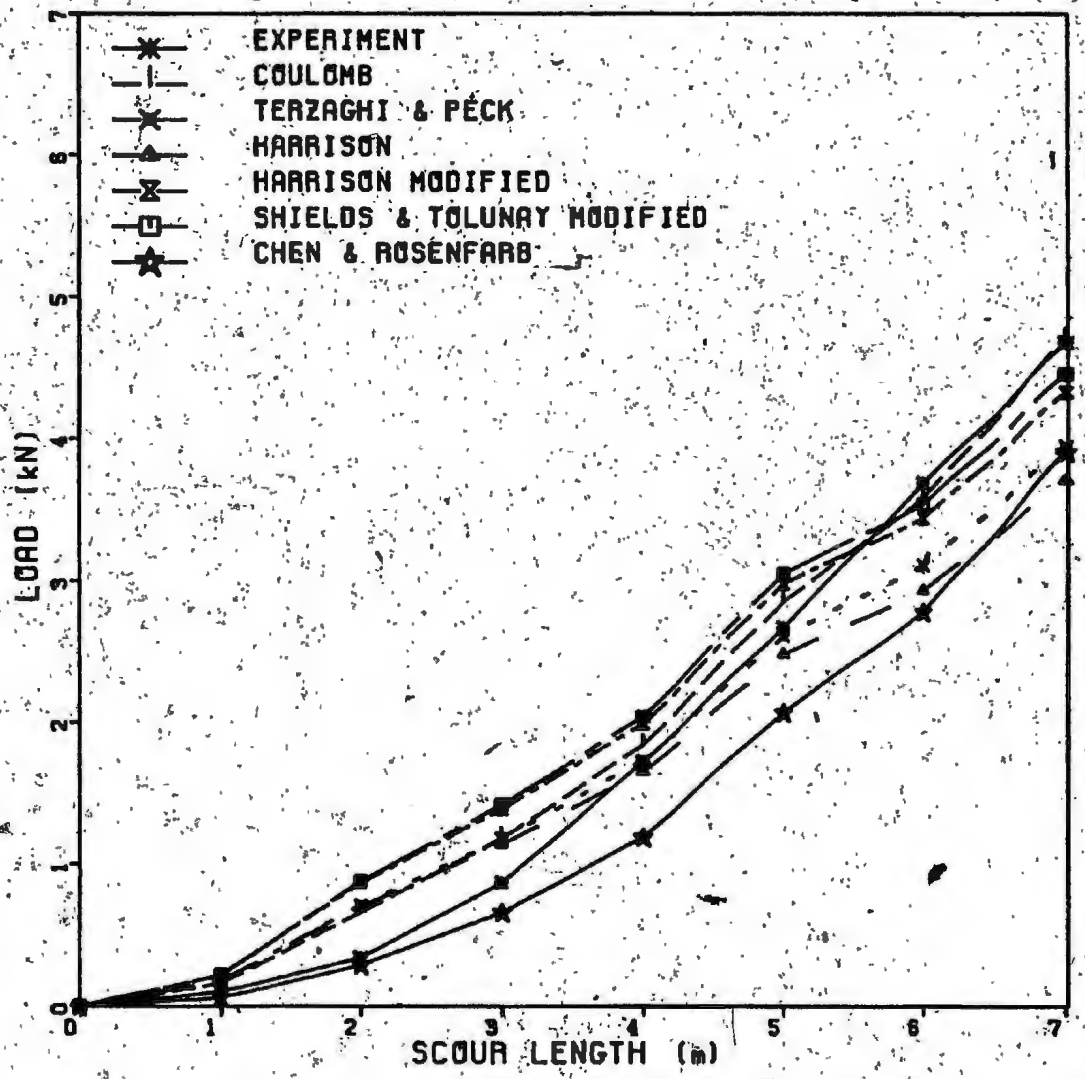

FIGURE 52 CORRELATION OF MEASURED AND COMPUTED FRONT FACE RESISTANCE FOR RECTANGULAR PRISMATIC SHAPE (M1)

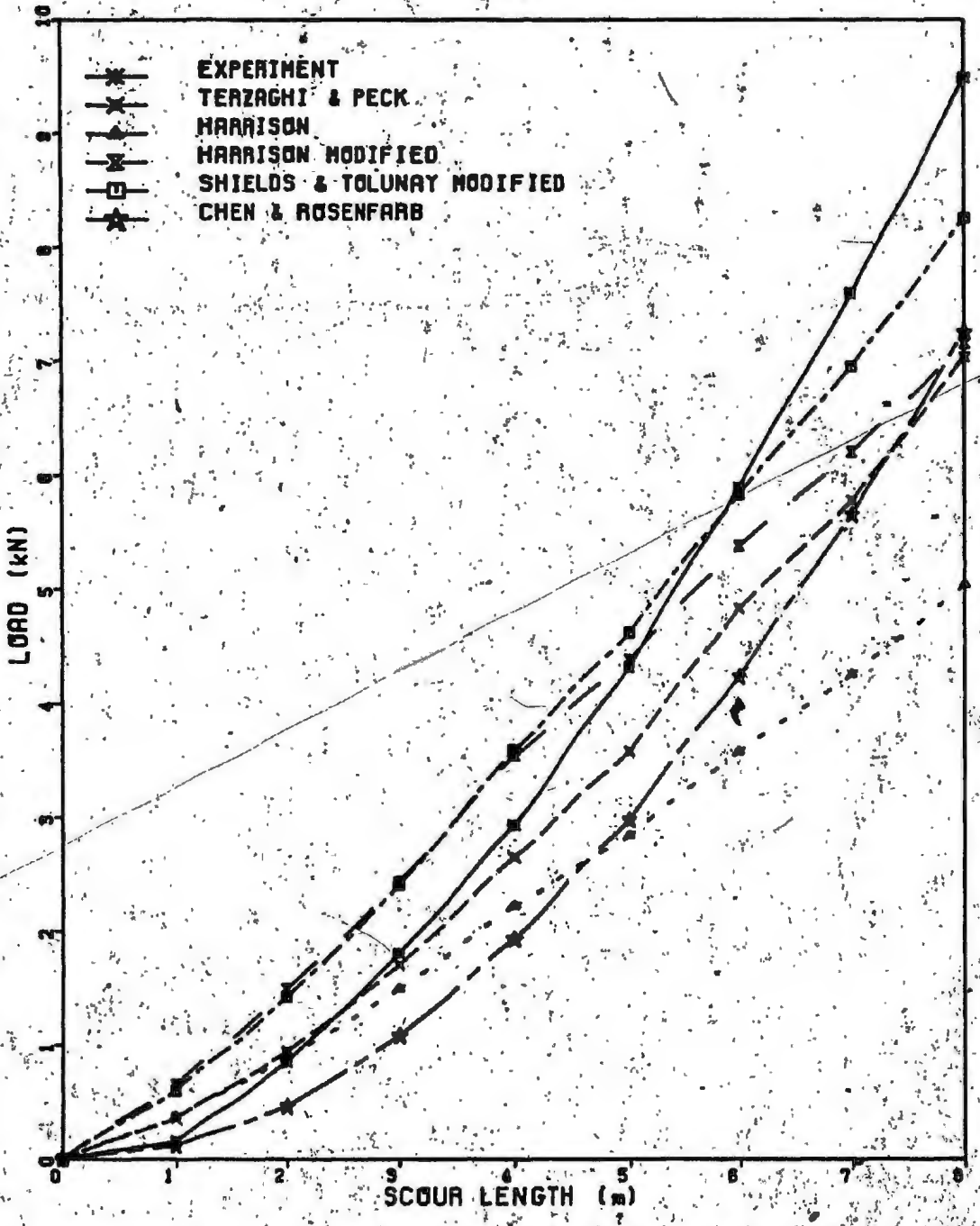

FIGURE 53 CORRELATION OF MEASURED AND COMPUTED FRONT FACE RESISTANCE FOR 30° INCLINED PROFILE (M2)

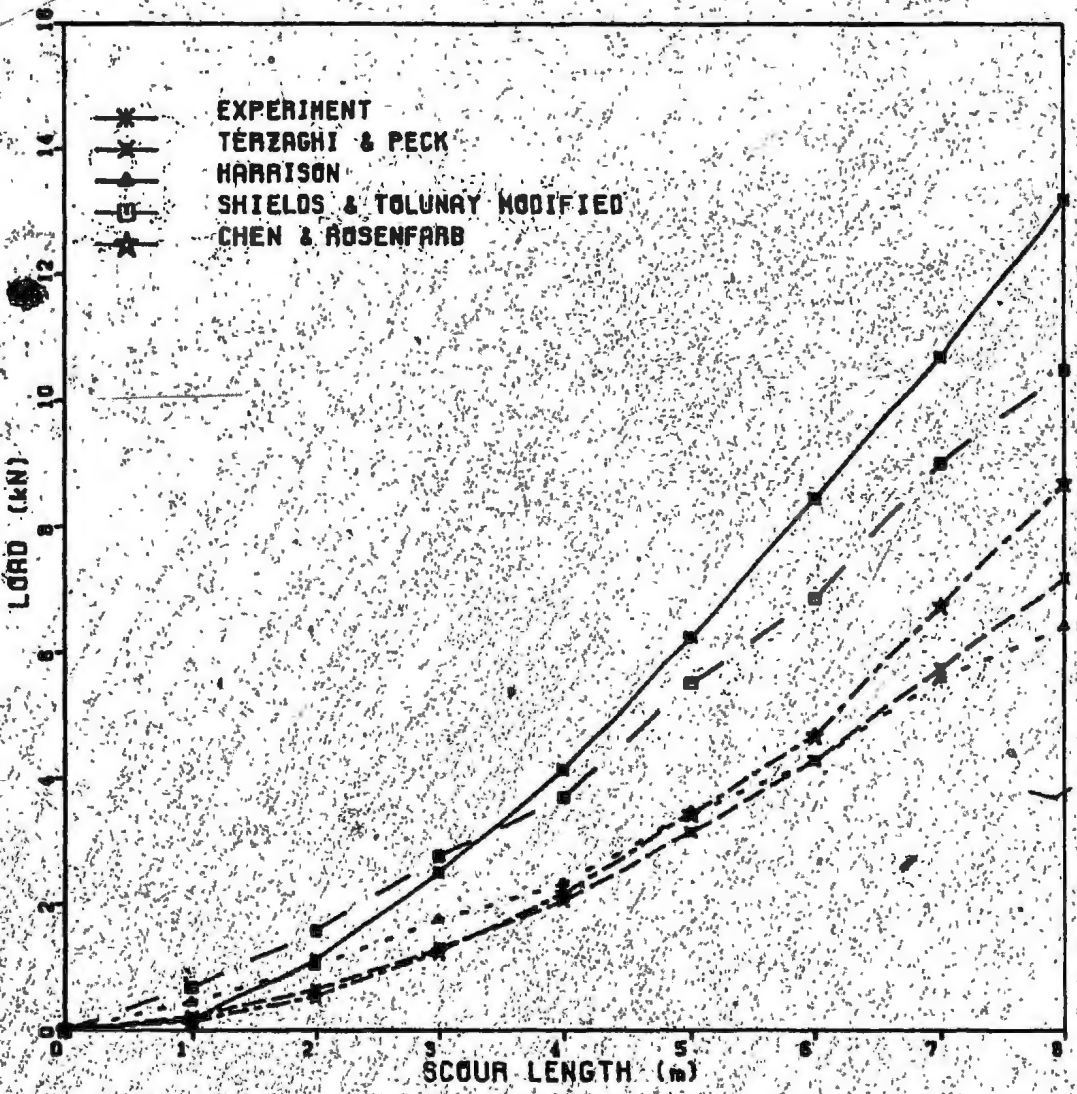

FIGURE 54 CORRELATION OF MEASURED AND COMPUTED FRONT FACE RESISTANCE FOR 60° INCLINED PROFILE (M3)

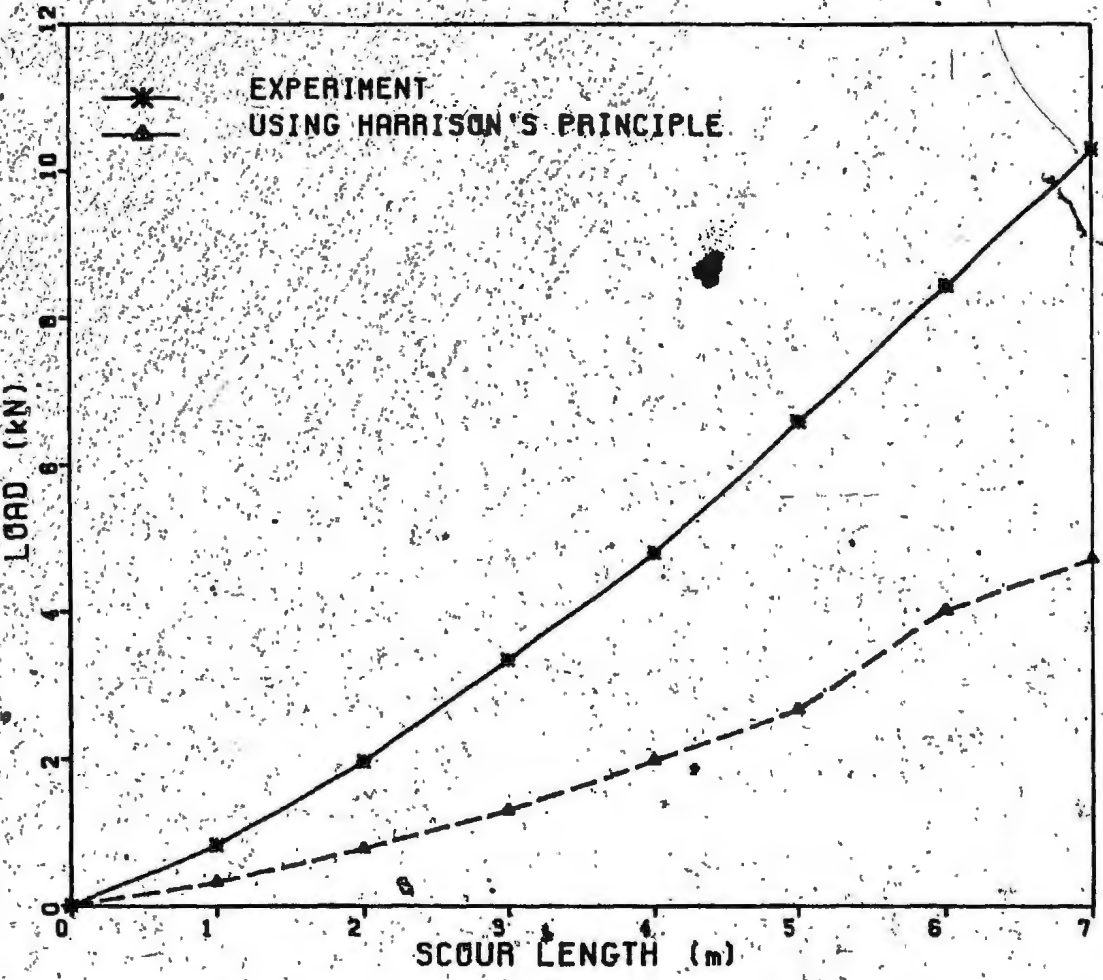

FIGURE 55 CORRELATION OF MEASURED AND COMPUTED FRONT FACE RESISTANCE FOR CURVED PROFILE (M4)

Terzaghi (1943). For large inclinations of the wall, if such an assumption is made, the horizontal component of the force will be in the direction of the wall movement; a condition which will not occur. On the other hand, the method of Harrison (1973) facilitates the calculation of the mobilized friction angle from the wall geometry and soil parameters which are then used in computing the soil resistance. However, even in this case, for large inclinations of the front face, this computed friction angle turns out to be negative and underestimates the passive resistance. In fact, a comparison of Harrison's (1973) own experimental results with his predictions were 28% higher. A similar trend is seen with the results obtained from this investigation. As already mentioned, there is a present need to develop a suitable theory of earth pressure for walls of large inclinations and curved profiles.

The theoretical expression for passive resistance on the cylindrical model (M5) was derived using the approach of Prater (1976) in which the pressure on mine shaft linings has been examined. The results of horizontal force can be given as:

$$P_h = \frac{\pi\gamma D^3}{\sin(\alpha-\beta)} \left[\frac{\tan(\alpha+\phi)\cos\alpha\cos\beta}{6\sin(\alpha-\beta)} + \frac{r_o \tan(\alpha+\phi)}{2H'} \right] - \frac{k_o}{6}\left(1 - \frac{\cos\alpha\sin\beta}{\sin(\alpha-\beta)}\right) \frac{\cos(\alpha+\phi)\cos\delta}{\cos(\alpha+\phi+\delta)} \quad [14]$$

where γ = unit weight of sand

D = depth of cut

α = failure surface inclination to horizontal

β = slope angle of backfill

ϕ = internal friction of soil

α = wall friction

r_o = radius of cylinder

The above expression can be minimized with respect to the angle of inclination α of the failure surface and the passive earth pressure computed. Figure 56 shows that a good correlation is obtained when the mobilized friction angle is assumed to be between $\frac{\phi}{2}$ and $\frac{\phi}{3}$.

For the wedge shaped model (M6), passive earth pressures developed on both faces of the wedge were computed and the horizontal component in the direction of travel of the model was calculated using Coulomb's method. There is a good correlation between measured and computed values as shown in Fig. 57.

5.6 Application of Experimental Results to the Scour Model

Results of laboratory tests with models of different shapes has shown that the soil resistance varies with the keel shape. Assuming the idealized prismatic model (M1) as the reference, the total forces on the other shapes were normalized as shown in Fig. 58. From this comparison,

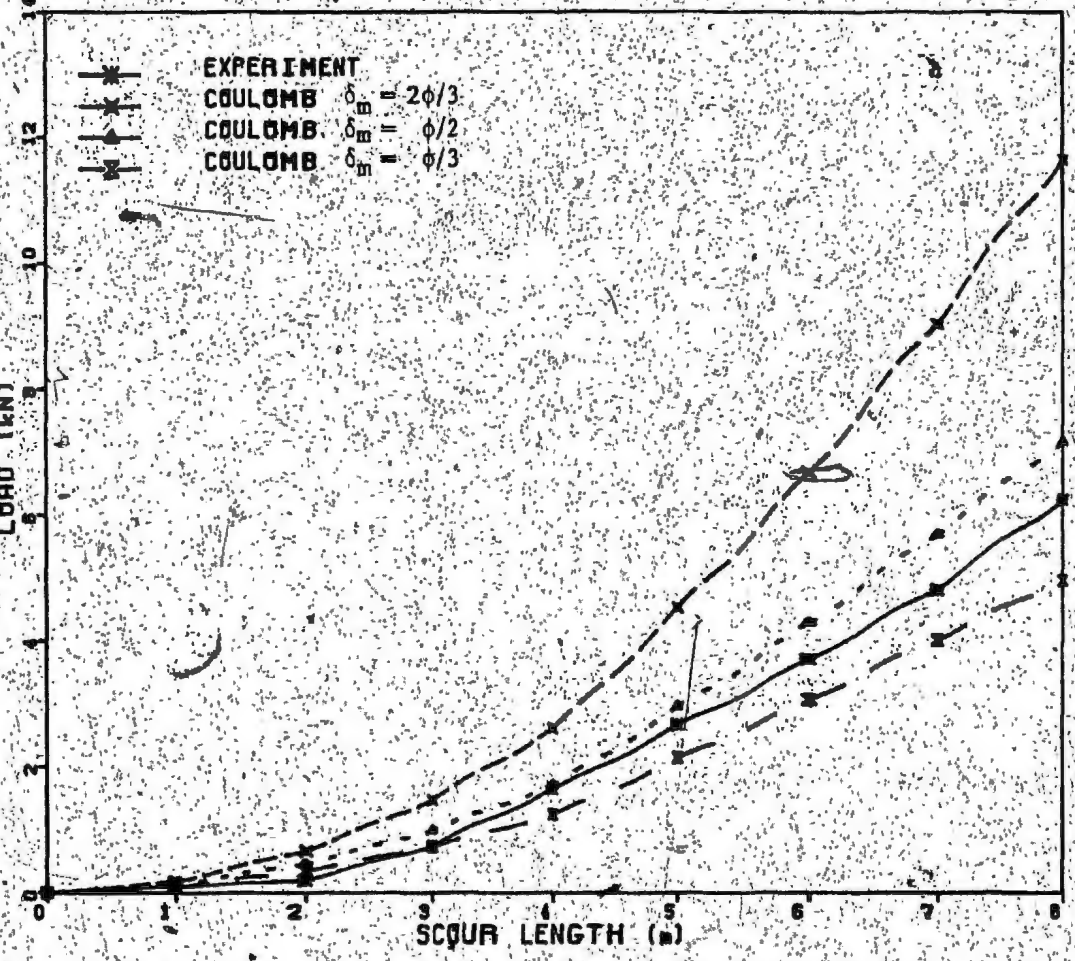

FIGURE 55 CORRELATION OF MEASURED AND COMPUTED FRONT FACE RESISTANCE FOR CYLINDRICAL MODEL (45)

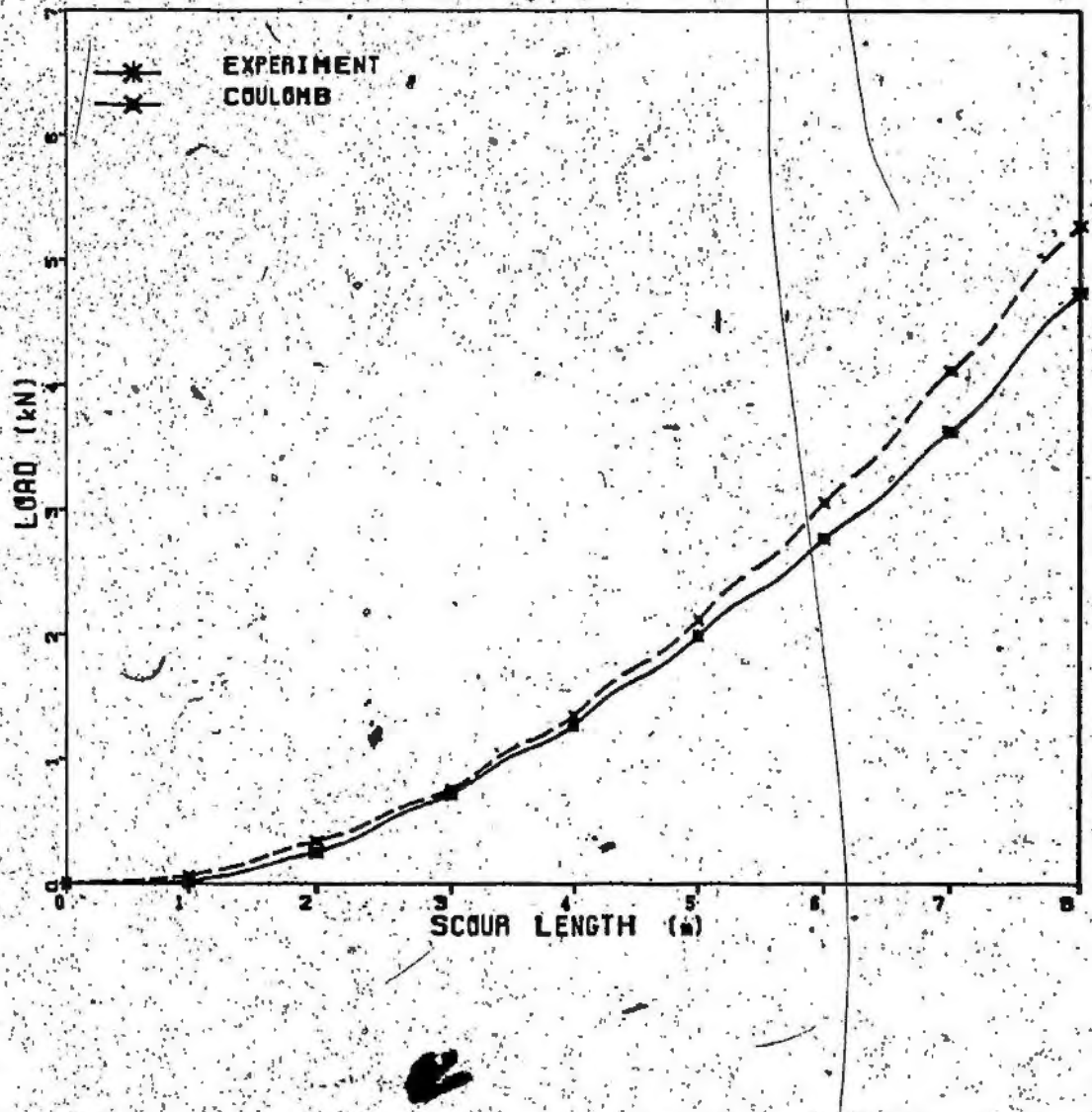

FIGURE 57 CORRELATION OF MEASURED AND COMPUTED FRONT FACE RESISTANCE FOR WEDGE SHAPED MODEL (M6)

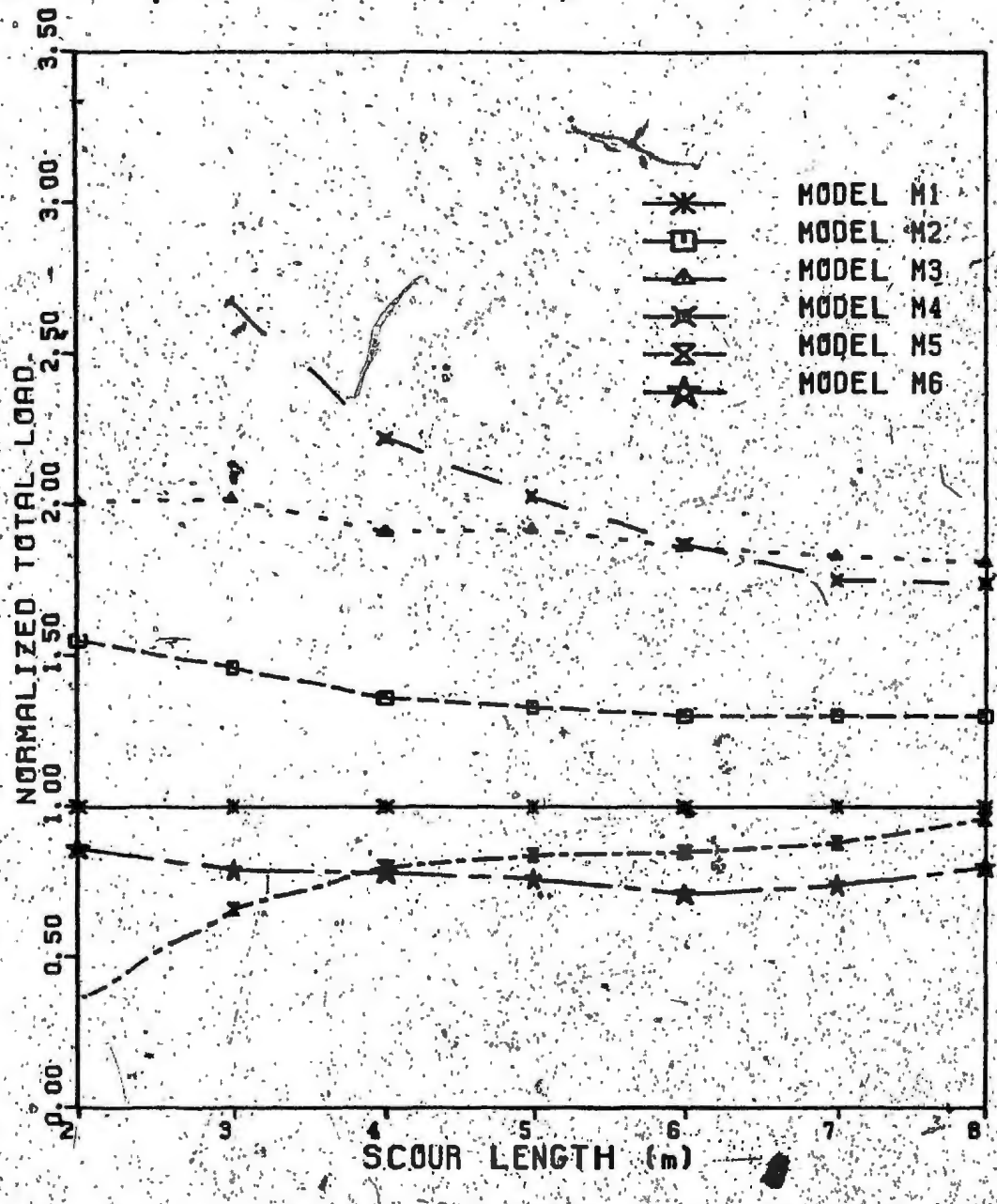

FIGURE 58 NORMALIZED TOTAL LOAD FOR DIFFERENT SHAPES WITH RESPECT TO RECTANGULAR PRISMATIC SHAPE

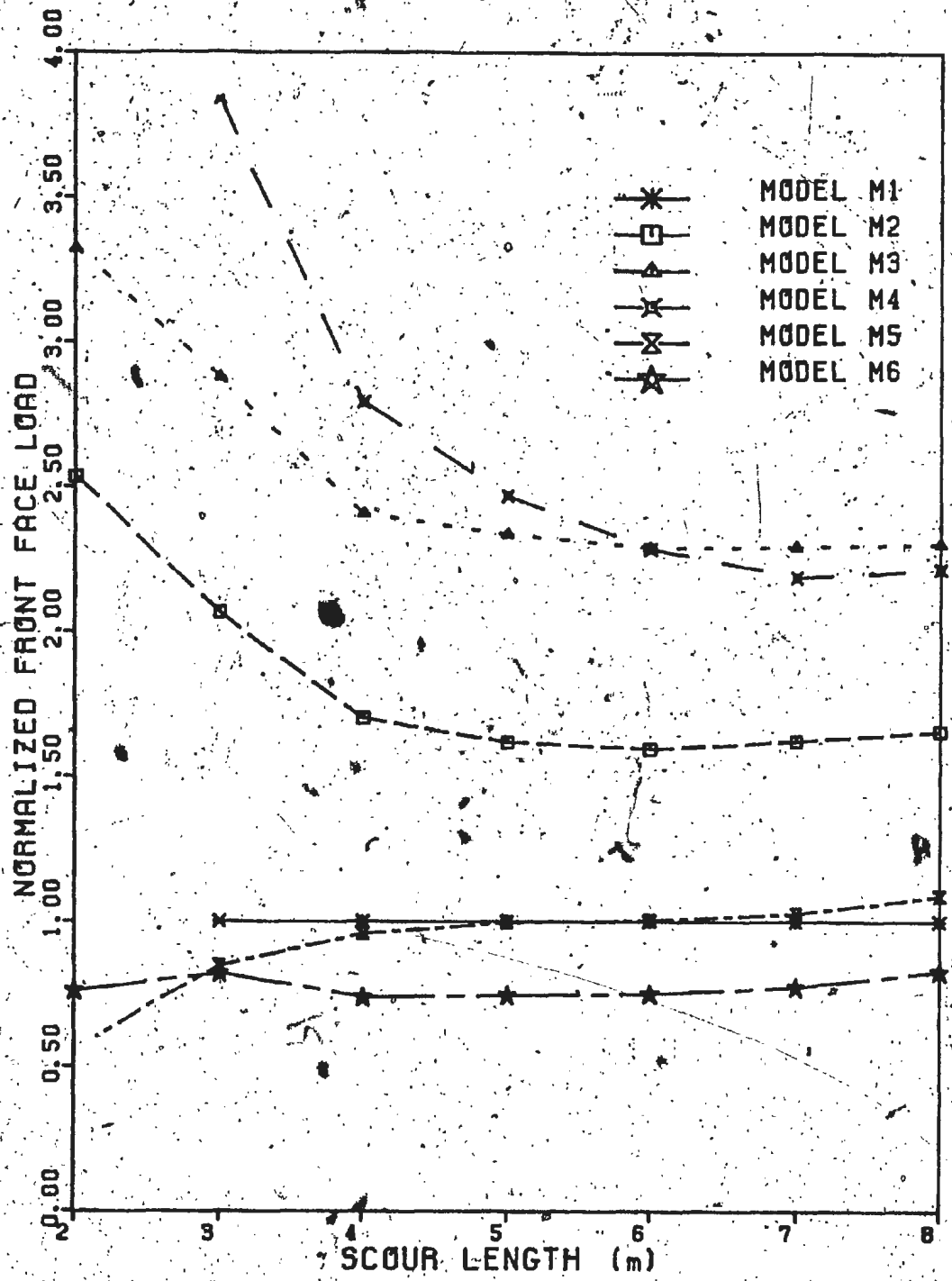

FIGURE 59 NORMALIZED FRONT FACE LOAD FOR DIFFERENT SHAPES WITH RESPECT TO RECTANGULAR PRISMATIC SHAPE

it may be seen that the total soil resistance on the models increases with an increase in the inclination of the front keel. For the curved profile (M4), the averaged slope of the contact area gradually decreases with increasing scour depth. This is clearly reflected in the total load on the model. A comparison of the loads on the curved keel (M4) and the 60° keel (M3) shows that the total load on the curved keel gradually becomes equal to that on the 60° keel and finally drops below it. Similar normalized graphs for the force on the front force alone are shown in Fig. 59. The resistance on iceberg keels which are curved in plan (M5) or wedge shaped (M6) is smaller than the force on a vertical surface of the same projected width. In general, real iceberg keels are not likely to have a plane slanted surface such as M2 or M3 nor are they likely to have a convex cylindrical face such as model M5. It is most likely that the contact surface may be a combination of these two. Thus, the use of the idealized shape of the analytical model is not likely to be too much in error, perhaps the estimates of maximum scour depths will be marginally on the conservative side.

In order to examine the shape effect further, relative factors were assigned for the frontal force on keels of different shapes as obtained from Fig. 59. Using these factors, the normalized scour depths were obtained for

different keel shapes for bergs of various sizes and the results are shown in Fig. 60. For the set of standard parameters considered in Chapter III, the variation of the estimated maximum scour depth ranges from 0.5 to 1.3 times the maximum scour depth calculated for the idealized shape. Thus, under the worst conditions, the shape of the keel is likely to cause a margin of error of +30% to -50% if the scour depths were computed using Eqns. 8 and 9. In reality, because of the complexity of the keel shape, this error is likely to be far less.

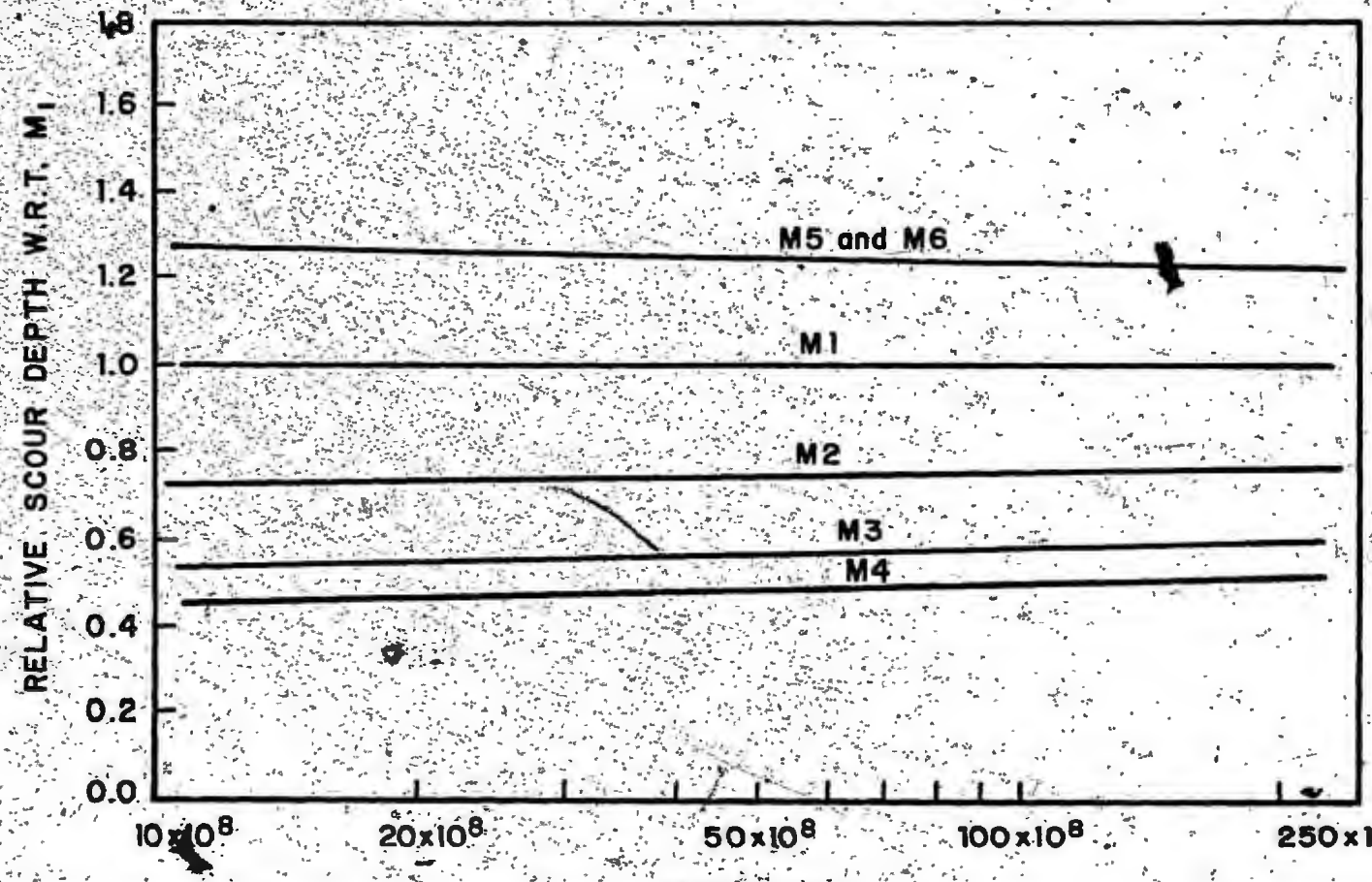

FIGURE 60 INFLUENCE OF ICEBERG SIZE AND KEEL SHAPE ON THE ESTIMATED SCOUR DEPTH

CHAPTER VI

SUMMARY AND CONCLUSIONS

The results of the research reported in this thesis are part of the ongoing project aimed at understanding the geotechnical aspects of the phenomenon of iceberg scouring. In the earlier analytical model (Chari 1979) it was assumed that the iceberg velocity decreases linearly during the process of scouring. This earlier model has now been examined further, and using a step by step iteration technique, it was found that the iceberg velocity variation during scouring is nonlinear. The model (Chari 1979) has now been extended to take into account the nonlinear velocity. Further parametric analyses show that under the combination of a set of environmental parameters, the difference in the scour depth computations between the linear and nonlinear velocity assumptions could be as much as about 20%.

The scour potential of a capsizing and bottom penetrating iceberg was examined and it was found that such icebergs could cause a long scour track or a pockmark on the seafloor, depending on the initial depth of penetration, iceberg size, and the type of the seafloor. Upper and lower bound values were established for such initial penetration for icebergs of a given size.

Physical models of iceberg scouring are only partial models as they do not simulate the phenomenon in its entirety. Nevertheless, these models are essential in understanding the geotechnical aspects of the iceberg-seabed interaction and as a subsequent feedback into the analytical model. Tests were conducted with models of different keel shapes.

For a rectangular prismatic model, the measured frontal force due to soil pressure is in good agreement with Coulomb's method.

The soil resistance on models with an inclined keel increases with the angle of inclination of the keel. The soil pressure on a curved keel is nonlinear. The total soil resistance on such keels depsnds on the avetage slope of the soil-keel contact surface. There is at present no satisfactory theory for computing the earth pressure on such curved surfaces.

The soil resistance on wedge shaped and cylindrical models is less than that for an equivalent rectangular prismatic model.

Results of tests on phybical models of different shapes were fedback into the analytical model and the results were normalized with reference to the idealized prismatic shape. It is concluded that the range of the theoretical scour depths obtained from the idealized model will be

acceptable in normal engineering practice, considering the fact that the keel of a real iceberg is likely to be curved or inclined in two planes if not three.

It is recommended that further experimental and theoretical research should be conducted with curved keel shapes for which there are no solutions at present. Previous investigation has shown that (Chari 1975, Green 1984) there is soil movement below the scour and this effect was examined for the rectangular prismatic models. It is recommended that further work be conducted for keels of different shapes so that a proper evaluation may be made of the pressures on pipelines buried below the potential depth of maximum scour.

REFERENCES

1. Abdelnour, R. and Lapp, D. (1980): "Model Tests of Sea Bottom Ice Scouring", Arctic Petroleum Operators Association (APOA), Project #150.

2. Andersen, K. H. (1976): "Behaviour of Clay Subjected to Cyclic Loading", International Conference on Offshore Structures, Trondheim.

3. Arctic Petroleum Operators Association (APOA) (1975): "An Analytical Study of Ice Scour on the Sea Bottom Scouring", in proceedings of APOA 69-1, report by FENCO Ltd.

4. Banke, E. G. and Smith, D. D. (1974): "Measurements of Towing Drag on Small Icebergs", Proceedings IEEE Ocean 74, International Conference on Engineering in the Ocean Environment, Vol. 1, Halifax, Canada, pp. 130 - 132.

5. Barnes, P.W., McDowell, D. and Reimnitz (1978): "Ice Gouging Characteristics: Their Changing Patterns from 1975 - 1977", Beaufort Sea, Alaska, U.S. Geological Survey, open file report 78-730, 40 p.

6. Barsvary, A. K., Klym, T. W. and Franklin, J. A. (1980): "List of Terms, Symbols and Recommended SI units and Multiples for Geotechnical Engineering", Canadian Geotechnical Journal, Vo. 17, pp. 89 - 96.

7. Bass, D. W. and Peters, G. R. (1984): "Computer Simulation of Iceberg Instability", Cold Regions Science and Technology, Vol. 9, pp. 163 - 169.

8. Bureau Veritas (1975): "Rules and Regulations for the Construction and Classification of Offshore Platforms", International Register for the Classification of Ships and Aircraft, Paris.

9. Chari, T. R. (1975): "Some Geotechnical Aspects of Iceberg Grounding", Ph.D. Thesis, Memorial University of Newfoundland, St. John's, 181 p.

10. Chari, T. R. (1979): "Geotechnical Aspects of Iceberg Scours on Ocean Floors", Canadian Geotechnical Journal, Vol. 16, No. 2, pp. 379 - 390.

11. Chari, T. R. (1980): "A Model Study of Iceberg Scouring in the North Atlantic", Journal of Petroleum Technology, December, pp. 2247 - 2252.

12. Chari, T. R. and Allen, J. H. (1972): "Iceberg Grounding - A Preliminary Theory", Applications of Solid Mechanics, Proceedings of the Symposium held at the University of Waterloo, June 1972, pp. 81 - 95.

13. Chari, T. R. and Green, H. P. (1981): "Iceberg Scour Studies in Medium Dense Sands", Proceedings of POAC 81, Vol. 2, pp. 1012 - 1019.

14. Chari, T. R. and Muthukrishnaiah, K. (1978): "Model Studies of Ocean Floor Scouring by Icebergs", in Proceedings of the Speciality Conference on Applied Techniques for Cold Environments, ASCE, pp. 828 - 839.

15. Chari, T. R. and Peters, G. R. (1981): "Estimates of Iceberg Scour Depths", Proceedings of the Symposium on Production and Transportation Systems for the Hibernia Discovery, St. John's, Nfld., pp. 178 - 188; 432 - 455.

16. Chen, W. F. and Rosenfarb, J. L. (1973): "Limit Analysis Solutions of Earth Pressure Problems", Soils and Foundations, Vol. 13, No. 4, pp. 45 - 60.

17. Dinsmore, R. P. (1972): "Ice and its Drift into the North Atlantic Ocean", Symposium on Environmental Conditions in the Northwest Atlantic, 1960 - 1969, ICNAF Special Publications No. 8, pp. 89 - 128.

18. Duval, B. C. (1975): "Exploratory Drilling on the Canadian Continental Shelf, Labrador Sea", Offshore Technology Conference, Houston, TX, OTC 2155, Vol. 1, pp. 59 - 67.

19. Green, H. P. (1984): "Geotechnical Modelling of Iceberg-Seabed Interaction", M.Eng. Thesis, Memorial University of Newfoundland, St. John's, 165 p.

20. Harris, I. M. and Jollymore, P. G. (1974): "Iceberg Furrow Marks on the Continental Shelf Northeast of Belle Isle, Newfoundland", Canadian Journal of Earth Sciences, 11, pp. 43 - 52.

21. Harrison, W. L. (1973): "Soil Failure Under Inclined Loads", Journal of Terramechanics, Vol. 9, No. 4, pp. 41 - 63, also Vol. 10, No. 1, pp. 89 - 107.

22. Jaky, J. (1948): "Pressure in Silos," 2nd International Conference on Soil Mechanics and Foundation Engineering, Rotterdam, Holland, Vol. 1, pp. 103 - 107.

23. Joo, J. S. (1985): "Behaviour of Large Scale Rigid Model Piles Under Inclined Loads in Sand", M.Eng. Thesis, Memorial University of Newfoundland, 135 p.

24. Kivisild, H. R. (1982): "The Influence of Soil Properties on Scour", Paper Presented at the Second Canadian Conference on Marine Geotechnical Engineering, Halifax, Nova Scotia, 7 p.

25. Kivisild, H. R., Pilkington, G. R. and Iyer, S. H. (1981): "Mathematical Analysis of Ice Scour," ASME, Energy Sources Technology Conference, January 19 - 21, 1981, Houston, Texas, 16 p.

26. Kollemeyer, R. C. (1980): "West Greenland Outlet Glaciers An Inventory of Major Iceberg Producers", Cold Regions Science and Technology, Vol. 1, pp. 175 - 181.

27. Lewis, C. F. M. and Barrie, J. V. (1981): "Geological Evidence of Iceberg Groundings and Related Seafloor Processes in the Hibernia Discovery Area of Grand Banks, Newfoundland", Proceedings of the Symposium on Production and Transportation Systems for the Hibernia Discovery, St. John's, pp. 146 - 177.

28 Lewis, J. K. C. and Benedict, C.P. (1981): "Burial Parameters: An Integrated Approach to Limit Overdesign", Proceedings of the Symposium on Production and Transportation Systems for the Hibernia Discovery, St. John's, February 16 - 18, pp. 189 - 203.

29. Lopez, R., Chari, T. R., Moore, E., Peters, G. R. and Zielinski, A. (1981): "Hydrodynamic Effects of Iceberg Gouging", Cold Regions Science and Technology, Vol. 4, No. 1, pp. 55 - 61.

30. Mountain, D. C. (1980): "On Predicting Iceberg Drift", Cold Regions Science and Technology, Vol. 1, pp. 273 - 282.

31. Milne, A. R. (1973): "Methods for Launch and Recovery of Sea Bottom Instrument Package", Underwater Journal, Vol. 5, No. 5, pp. 213 - 220.

32. Murray, J. E. (1969): "The Drift, Deterioration and Distribution of Icebergs in the North Atlantic Ocean", Ice Seminar, Canadian Institute of Mining and Metallurgy, Special Vol. 10, pp. 3 - 18.

33. Prasad, K. S. R. and Chari, T. R. (1984): "Some Factors Influencing Iceberg Scour Estimates", 4th International Symposium on Offshore Mechanics and Arctic Engineering, Dallas, Texas, February 17 - 22.

34. Prater, E. G. (1976): "An Examination of Some Theories of Earth Pressure on Shaft Linings", Canadian Geotechnical Journal, Vol. 14, pp. 91 - 106.

35. Russell, W. E. and Muggeridge, D. B. (Editors) (1981): "Symposium on Production and Transportation Systems for the Hibernia Discovery", St. John's, Nfld., 522 p.

36. Sanderson, R. M. and Davis, G. P. (1972): "Ice Conditions Through the Northwest Passage", Marine Observer 42, No. 236, pp. 69 - 80.

37. Schuring, D. J. and Emori, R. I. (1964): "Soil Deforming Processess and Dimensional Analysis", Society of Automotive Engineers, Report 897C.

38. Shields, D. H. and Tolunay, A. Z. (1973): "Passive Pressure by Method of Slices", Journal of the Soil Mechanics and Foundations Division, Proceedings ASCE, Vol. 99, No. SM12, pp. 1043 - 1053.

39. Shirasawa, K., Riggs, N. P. and Muggeridge, D. B. (1984): "The Drift of a Number of Idealized Model Icebergs", Cold Regions Science and Technology (in press).

40. Siemens, J. C. (1963): "Mechanics of Soil Under the Influence of Model Tillage Tolls", Ph.D. Thesis, University of Illinois at Urbana, 139 p.

41. Smith, E. H. (1931): "The Marion Expedition to Davis Strait and Baffin Bay", U.S. Coast Guard Bulletin, No. 19, Part 3, Scientific Results, pp. 60 - 216.

42. Terzaghi, K. (1943): "Theoretical Soil Mechanics", John Wiley and Sons, Inc., New York.

43. Terzaghi, K. and Peck, R. B. (1967): "Soil Mechanics in Engineering Practice", John Wiley & Sons, Inc., New York.

APPENDIX - A

COMPUTER PROGRAMS

```
C  THIS PROGRAMME COMPUTES THE MAXIMUM DEPTH OF
C  SCOUR IN COHESIVE SOILS ACCOUNTING NON-LINEAR
C  VELOCITY AND INITIAL DEPTH OF SCOUR
      REAL LSTAR,L,LD,LNEW,LDN,V,C,K,K2,SLP,REP,DENS,B,W,KE,A,DRAFT
      OPEN(UNIT=20,FILE='ICEBRG.ANS',TYPE='NEW')
   06 ROW=1.025
      OPEN(UNIT=21,FILE='ICEBRG.DAT',TYPE='OLD')
      READ(21,*) NDATA
      DO 180 I=1,NDATA
      READ(21,*) V,DENS,C,SLP,W,B,CD,S,FAC
      WRITE(20,*)'*********************************************'
      WRITE(20,*) 'V=',V,' DENS=',DENS,' TAU=',C,' SLP=',SLP,
     1  ' W=',W,' B=',B,' CD=',CD,' S=',S
      REP=SLP
      VCUR=V
      GAMA=DENS-10.05
C ANALYSIS IS BEING DONE IN INCREMENTS OF LENGTH
      DL=5.0
      L=0.0
      DLSTOP=0.001
      VLIMIT=0.0001
   30 K = 1.0/SLP + 1.0/REP
   40 KE=W*V*V/(2.0*9.806)
      AB3=KE
   41 A = 2.644*(3*W/(4*3.14*8.8))**0.67
   42 DRAFT = 1.57*(3*W/(4*3.14*8.8))**.33


      BLIMIT=(GAMA*S**3*B/6.0+C*B*S*S+1.414/3*C*S**3)*SLP
      VOLD=VCUR
      ES=0.0
      EP=KE
      EADD=0.0
      ENET=KE
      VNEW=VCUR
      ESCUM=0,0
      SMEADD=0.0
      LPRINT=L/100
C      TYPE*,L,ES,EP,EADD,KE,VNEW,ESCUM,SMEADD
      L=L+DL
      D=L/SLP
C  LD IS NOW OBTAINED BY NEWTON - RAPHSON METHOD
C
      LD=L/10
   49 ITER=1
```

```
   50 FX = 2.0*K*K*LD**4 + 4.0*K*K*L*LD**3 + LD*LD*(2.0*K*K*L*L
     2  + 3.0*K*L*B/REP) - 3.0*L**3*B/REP/SLP-6.0*S*L*L*B/REP
   60 FDX = 8.0*K*K*LD**3 + 12.0*K*K*L*LD*LD
     2 + 2.0*LD*(2.0*K*K*L*L + 3.0*K*L*B/REP)
   70 LDN = LD - FX/FDX
   71 IF(ABS(LD-LDN).LT.0.1) GO TO 74
      ITER=ITER+1
      IF(ITER.GE.50) GO TO 96
   72 LD = LDN
   73 GO TO 50
   74 LD = LDN
C     TYPE*,'LD=',LD
   75 H = L/SLP  +  LD/REP + LD/SLP
   76 HD = LD/REP + LD/SLP
      D1=S+L/SLP
      K2=LD*K/(S+L/SLP)
      RESIST=GAMA*(H+S)**2*B/2.0+2.0*C*D1*B+1.414*C*D1*D1
      TLIMIT=(GAMA*(H+S)**2*D1*B/6.0+C*D1*D1*B+
     1  1.414*C*D1**3/3.0)*SLP
      TLIMIT=TLIMIT*FAC
      LPRINT=L/100
      IF(LPRINT*100.EQ.L.OR.L-LAST.GE.100)TYPE*,'L=',L,LD,K2
      LAST=L
      ES=TLIMIT-BLIMIT
      ETEMP=ENET-ES+0.5*CD*ROW*A*(VCUR-VOLD)**2*DL
       VNEW=SQRT(ETEMP*2.0*9.806/W)
      IF(VNEW.LT.VLIMIT.OR.ENET.LT.50.0)GO TO 96
      VAVSQ=((VNEW-VCUR)**2+(VOLD-VCUR)**2)/2.0
      EADD=CD*ROW*A*VAVSQ/2.0*DL
      ENET=KE-ES+EADD
C*********************OUTPUT INFORMATION
      IF(ES.GT.ENET)TYPE*,'FOR L=',L,'ES>ENET=',ENET,'DL=',DL
      IF(ES.GT.ENET)TYPE*,'L=',L,'FDRAG=',EADD/DL,'V=',VNEW,
     1  'RVSQ=',(VCUR-VNEW)**2,'P=',RESIST
C     IF(ES.GT.ENET)WRITE(20,*)'L=',L,'FDRAG=',EADD/DL,'V=',VNEW,
C    1  'RVSQ=',(VCUR-VNEW)**2,'P=',RESIST
C**********************
      IF(ENET.LE.ES) GO TO 90
      ESCUM=ESCUM+ES
      AB1=ESCUM
      SMEADD=SMEADD+EADD
      AB2=SMEADD
      AB4=AB3/AB1*100
      AB5=AB2/AB1*100
      KE=ENET
```

```
      LPRINT=L/100
      IF(LPRINT*100.EQ.L)GO TO 81
      IF(DL.GE.1.0)GO TO 85
      IF(DL.LT.1.0.AND.L-LPAST.LT.25) GO TO 85
   81 LPAST=L
C*********************************
C     TYPE*,'L=',L,'FDRAG=',EADD/DL,'V=',VNEW,'P=',RESIST
C  84 TYPE*,L,ES,EP,EADD,KE,VNEW,ESCUM,SMEADD
      WRITE(20,*)'L=',L,'V=',VNEW,'P=',RESIST,'WSOIL=',ESCUM,
     1 'FDRAG=',EADD/DL,'EDRAG=',SMEADD,AB3+SMEADD
C*********************************
   85 VOLD=VNEW
      BLIMIT=TLIMIT
   90 IF(ENET.LE.ES.AND.DL.LE.DLSTOP)GO TO 96
      IF(ENET.GT.ES)GO TO 95
      L=L-DL
      IF(DL.EQ.1.0)GO TO 94
      IF(DL.EQ.5.0)DL=1.0
      IF(DL.EQ.1.0)GO TO 95
   94 IF(DL.LT.5.0)DL=DL/10.0
   95 L=L+DL
      IF(KE.LE.0.0) GO TO 96
      IF(KE.GT.0.0)GO TO 49
   96 WRITE(20,*)'L=',L,'D=',D1,'V=',VNEW,'  ENET=',KE
      D=L/SLP
  180 CONTINUE
      STOP
      END
```

```
C THIS PROGRAMME COMPUTES THE MAXIMUM SCOUR DEPTH
C FOR COHESIVE FRICTIONAL SOIL TAKING INTO ACCOUNT
C NONLINEAR VELOCITY

      REAL L,L1,KE
      COMMON/BLOC1/C,PHID,SLP,B,L,L1,WO,GAMA,H,D,P

      OPEN(UNIT=20,FILE='ICEBRG.ANS',TYPE='NEW')
C
 06 ROW=1.025
      OPEN(UNIT=21,FILE='ICEBRG.DAT',TYPE='OLD')
      READ(21,*) NDATA
      DO 180 I=1,NDATA
      READ(21,*) V,DENS,C,SLP,W,B,CD,PHID
      WRITE(20,*)'*********************************************'
      WRITE(20,*) 'V=',V,' DENS=',DENS,' C=',C,' SLP=',SLP,
     1 ' W=',W,' B=',B,' CD=',CD,' PHI=',PHID
      VCUR=V
      GAMA=DENS-10.05
C ANALYSIS IS BEING DONE IN INCREMENTS OF LENGTH
      DL=5.0
      L=0.0
      DLSTOP=0.001
      VLIMIT=0.0001

 40 KE=W*V*V/(2.0*9.806)
 41 A = 2.644*(3*W/(4*3.14*8.8))**0.67
 42 DRAFT = 1.57*(3*W/(4*3.14*8.8))**.33


      POLD=0
      VOLD=VCUR
      ES=0.0
      EP=KE
      EADD=0.0
      ENET=KE
      VNEW=VCUR
      ESCUM=0.0
      SMEADD=0.0
      LPRINT=L/100
C      TYPE*,L,ES,EP,EADD,KE,VNEW,ESCUM,SMEADD
      L=L+DL
49     CALL SURCH
      D=L/SLP
      CALL RESIST
```

```
      PNEW=P

      LPRINT=L/100
      ES=0.5*(PNEW+POLD)*DL
      ETEMP=ENET-ES+0.5*CD*ROW*A*(VCUR-VOLD)**2*DL
       VNEW=SQRT(ETEMP*2.0*9.806/W)
      IF(VNEW.LT.VLIMIT.OR.ENET.LT.50.0)GO TO 96
      VAVSQ=((VNEW-VCUR)**2+(VOLD-VCUR)**2)/2.0
      EADD=CD*ROW*A*VAVSQ/2.0*DL
      ENET=KE-ES+EADD
C*********************OUTPUT INFORMATION
      IF(Enet.LT.Es)TYPE*,'FOR L=',L,'ES>ENET=',ENET,'DL=',DL,'L1=',L1
      IF(ENET.LE.ES) GO TO 90
      ESCUM=ESCUM+ES
      SMEADD=SMEADD+EADD
      KE=ENET
      LPRINT=L/100
      IF(LPRINT*100.EQ.L)GO TO 81
      IF(DL.GE.1.0)GO TO 85
      IF(DL.LT.1.0.AND.L-LPAST.LT.25) GO TO 85
 81   LPAST=L
      TYPE*,'L=',L,'FDRAG=',EADD/DL,'V=',VNEW,'P=',PNEW,'Li=',L1
      WRITE(20,*)'L=',L,'V=',VNEW,'P=',PNEW,'WSOIL=',ESCUM,
     1 'FDRAG=',EADD/DL,'EDRAG=',SMEADD,AB3+SMEADD
 85   VOLD=VNEW
      POLD=PNEW
      IF(ENET.GT.ES)GOTO 95
 90    IF(VNEW.LT.VLIMIT. AND. DL.LE.DLSTOP)GOTO 96
      IF(ENET.LE.ES .AND. DL.LE.DLSTOP)GO TO 96

      L=L-DL
      IF(DL.EQ.5.0)DDL=1.0
      IF(DL.EQ.1.0)DDL=0.1
      IF(DL.EQ.0.1)DDL=0.01
      IF(DL.EQ.0.01)DDL=0.001
      DL=DDL
 95    L=L+DL
      IF(KE.GT.0.0)GO TO 49
C*********************************
 96    WRITE(20,*)'L=',L,'D=',D,'V=',VNEW,'  ENET=',KE
C      TYPE*,'L=',L,'L1=',L1,'WO=',WO
C*********************************
 180   CONTINUE
      STOP
      END
```

```
      SUBROUTINE RESIST
      REAL L,L1
      COMMON/BLOC1/C,PHID,SLP,B,L,L1,WO,GAMA,H,D,P
C      TYPE*,'C=',C,PHID,SLP,GAMA,B,D,H,WO,P,L
      Q=WO
      ALPC=0.0
      CA=ALPC*C
      DELTAD=PHID/3.0
      REP=SLP
      PI=3.1415927
      FAC=PI/180.0
      PHI=PHID*FAC
      DELTA=DELTAD*FAC
      BETA=ATAN(1.0/SLP)
      ALP=ATAN(1.0/REP)

      IF(D.EQ.0.0)GOTO 15
      AK0=0.0
      TITAD=5.0
      PMIN=100000000.0
5     TITA=TITAD*FAC
      IF(TITA-BETA.EQ.0.0)GOTO 10

      WO=Q-0.5*GAMA*B*SIN(ALP+BETA)*
     1  (L1/COS(ALP)-(H+D)*COS(TITA)/SIN(ALP+TITA))*
     2  (L1/COS(BETA)-D*COS(TITA)/SIN(TITA-BETA))

      W=GAMA*B*(0.5*D*D*COS(BETA)*COS(TITA)/SIN(TITA-BETA))
      S=(B*D*COS(BETA)/SIN(TITA-BETA))*C
      SS=(0.5*D*D*COS(BETA)*COS(TITA)/SIN(TITA-BETA))*
     1   (C+AK0*(GAMA*D/3.0+WO*SIN(TITA-BETA)/(B*D*COS(TITA)))
     2    *TAN(PHI))


      CCA=(H+D)*B*CA
      P=((WO+W+(S+2.0*SS)*SIN(TITA)+CCA)*SIN(TITA+PHI)+(S+2.0*SS)*
     1  COS(TITA)*cos(tita+phi))/COS(DELTA+PHI+TITA)


      IF(P.GE.PMIN)GOTO 12
      IF(P.GT.0.0 .AND. P.LE.PMIN)TMIN=TITAD
      IF(P.GT.0.0 .AND. P.LE.PMIN) PMIN=P
10     TITAD=TITAD+1.0
      IF(TITAD.LT.50.0)GO TO 5
C      TYPE*,'PMIN=',PMIN,'AT TITA=',TMIN
```

```
12    P=PMIN
15    IF(D.EQ.0.0)P=0.0
      RETURN
      END

      SUBROUTINE SURCH
      REAL K,L,L1
      COMMON/BLOC1/C,PHID,SLP,B,L,L1,WO,GAMA,H,D,P
      REP=SLP
      K=1.0/SLP+1.0/REP
      L1=L/10.0
      DO 10 I=1,50
      F=2.0*K*K*L1**4+4.0*K*K*L*L1**3+LT*L1*(2.0*K*K*L*L
     1   +3.0*K*L*B/REP)-3.0*L**3*B/REP/SLP
      FD=8.0*K*K*L1**3 + 12.0*K*K*L*L1*L1
     1    +2.0*L1*(2.0*K*K*L*L + 3.0*K*L*B/REP)
      AL1N=L1-F/FD
      IF(ABS(AL1N-L1).LT.0.1)GOTO 15
C     TYPE*,L1,AL1N
      L1=AL1N
      IF(I.EQ.50)TYPE*,'ITERATION EXCEEDED'
10    CONTINUE
15    L1=AL1N
      H=K*L1
      VOLF=L1*H*B/2.0
C     TYPE*,'L=',AL,'L1=',AL1,'VOLF=',VOLF
      WO=GAMA*VOLF
      RETURN
      END
```

```
C  THIS IS A GENERALIZED PROGRAMME FOR MODELS
C  M1, M2 AND M3 TO COMPUTE FRONT FACE RESISTANCE
C  USING COULOMB'S METHOD.  RHO IS FRONT FACE INCLINATION
C  ALL VARIABLES ARE SELF EXPLANATORY

      OPEN(UNIT=10,FILE='EXP.DAT',TYPE='OLD')
      OPEN(UNIT=20,FILE='EXP.ANS',TYPE='NEW')
      READ(10,*)N
      DO 5,I=1,N
      READ(10,*)AL,VO
      GAMA=17.0
      AK0=0.5
      D=AL/35.0
      B=0.5

      WRITE(20,7)AL,VO
7     FORMAT(2X,'RECTANGULAR PRISMATIC',//,'SCOUR
     1 LENGTH=',F4.2,5X,'VOL. OF OVERBURDEN=',E8.2)
      PHI=35.5*3.142/180.0
      DELTA=23.0*3.142/180
      BETA=1.637*3.142/180.0
      RHO=0.0*3.142/180.0
C TOTAL WEIGHT = WT. OF VARIABLE WEDGE + WT. OF OVERBURDEN
C      WT  =  WW + WO
      WO=GAMA*VO
      TITAD=5.0
10    TITA=TITAD*3.142/180.0
      WW=GAMA*B*(0.5*(D*COS(BETA))**2*COS(RHO+TITA)/
     1 COS(RHO+BETA)/ SIN(TITA-BETA))
      WT=WW + WO
C     TYPE*,'WW=',WW,'WO=',WO,'WT=',WT
      Q=WO*COS(RHO+BETA)*SIN(TITA-BETA)/B/D/
     1 COS(RHO+TITA)/COS(BETA)
      FS=2.0*(WW/GAMA/B)*(AK0*(Q+GAMA*D/2.0))*TAN(PHI)
      P=(WT*SIN(TITA+PHI)+FS*COS(PHI))/COS(TITA+PHI+DELTA+RHO)
      PH=P*COS(RHO+DELTA)
C     TYPE*,'Q=',Q,'FS=',FS,'P=',P,'PH=',PH
      WRITE(20,9)TITAD,WO,WW,WT,PH
9     FORMAT('FOR TITA=',F4.1,2X,'WO=',E8.2,2X,'WW=',E8.2,
     1 2X,'WT=',E8.2 ,2X,'P=',F9.4)
      TITAD=TITAD+1.0
      IF(TITAD.LE.30)GO TO 10
5     CONTINUE
      STOP
      END
```

```
C  THIS PROGRAMME COMPUTES THE FRONTFACE RESISTANCE
C  FOR MODELS M1, M2 AND M3 USING LOGARITHMIC SPIRAL
C  METHOD AND REFERRED TO AS TERZAGHI AND PECK METHOD.

      OPEN(UNIT=20,FILE='EXP.DAT',TYPE='OLD')
      OPEN(UNIT=21,FILE='EXP.ANS',TYPE='NEW')
      OPEN(UNIT=22,FILE='WASTE.ANS',TYPE='NEW')
      ALPHAD=90.0
      PHID=35.5
      GAMA=17.0
      B=0.5
      BETA=ATAN(1.0/35.0)
      PI=3.1415927
      FAC=PI/180.0
      ALP1=28.66*FAC
      ALP2=27.84*FAC
      ALPHA=ALPHAD*FAC
      PHI=PHID*FAC
      READ(20,*)N
      DO 10 I=1,N
      READ(20,*)AL,VO
      WO=VO*GAMA
      D=AL/35.0
      DO 10 J=1,116
      TITAD=J-26
      TITA=TITAD*FAC
      AB=D/SIN(ALPHA)
      ETA=PHI-TITA
      ANGOAB=ALPHA-(TITA+PI/2.0-PHI)
      ANGOBA=(PI-ALPHA)+(ALP1-BETA)
      TITAM=PI-ANGOAB-ANGOBA
      delta=23.0*fac
      DELTAD=DELTA/FAC
      ALP3=PI-ALP1-(PI/4.0+PHI/2.0)
      ALP4=BETA+ALP3-PI/2.0
      ALP5=ALPHA-PI/2.0+DELTA
      AO=AB*SIN(ANGOBA)/SIN(TITAM)
      R0=AO
      CO=R0*EXP(TITAM*TAN(PHI))
      BO=AB*SIN(ANGOAB)/SIN(TITAM)
      BC=CO-BO
      BD=BC*SIN(PI/4.0+PHI/2.0)/SIN(ALP3)
      CD=BC*SIN(ALP1)/SIN(ALP3)
      CE=CD*SIN(ALP3)/SIN(ALP2)
      DE=CD*SIN(PI/4.0+PHI/2.0)/SIN(ALP2)
```

```
      XA=0.0
      YA=0.0
      XB=D*SIN(ALPHA-PI/2.0)/SIN(ALPHA)
      YB=D
      XO=XA-AO*SIN(ETA)
      YO=YA+AO*COS(ETA)
      XC=XB+BC*COS(ALP1-BETA)
      YC=YB-BC*SIN(ALP1-BETA)
      XD=XB+BD*COS(BETA)
      YD=YB+BD*SIN(BETA)
      XE=XD+DE*COS(BETA)
      YE=YD+DE*SIN(BETA)
      XF=XC+(XD-XC)/3.0
      YF=YC+(YD-YC)/3.0
      XG=XC+(XD-XC)/2.0
      YG=YC+(YD-YC)/2.0
      XH=XA+(XB-XA)/3.0
      YH=YA+(YB-YA)/3.0
      XI=XA+(XB-XA)/2.0
      YI=YA+(YB-YA)/2.0
      XABO=(XA+XB+XO)/3.0
      YABO=(YA+YB+YO)/3.0
      XBCD=(XB+XC+XD)/3.0
      YBCD=(YB+YC+YD)/3.0
      CGACBO=4.0*R0*TAN(PHI)/3.0/(EXP(2.0*TITAM*TAN(PHI))-1)
     1  *(3.0*TAN(PHI)*SIN(TITAM+ETA)*EXP(3.0*TITAM*TAN(PHI))
     2   -COS(TITAM+ETA)*EXP(3.0*TITAM*TAN(PHI))-3.0*TAN(PHI)*
     3   SIN(ETA)+COS(ETA))/(1.0+9.0*TAN(PHI)**2)

      XACBO=XO+CGACBO

      AABO=(XA*YB-XB*YA+XB*YO-XO*YB+XO*YA-XA*YO)*0.5
      ABCD=0.5*(XB*YC-YB*XC+XC*YD-YC*XD+XD*YB-YD*XB)
      AACBO=R0**2/4.0/TAN(PHI)*(EXP(2.0*TITAM*TAN(PHI))-1)
      FG=0.5*GAMA*CD**2*TAN(PI/4.0+PHI/2.0)**2
      Q=WO/(B*(BD+DE))
      FQ=Q*TAN(PI/4.0+PHI/2.0)**2*CD
      AMABO=AABO*GAMA*(XABO-XO)
      AMACBO=AACBO*GAMA*(XACBO-XO)
      AMBCD=ABCD*GAMA*(XBCD-XO)
      AMFG=FG*COS(ALP4)*(YO-YF)+FG*SIN(ALP4)*(XF-XO)
      AMFQ=FQ*COS(ALP4)*(YO-YG)+FQ*SIN(ALP4)*(XG-XO)
      PG=(AMACBO+AMBCD-AMABO+AMFG)/(COS(ALP5)*(YO-YH)
     1    -SIN(ALP5)*(XH-XO))
      PQ=(AMFQ+Q*BD*((XB+XD)/2.0-XO))/(COS(ALP5)*(YO-YI)
```

```
     1      -SIN(ALP5)*(XI-XO))
            P=PG+PQ

            PH=P*COS(ALP5)
            PH=0.5*PH
            WRITE(21,*)AL,TITAD,DELTAD,PH
     C      TYPE*,AL, TITAD,DELTAD,PH
     10     CONTINUE
            STOP
            END
```

```
C  THIS PROGRAMME IS USED TO COMPUTE FRONT FACE RESISTANCE
C  OF MODELS M1, M2 AND M3 WITH SLOPING BACKFILL AND
C  SURCHARGE USING HARRISON'S METHOD.
C  FOR NOTATION, PLEASE REFER TO TEXT.

      OPEN(UNIT=20,FILE='EXP.DAT',TYPE='OLD')
      OPEN(UNIT=21,FILE='EXP.ANS',TYPE='NEW')

      PHID=35.5
      ALPHAD=150.0
      ALP1D=26.66
      ALP2D=27.84
      GAMA=17.0
      B=0.5
      BETA=ATAN(1.0/35.0)
      WRITE(21,5)ALPHAD
C     WRITE(21,6)
 5    FORMAT(/,5X,'INCLINED PROFILE',F5.1,/)
 6    FORMAT(5X,'L,XO,YO,XC,YC,XD,YD,XE,YE,TITA,DELTA,PH',/)
      PI=3.1415927
      FAC=PI/180.0
      PHI=PHID*FAC
      ALPHA=ALPHAD*FAC
      ALP1=ALP1D*FAC
      ALP2=ALP2D*FAC
      READ(20,*)N
      DO 10 I=1,N
      READ(20,*)AL,VO
      D=AL/35.0
      WO=VO*GAMA

      ETA=PHI
      TITAM=PI/2.0-PHI-ALP1+BETA
      ALP3=PI-ALP1-(PI/4.0+PHI/2.0)
      ALPG=BETA+ALP3-PI/2.0
      ALPH=ALPG

      BC=D/COS(PHI)
      R0=BC
      BD=R0*EXP(TITAM*TAN(PHI))
      BE=SIN(PI/4.0+PHI/2.0)*BD/SIN(ALP3)
      DE=SIN(ALP1)*BD/SIN(ALP3)
      EF=SIN(PI/4.0+PHI/2.0)*DE/SIN(ALP2)
```

```
      BF=BE+EF


      XA=0.0
      YA=0.0
      XB=D*SIN(ALPHA-PI/2.0)/SIN(ALPHA)
      YB=D.
      XC=XB+BC*SIN(PHI)
      YC=0.0
      XD=XB+BD*COS(ALP1-BETA)
      YD=YB-BD*SIN(ALP1-BETA)
      XE=XB+BE*COS(BETA)
      YE=YB+BE*SIN(BETA)
      XF=XB+BF*COS(BETA)
      YF=YB+BF*SIN(BETA)
      XG=XD+(XE-XD)*1.0/3.0
      YG=YD+(YE-YD)*1.0/3.0
      XH=XD+(XE-XD)*1.0/2.0
      YH=YD+(YE-YD)*1.0/2.0

      XBDE=(XB+XD+XE)/3.0
      CGBCD=4.0*R0*TAN(PHI)/3.0/(EXP(2.0*TITAM*TAN(PHI))-1)
     1  *(3.0*TAN(PHI)*SIN(TITAM+ETA)*EXP(3.0*TITAM*TAN(PHI))
     2   -COS(TITAM+ETA)*EXP(3.0*TITAM*TAN(PHI))-3.0*TAN(PHI)*
     3   SIN(ETA)+COS(ETA))/(1.0+9.0*TAN(PHI)**2)
      XBCD=CGBCD+XB


      ABDE=ABS(0.5*(XB*YD-XD*YB+XD*YE-XE*YD+XE*YB-XB*YE))
      ABCD=ABS(R0**2/(4.0*TAN(PHI))*(EXP(2.0*TITAM*TAN(PHI))-1))
      AABC=ABS(0.5*(XA*YB-YA*XB+XB*YC-YB*XC+XC*YA-YC*XA))


      FG=0.5*GAMA*DE**2*TAN(PI/4.0+PHI/2.0)**2
      Q=WO/(B*(BE+EF))
      FQ=Q*TAN(PI/4.0+PHI/2.0)**2*DE
      AMBDE=ABDE*GAMA*(XBDE-XB)
      AMBCD=ABCD*GAMA*(XBCD-XB)
      AMFG=FG*COS(ALPG)*(YB-YG)+FG*SIN(ALPG)*(XG-XB)
      AMFQ=FQ*COS(ALPH)*(YB-YH)+FQ*SIN(ALPH)*(XH-XB)
      PPG=(AMBDE+AMBCD+AMFG)/(2.0/3.0*BC*COS(PHI))
      PPQ=(AMFQ+Q*BE*(XE-XB)/2.0)/(1.0/2.0*BC*COS(PHI))
      PP=PPG+PPQ
      TITA=(270-2.0*ALPHAD-PHID)*FAC
      TITAD=TITA/FAC
```

```
      DELTA=ATAN(SIN(TITA)*SIN(PHI)/(1.0+COS(TITA)*SIN(PHI)))
      IF(DELTA/FAC.GT.23.0) DELTA=23.0*FAC
      IF(DELTA/FAC.LT.-23.0) DELTA=-23.0*FAC
      DELTAD=DELTA/FAC
      P=COS(PHI)*(PP+AABC*GAMA*TAN(PHI))/COS(ALPHA-
     *1   PI/2.0+DELTA+PHI)
      PH=P*COS(ALPHA-PI/2.0+DELTA)
           PH=PH*B
C     WRITE(21,7)D,XO,YO,XC,YC,XD,YD,XE,YE,TITAD,PHID,DELTAD,PH
7     FORMAT(2X,F4.2,8(2X,F6.2),2X,F6.2,2X,F6.2,2X,F6.2,F8.4)
      TYPE*,AL, ALPHAD,DELTAD,'PH=',PH
      WRITE(21,8)AL,ALPHAD,DELTAD,PH
8     FORMAT(2X,'L=',F4.1,2X,'ALPHA=',F6.2,2X,'DELTA=',F6.2,
     1   2X,'PH=',F9.4)
C-----------------------------------------------------------
C      TYPE*,'ALPHA=',ALPHAD,'TITA=',TITAD,'ETA=',ETA/FAC
C     TYPE*,'TITAM=',TITAM/FAC,'ALP3=',ALP3
C     TYPE*,'ALPG=',ALPG/FAC,'ALPH=',ALPH/FAC
C     TYPE*,'BC=',BC,'BD=',BD,'BE=',BE,'DE=',DE,'EF=',EF,'BF=',BF
C     TYPE*,'XB=',XB,'YB=',YB
C     TYPE*,'XC=',XC,'YC=',YC
C     TYPE*,'XD=',XD,'YD=',YD
C     TYPE*,'XE=',XE,'YE=',YE
C     TYPE*,'XF=',XF,'YF=',YF
C     TYPE*,'XG=',XG,'YG=',YG
C     TYPE*,'XH=',XH,'YH=',YH
C      TYPE*,'AABC=',AABC,'ABCD=',ABCD,'ABDE=',ABDE
C      TYPE*,'FG=',FG,'FQ=',FQ
C     TYPE*,'WABC=',AABC*GAMA,'WBCD=',ABCD*GAMA,
C        'WBDE=',GAMA*ABDE
C     TYPE*,'AMBCD=',AMBCD,'AMBDE=',AMBDE,AMFG,AMFQ
C-----------------------------------------------------------


10    IF(DELTAD.LT.-24.0 .OR. DELTAD.GT.24) TYPE*,'NO VALUE'
      STOP
      END
```

```
C THIS PROGRAMME IS SET TO COMPUTE FRONT FACE RESISTANCE OF
C CURVED PROFILE (M4) USING THE PRINCIPLE OF HARRISON (1973).
C THE CURVED PROFILE IS APPROXIMATED AS INCLINED PLANE
C SURFACE HAVING THE AVERAGE INCLINATION OF CONTACT
C SURFACE.

      OPEN(UNIT=20,FILE='EXP.DAT',TYPE='OLD')
      OPEN(UNIT=21,FILE='EXP.ANS',TYPE='NEW')

      PHID=35.5
      ALP1D=26.66
      ALP2D=27.84
      GAMA=17.0
      B=0.5
      BETA=ATAN(1.0/35.0)
      WRITE(21,5)
C     WRITE(21,6)
 5    FORMAT(/,5X,'CURVED PROFILE',F5.1,/)
 6    FORMAT(5X,'L,XO,YO,XC,YC,XD,YD,XE,YE,TITA,DELTA,PH',/)
      PI=3.1415927
      FAC=PI/180.0
      PHI=PHID*FAC
      ALP1=ALP1D*FAC
      ALP2=ALP2D*FAC
      READ(20,*)N
      DO 10 I=1,N
C THE POINT OF APPLICATION OF RESISTANCE , COMPUTED FROM
C MEASURED PRESSURE DISTRIBUTION IS SUPPLIED (CGF)
      READ(20,*)AL,VO,CGF
      D=AL/35.0
      WO=VO*GAMA

      XB=SQRT(0.09-(0.3-D)**2)
      YB=D
      ALPHA=PI-ATAN(YB/XB)
      ALPHAD=ALPHA/FAC
      OMEGA=ATAN(XB/(0.3-D))
      OMEGAD=OMEGA/FAC

      ETA=PHI
      TITAM=PI/2.0-PHI-ALP1+BETA
      ALP3=PI-ALP1-(PI/4.0+PHI/2.0)
      ALPG=BETA+ALP3-PI/2.0
```

```
      ALPH=ALPG

      BC=D/COS(PHI)
      R0=BC
      BD=R0*EXP(TITAM*TAN(PHI))
      BE=SIN(PI/4.0+PHI/2.0)*BD/SIN(ALP3)
      DE=SIN(ALP1)*BD/SIN(ALP3)
      EF=SIN(PI/4.0+PHI/2.0)*DE/SIN(ALP2)
      BF=BE+EF


      XA=0.0
      YA=0.0
      XC=XB+BC*SIN(PHI)
      YC=0.0
      XD=XB+BD*COS(ALP1-BETA)
      YD=YB-BD*SIN(ALP1-BETA)
      XE=XB+BE*COS(BETA)
      YE=YB+BE*SIN(BETA)
      XF=XB+BF*COS(BETA)
      YF=YB+BF*SIN(BETA)
      XG=XD+(XE-XD)*1.0/3.0
      YG=YD+(YE-YD)*1.0/3.0
      XH=XD+(XE-XD)*1.0/2.0
      YH=YD+(YE-YD)*1.0/2.0

      XBDE=(XB+XD+XE)/3.0
      CGBCD=4.0*R0*TAN(PHI)/3.0/(EXP(2.0*TITAM*TAN(PHI))-1)
     1  *(3.0*TAN(PHI)*SIN(TITAM+ETA)*EXP(3.0*TITAM*TAN(PHI))
     2  -COS(TITAM+ETA)*EXP(3.0*TITAM*TAN(PHI))-
     3  3.0*TAN(PHI)* SIN(ETA)+COS(ETA))/(1.0+9.0*TAN(PHI)**2)
      XBCD=CGBCD+XB


      ABDE=ABS(0.5*(XB*YD-XD*YB+XD*YE-XE*YD+XE*YB-XB*YE))
      ABCD=ABS(R0**2/(4.0*TAN(PHI))*(EXP(2.0*TITAM*
     1  TAN(PHI))-1))
      AABC=ABS(0.5*(XA*YB-YA*XB+XB*YC-YB*XC+XC*YA-YC*XA))
      COFAR=OMEGA*0.09/2.0-0.5*0.09*SIN(OMEGA)
      AABC=AABC-COFAR


      FG=0.5*GAMA*DE**2*TAN(PI/4.0+PHI/2.0)**2
      Q=WO/(B*(BE+EF))
      FQ=Q*TAN(PI/4.0+PHI/2.0)**2*DE
```

```
      AMBDE=ABDE*GAMA*(XBDE-XB)
      AMBCD=ABCD*GAMA*(XBCD-XB)
      AMFG=FG*COS(ALPG)*(YB-YG)+FG*SIN(ALPG)*(XG-XB)
      AMFQ=FQ*COS(ALPH)*(YB-YH)+FQ*SIN(ALPH)*(XH-XB)
      PPG=(AMBDE+AMBCD+AMFG)/(2.0/3.0*BC*COS(PHI))
      PPQ=(AMFQ+Q*BE*(XE-XB)/2.0)/(1.0/2.0*BC*COS(PHI))
      PP=PPG+PPQ
      ALPHAD=180.0-OMEGAD*CGF
      ALPHA=PI-OMEGA*CGF
      TITA=(270-2.0*ALPHAD-PHID)*FAC
      TITAD=TITA/FAC
      DELTA=ATAN(SIN(TITA)*SIN(PHI)/(1.0+COS(TITA)*SIN(PHI)))
      IF(DELTA/FAC.GT.23.0) DELTA=23.0*FAC
      IF(DELTA/FAC.LT.-23.0) DELTA=-23.0*FAC
      DELTAD=DELTA/FAC
      P=COS(PHI)*(PP+AABC*GAMA*TAN(PHI))/COS(ALPHA-
     1  PI/2.0+DELTA+PHI)
      PH=P*COS(ALPHA-PI/2.0+DELTA)
           PH=PH*B
C      WRITE(21,7)D,XO,YO,XC,YC,XD,YD,XE,YE,TITAD,PHID,DELTAD,PH
 7    FORMAT(2X,F4.2,8(2X,F6.2),2X,F6.2,2X,F6.2,2X,F6.2,F8.4)
      TYPE*,AL, ALPHAD,DELTAD,'PH=',PH
      WRITE(21,8)AL,ALPHAD,DELTAD,PH
 8    FORMAT(2X,'L=',F4.1,2X,'EQUIVALENT ALPHA=',F7.2,2X,
     1  'DELTA=',F6.2,2X,'PH=',F8.3)
C ---------------------------------------------
C      'TYPE*,'ALPHA=',ALPHAD,'TITA=',TITAD,'ETA=',ETA/FAC '
C      TYPE*,'TITAM=',TITAM/FAC,'ALP3=',ALP3
C      TYPE*,'ALPG=',ALPG/FAC,'ALPH=',ALPH/FAC
C      TYPE*,'BC=',BC,'BD=',BD,'BE=',BE,'DE=',DE,'EF=',EF,'BF=',BF
C      TYPE*,'XB=',XB,'YB=',YB
C      TYPE*,'XC=',XC,'YC=',YC
C      TYPE*,'XD=',XD,'YD=',YD
C      TYPE*,'XE=',XE,'YE=',YE
C      TYPE*,'XF=',XF,'YF=',YF
C      TYPE*,'XG=',XG,'YG=',YG
C      TYPE*,'XH=',XH,'YH=',YH
C      TYPE*,'AABC=',AABC,'ABCD=',ABCD,'ABDE=',ABDE'
C      TYPE*,'FG=',FG,'FQ=',FQ
C      TYPE*,'WABC=',AABC*GAMA,'WBCD=',ABCD*GAMA,'WBDE=',GAMA
C      TYPE*,'AMBCD=',AMBCD,'AMBDE=',AMBDE,AMFG,AMFQ
C ---------------------------------------------

10    IF(DELTAD.LT.-24.0 .OR. DELTAD.GT.24) TYPE*,'NO VALUE'
```

```
STOP
END
```

```
C  THIS PROGRAMME CALCULATES FORCE ON THE
C  CYLINDRICAL MODEL.  COULOMB'S METHOD IS USED
C  ON SIMILAR LINES SUGGESTED BY
C  PRATER.  SLOPE OF BED AND SURCHARGE ARE CONSIDERED.

      OPEN(UNIT=20,FILE='EXP.DAT',TYPE='OLD')
      OPEN(UNIT=21,FILE='EXP.ANS',TYPE='NEW')
      OPEN(UNIT=22,FILE='EFFORT.ANS',TYPE='NEW')
      PHID=35.5
      DELTAD=23.0
      BETA=0.0
      GAMA=17.0
      PI=3.1415927
      FAC=PI/180.0
      PHI=PHID*FAC
      DELTA=DELTAD*FAC
      READ(20,*)N
      DO 10 I=1,N
      READ(20,*)AL,VO
      WO=VO*GAMA
      PMIN=1000
      D=(AL-0.125)/35.0
      ALPHAD=5
      DO 20 J=1,30
      ALPHA=ALPHAD*FAC
      TRM1=COS(ALPHA)*COS(BETA)/SIN(ALPHA-BETA)
      W1=PI*GAMA*(D**3/6.0*TRM1**2+D*D*0.25/2.0*TRM1)
      WT=WO+W1
      AK0=1.0-SIN(PHI)
      TRM2=COS(ALPHA)*SIN(BETA)/SIN(ALPHA-BETA)
      T=AK0*GAMA*D**3/6.0*TRM1*(1.0-TRM2)
      F=T*PI
      P=(WT*SIN(ALPHA+PHI)-F*COS(ALPHA+PHI))/
     1   COS(ALPHA+PHI+DELTA)
      PH=P*COS(DELTA)
      IF(PH.LT.0 .OR. PH.GT.1000)GOTO 20
C     IF(PH.GT.PMIN)GOTO 21
      IF(PH.LE.PMIN)ALPMIN=ALPHAD
      IF(PH.LE.PMIN)PMIN=PH
C     WRITE(22,*)AL,ALPHAD,PMIN,PH
      ALPHAD=ALPHAD+1
 20   CONTINUE
 21   WRITE(21,22)AL,VO,ALPMIN,PMIN
 22   FORMAT(5X,'L=',F3.2X,'VOL.SURCHARGE=',F9.7,2X,
```

```
    1  'ALPHA=',F5.2,2X,'PH=',F8.5)
10     CONTINUE
       STOP
       END
```

```
C   THIS PROGRAMME CALCULATES THE FRONT FACE RESISTANCE
C   FOR MODEL M6 USING COULOMB'S METHOD. THE COMONENTS
C   OF PASSIVE AND FRICTIONAL RESISTANCE ON TWO INCLINED
C   FACES IN THE DIRECTION OF MOVEMENT IS CONSIDERED.


      OPEN(UNIT=19,FILE='EXP.DAT',TYPE='OLD')
      OPEN(UNIT=20,FILE='EXP.ANS',TYPE='NEW')
      READ(19,*)N
      DO 5,I=1,N
      READ(19,*)AL,VO
      GAMA=17.0
      AK0=0.5
      B=0.25/COS(67.5*3.142/180.0)
      RHO=0.0
      D=(AL-0.302)/35.0
      VO=VO/2.0
      WRITE(20,7)AL,2.0*VO
7     FORMAT(2X,'TRIANGULAR WEDGE',//,'SCOUR LENGTH=',F4.2,5X,
     1  'VOL. OF OVERBURDEN=',E8.2)
      PHI=35.5*3.142/180.0
      DELTA=23.0*3.142/180
      BETA=1.637*3.142/180.0
      RHO=RHO*3.142/180.0
C TOTAL WEIGHT = WT. OF VARIABLE WEDGE + WT. OF OVERBURDEN
C       WT  =  WW + WO
      WO=GAMA*VO
      TITAD=5.0
10    TITA=TITAD*3.142/180.0
      WW=GAMA*B*(0.5*(D*COS(BETA))**2*COS(RHO+TITA)
     1   /COS(RHO+BETA)/  SIN(TITA-BETA))
      WT=WW + WO
C      TYPE*,'WW=',WW,'WO=',WO,'WT=',WT
      P=(WT*SIN(TITA+PHI))/COS(TITA+PHI+DELTA+RHO)
      PH=P*COS(RHO+DELTA)
C ** FOR TRIANGULAR PRISM
       PH=PH*0.7740*2.0
      WRITE(20,9)TITAD,WO,WW,WT,PH
9     FORMAT('FOR TITA=',F4.1,2X,'WO=',E8.2,2X,'WW=',
     1  E8.2,2X,'WT=',E8.2 ,2X,'P=',F9.4)
      TITAD=TITAD+1.0
      IF(TITAD.LE.30)GO TO 10
5     CONTINUE
      STOP
      END
```

APPENDIX - B

SPECIFICATIONS AND CALIBRATION OF TRANSDUCERS

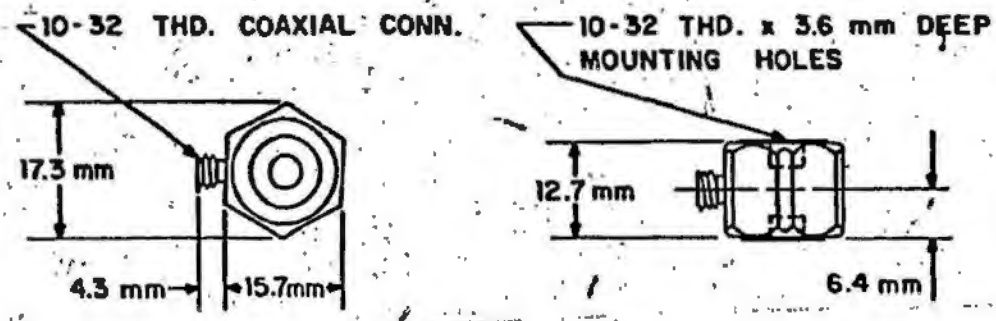

LOAD CELL

SCALE: FULL SIZE

Kistler Model 912 Quartz Dynamic Load Cell

Specifications:

Range: compression	5000 lbs (2268 kg)
Resolution	0.002 lb (0.9 gr)
Overload	20%
Sensitivity (nominal)	50 pcb/lb (110 pcb/kg)
Resonant frequency (nominal) (no load)	70,000 Hz
Rigidity	20×10^{-8} in/lb (1×10^{-8} m/kg)
Rise time	5 microsec
Linearity (zero based best straight line)	1%
Capacitance (nominal)	58 picofarads
Insulation resistance (minimum)	10^{13} ohms
Temperature sensitivity	0.01% per °F
Temperature range	-400 ° to 300°F
Side force (maximum)	100 lbs (45 kg)
Shock and vibration	10,000 g
Cable connector, side coaxial, teflon insulation	10:32 thread
Case materials	416 SS, 17-4PH SS
Weight	0.6 oz (17 gm)

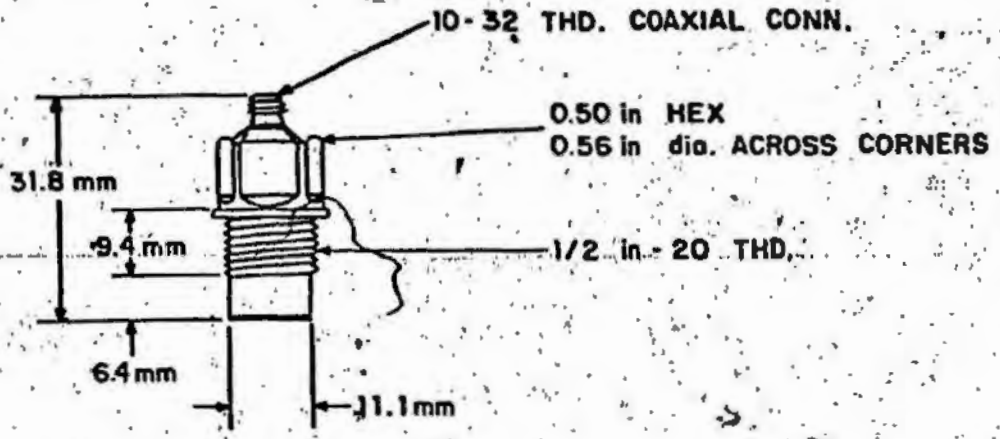

PRESSURE TRANSDUCER

SCALE: FULL SIZE

Kistler Model 606A/606L Quartz Pressure Transducer

Specifications:	606A*
Range full scale	3000 psi (21 MPa)
Resolution	0.005 psi (0.03 KPa)
Maximum pressure	5000 psi (34 MPa)
Sensitivity (nominal)	5.5 pcb/psi (0.8 pcb/KPa)
Resonant frequency (nominal)	130 kHz
Rise time	3.0 microsec
Linearity (zero based best straight line)	1%
Capacitance (nominal)	50 picofarads
Insulation resistance	10^{13} ohms
Acceleration sensitivity	<0.005 psi/g (0.03 KPa/g).
Temperature effect on sensitivity	<0.03% per °F
Temperature range	-350° to +450°F
Shock, 1 ms pulse width	1000 g
Case material	SS
Weight	0.5 oz (14 gm)

*Model 606L is identical to 606A except for range of 30 psi and maximum pressure of 300 psi
30 psi equals approximately 207 KPa
300 psi equals approximately 2068 KPa

CALIBRATION

All the pressure transducers and load cells used in this investigation were originally factory calibrated and were recalibrated by Chari (1975) and Green (1984). However, the calibration was rechecked both at the beginning and end of the experimental work. Load cells were subjected to direct compressive axial force using Instron Testing Machine. Keeping the amplifier under long time constant, a static force was applied in increments of 1 kN, over sufficient length of time and the response was monitored. Pressure transducers were calibrated using a piston activated oil pressure chamber and also by using a mercury column. In all the repetitions, good consistency was observed indicating the reliability of the pressure transducers.